# Scientific Opportunities with Fast Fragmentation Beams from RIA

*National Superconducting Cyclotron Laboratory*
*Michigan State University*

March 2000

---

INDEX OF ASTROPHYSICAL INSERTS:

# EXECUTIVE SUMMARY

This document highlights the scientific opportunities at the future Rare Isotope Accelerator (RIA) with fast beams produced by in-flight separation of isotopes from projectile fragmentation or fission. It is intended to augment the 1997 report *Scientific Opportunities with an Advanced ISOL Facility* that made the scientific case for an advanced ISOL (isotope separation on-line) facility. For medium-mass to heavy nuclei, fast beams will extend the study of very short-lived, neutron-rich nuclei into a region more than 10 neutrons further from the valley of stability than is presently possible and about 3 – 4 neutrons further than possible with re-accelerated (ISOL) beams. A compelling scientific case exists for the incorporation of an advanced fast fragmentation beam capability into the base plan of RIA.

The atomic nucleus consists of Z positively charged protons and N electrically neutral neutrons. The atomic number Z determines the number of electrons of the neutral atom and, consequently, its chemical properties. Since neutrons and protons have approximately the same mass, the mass of an atom is largely determined by its mass number A = N + Z. Slightly fewer than 300 isotopes make up the assortment of the 82 stable elements that exist in nature. When displayed on a graph of N versus Z, these stable isotopes lie along a slightly curved line, called the line of stability (or, figuratively, the valley of stability in the nuclear landscape).

A few more (unstable) isotopes exist on earth, but all unstable isotopes eventually decay until the line of stability is reached, i.e., they are radioactive. Some radioactive isotopes provide major medical benefits through diagnosis or treatment of diseases; others have important applications, e.g., in biological sciences, environmental sciences, archeology, national security and energy generation. The average time for a specific isotope to decay (its lifetime) can range from less than a thousandth of a second to billions of years. Short-lived isotopes cannot be found naturally on earth – they have long decayed since the earth was formed some billions of years ago. Yet, thousands of short-lived isotopes are continually created in the cosmos. They may have only a fleeting existence, but they play a crucial role in the still ongoing creation of the elements in the cosmos, as they did in the creation of the elements in our solar system billions of years ago.

Scientists now think that most of the elements in the cosmos are formed in stellar environments via reactions that involve rare isotopes, i.e., short-lived nuclei very far from the line of stability. The properties of most of these rare isotopes are unknown and can only be inferred, with considerable uncertainty, from theoretical calculations. Recent developments in accelerators and experimental technology now make it possible to produce thousands of different new isotopes and explore this large *terra incognita* of rare isotopes in the nuclear landscape. The resulting data will help elucidate the astrophysical processes underlying the creation of the elements in the cosmos and will be of great value for improving our understanding of the nucleus and for interpreting the high-quality astronomical observations made available by new generations of ground and satellite based instruments.

Even with the most advanced technology, the creation of rare isotopes far from stability is excruciatingly difficult, and they can only be produced in very small quantities. For some of the most interesting isotopes the production rate is only a few atoms per day – and most then decay within fractions of a second. Yet, these rates are often sufficient to determine the most important properties of the isotopes, thanks to new and highly sensitive experimental techniques.

While significant first steps have been made in recent years, there is an international consensus that effective exploitation of this new scientific frontier of rare isotopes requires advanced, new facilities wholly dedicated to the production and study of short-lived rare isotopes. An optimally designed and dedicated rare isotope research facility will allow scientists to learn much about important questions, such as:

- *What is the origin of the elements of the cosmos – and what are the nuclear processes that determine the fate of stars and that lead to the synthesis of the elements we are made of?* Many elements are created in stars similar to our sun, but many others must be created in much hotter, explosive environments, e.g., in supernova explosions. While scientists are beginning to understand some of the general features of these element creation processes, many details remain unknown. Together with modern astronomical observations, experiments at an advanced rare isotope research facility will allow scientists to unravel this mystery.
- *Which combinations of protons and neutrons can make up a nucleus?* Scientists can answer this basic question only for the lightest eight elements. Theoretical predictions of the limits of stability are extremely challenging since they require very accurate solutions of the mesoscopic quantum problem for strongly interacting particles.
- *What are the properties of nuclei with extreme proton-to-neutron ratios?* In recent years, it has been discovered that some very light rare isotopes (e.g., the rare isotope $^{11}$Li) consist of nearly pure neutron matter in their outer periphery – a condition that does not exist in any nucleus close to the line of stability. More substantial neutron skins or halos may exist in heavier nuclei, but it has not been possible to produce and study them. Elsewhere, neutron matter exists only inside neutron stars – collapsed stars so dense that a mass as great as the entire mass of our solar system would fit into a sphere less than ten miles in radius.
- *What are the properties of bulk neutron-rich matter under extreme conditions of temperature and density?* Large objects of neutron-rich nuclear matter, neutron stars, are created in the cosmos during supernovae explosions which are triggered by the gravitational collapse of the cores of massive stars that have run out of nuclear fuel. While the existence of neutron stars is firmly established by astronomical observations, neither their properties nor the sequence of events which leads to their formation are well understood, in part due to our incomplete knowledge of the equation of state (EOS) of neutron-rich nuclear matter.

- *How must existing theoretical models be changed to describe the properties of rare isotopes?* Present models have been fine-tuned to reproduce the properties of nuclei close to the line of stability, but their predictions become increasingly uncertain as the neutron excess increases. They cannot predict the properties of the very neutron-rich rare nuclei that play a central role in the formation of heavy elements. It seems likely that long held concepts, such as the shell structure of nuclei, will undergo major revisions as one moves away from the line of stability.
- *How are the properties of rare isotopes related to the basic nucleon-nucleon interaction?* This question is closely related to one of the most challenging problems of modern science – how can one derive the properties of composite objects from those of their building blocks? Solutions of such mesoscopic problems require advanced computational techniques of ever increasing sophistication, whose development will have many cross-disciplinary applications. Nuclei, and especially rare isotopes with unusual properties, provide an ideal test bed for problems of mesoscopic quantum physics and a continuing stimulus for the development of new theoretical approaches.

The Nuclear Science Advisory Committee (NSAC) of the Department of Energy (DOE) and the National Science Foundation (NSF) has recommended the construction of a Rare Isotope Accelerator (RIA) in order to pursue these compelling scientific questions. RIA would be capable of delivering intense beams of all elements from hydrogen to uranium, with beam power in excess of 100 kW and beam energies per nucleon up to 400 MeV. The recently developed RIA concept is bold and novel; no present accelerator can provide such intense and diverse beams. It combines both major techniques of rare isotope production: (1) projectile fragmentation or fission and in-flight separation, and (2) target spallation or fission, and isotope separation on-line (ISOL) followed by acceleration of the isotope of interest. These two techniques are complementary in the species and energies of the beams that can be produced and drive different aspects of the science. Past facility concepts were based on the implicit assumption that these two techniques require two separate facilities. The integration of both production techniques into a single advanced rare isotope research facility is a paradigm change which allows cost-effective utilization of the full arsenal of experimental techniques being developed worldwide. The RIA approach is unique in the world.

The scientific case for a next-generation ISOL facility was elaborated in the 1997 Report *Scientific Opportunities with an Advanced ISOL Facility*. Since the RIA concept also allows the direct utilization of fast beams of projectile fragments separated in flight, it is appropriate and timely to delineate the additional scientific opportunities that arise from this capability. That is the purpose of the present document.

This document highlights the scientific opportunities that can be realized with fast beams of projectile fragments separated in flight at RIA and, therefore, complements the 1997 report mentioned above. For medium-mass to heavy nuclei, the direct utilization of fast fragmentation beams will extend the scientific reach of RIA by allowing studies of many very short-lived, neutron-rich nuclei in a region of more than 10 neutrons further from the line of stability than is presently possible and 3 – 4 neutrons further as compared to re-

accelerated beams. The effective utilization of fast fragmentation beams at RIA will thus be crucial for addressing the scientific objectives discussed above.

The following attractive features of experiments with fast beams enable this extended scientific reach:

- Economic production of medium-energy (E/A $\geq$ 50 MeV) beams of rare isotopes, without re-acceleration;
- Increased luminosity from the use of thick secondary targets (by up to a factor of 10,000);
- Reduced background from in-flight tracking and identification of individual isotopes in the beam on a particle-by-particle basis;
- Efficient particle detection from strong forward focusing;
- Short beam development times and low losses due to fast (sub-microsecond) and chemistry-independent separation and transport to the experiment.

The scientific case for the incorporation of an advanced fast fragmentation beam capability into the base plan of RIA is compelling. Experiments with fast beams can be performed for those hundreds of isotopes that are produced with intensities too low to be useful in experiments with low-energy re-accelerated beams. RIA provides unprecedented capabilities for both techniques, the ISOL re-acceleration technique and the projectile fragmentation technique, and thus unique access to the unknown territory of rare isotopes far from the valley of stability.

# 1. INTRODUCTION

Some distance from the valley of stability lies a frontier beyond which the properties of nuclei are unknown. Within the valley lie the stable isotopes, totaling almost 300. Thousands more are continually created in the cosmos and play a fleeting, though important role in stellar processes. Technical advances now make it possible to create many of these short-lived nuclei in the laboratory and to study their unusual properties. These are of considerable intrinsic scientific interest and are needed to provide a solid understanding of the nuclear processes that underlie the evolution of stars and the origin of the elements in the cosmos. Important investigations have begun at facilities developed mostly for studies of nuclei near the valley of stability, but a fully effective response to this scientific challenge requires advanced new facilities wholly dedicated to the production and study of short-lived, rare isotopes.

The importance of the physics and the nature of the technology necessary to advance this scientific frontier were examined in detail by the DOE/NSF Nuclear Science Advisory Committee (NSAC) in preparation of its 1996 Long Range Plan (LRP)[*] and by the National Research Council (NRC) Committee on Nuclear Physics in its assessment of the field, *Nuclear Physics, The Core of Matter, The Fuel of Stars* (1999).[†] At the international level, the nuclear physics working group of the Organization for Economic Cooperation and Development (OECD) Megascience Forum addressed this issue in its 1999 report.[‡] The conclusions of these groups strongly support exploration of nuclei far from the valley of stability, and the Megascience Forum report recommends that "a new generation of high-intensity RNB (Radioactive Nuclear Beam) facilities of each of the two basic types, ISOL (Isotope Separator On-Line) and In-Flight, should be built on a regional basis."

The NSAC LRP recognizes that: "The scientific opportunities made available by world-class radioactive beams are extremely compelling and merit very high priority." As the highest priority for new initiatives, the LRP strongly recommends the "immediate upgrade of the MSU facility to provide intense beams of radioactive nuclei via fragmentation" and "development of a cost-effective plan for a next generation ISOL-type facility and its construction when RHIC is essentially complete." The LRP notes further that "the fragmentation and Isotope Separator On-Line (ISOL) techniques are complementary in the species and energies of the beams produced. Thus they drive different aspects of the science."

Together, the two complementary techniques provide the tools needed to address important questions about the nature of nucleonic matter and the origin of the elements, and to test of the standard model of electroweak and strong interactions.

---

[*] http://pubweb.bnl.gov/~nsac/

[†] http://www.nap.edu/readingroom/books/nucphys

[‡] The OECD Megascience Forum: Report from the Working Group on Nuclear Physics, January 1999

The traditional ISOL technique is based upon isotope production at rest in thick targets via fragmentation or fission of a target nucleus, followed by extraction, ionization, separation and acceleration of the desired isotopes to modest energies. It is the technique of choice for the production of precision beams of low energy (E/A < 20 MeV). In most cases, beam development involves both physical and chemical methods and requires a considerable amount of time and effort. For very short-lived isotopes, losses due to decay can be appreciable. Beams created by the ISOL technique excel for precision studies at or near the Coulomb barrier, such as transfer reactions, multi-step Coulomb excitation, and sub-barrier fusion or capture reactions.

Projectile fragmentation (or fission) combined with in-flight separation, is the most economical way of producing medium-energy (E/A ≥ 50 MeV) beams of rare isotopes. This technique allows sub-microsecond isotope separation by purely physical methods, yielding short beam development times. Thus, projectile fragmentation/fission is the technique of choice for experiments requiring energetic beams, e.g., knockout reactions, charge-exchange reactions, spin-flip excitations, and studies of giant resonances.

While complementary, the two techniques also allow a seamless overlap. Several important questions can be addressed both with re-accelerated beams and with fast beams separated in flight, allowing case-by-case optimization as well as important crosschecks between complementary approaches when the extracted physics requires a solid understanding of the reaction mechanism.

Following NSAC's recommendations, the DOE and NSF took action: The NSCL upgrade is underway and will be completed by 2001. The scientific case for a next-generation ISOL facility was elaborated in the 1997 Report, *Scientific Opportunities with an Advanced ISOL Facility*,[*] and NSAC was charged in 1998 to establish a task force to provide a technical analysis of the various options for a new facility which would allow the research outlined in the 1997 report to be carried out.

In November 1999, NSAC received, endorsed, and forwarded the report and recommendations of the ISOL Task Force[†] to the agencies. Most notably, the ISOL Task Force recommends:

- "The design and construction of a Rare-Isotope Accelerator (RIA) facility that provides unprecedented beams of a diverse assortment of nuclei. The scientific potential of the RIA facility will be maximized by integrating multiple techniques for producing and separating, then accelerating and utilizing these rare isotopes. RIA will be based on a highly flexible superconducting linac driver capable of providing 100 kW, 400 MeV/nucleon beams of any stable isotope from hydrogen to uranium. The broad assortment of short-lived secondary beams needed for the experimental program will be produced by a combination of techniques: projectile fragmentation, target fragmentation, fission, and spallation."

[*] http://www.phy.anl.gov/div/W_PaperF.pdf

[†] http://srfsrv.jlab.org/isol/ISOLTaskForceReport.pdf

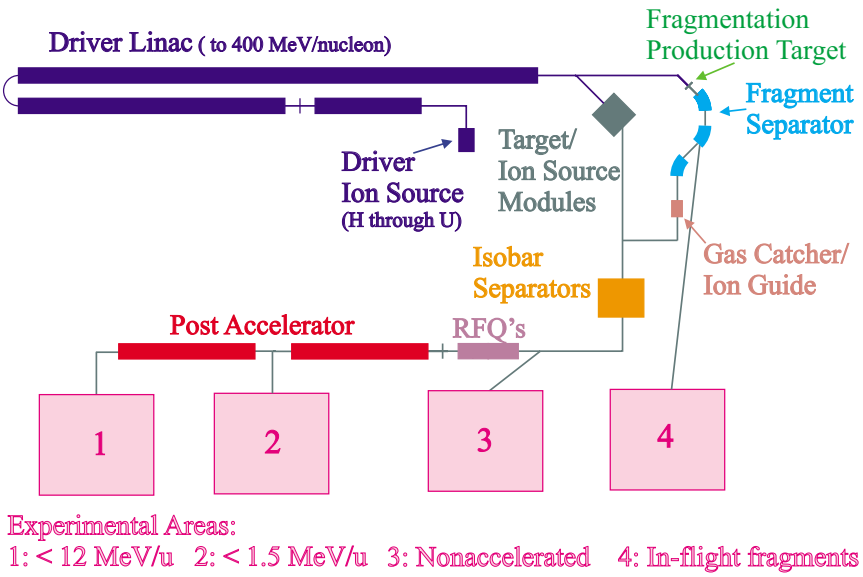


Figure 1: Schematic layout of an advanced ISOL facility. From ISOL Task Force Report to NSAC.

- "That an additional important opportunity be provided: fast in-flight separated beams of rare isotopes. This will extend the scientific reach of the RIA facility. We recommend that the RIA design accommodate this capability."

The schematic layout of the envisioned RIA facility is shown in Figure 1. Rare isotopes at rest in the laboratory will be produced by conventional ISOL target fragmentation, spallation, or fission techniques and, in addition, by projectile fragmentation/fission and stopping in a gas cell. Upon extraction, these stopped isotopes can be used at rest for experiments in Area 3, or they can be accelerated either to energies below the Coulomb barrier and used in Area 2 or above the Coulomb barrier and used in Area 1.

The fast beams of rare isotopes, which are produced by projectile fragmentation/fission, can also be used directly after separation in a high-resolution fragment separator (area 4). Thus, RIA combines the advantages of both techniques, the conventional thick-target ISOL technique and the transmission-target projectile fragmentation/fission technique – a paradigm change as compared to the original recommendation of the LRP. In transmitting the ISOL Task Force Report to the agencies, NSAC notes:

> "The beams from this accelerator, when combined with new developments in target and ion source technology and a superconducting post-accelerator, will generate high-quality beams of rare isotopes at unprecedented intensities. These capabilities are far in excess of those envisioned in the 1996 Long Range Plan and will give this rare isotope accelerator (RIA) physics discovery potential exceeding any existing or planned facility in the world. Furthermore, the choice of this highly flexible driver accelerator opens up the possibility of a whole new range of experiments using fast fragmentation, in addition to those originally envisaged for

> the ISOL facility and laid out in the 1997 physics report: 'Scientific Opportunities with an Advanced ISOL Facility.' … This innovative technical concept has generated great excitement within the potential user community of RIA. NSAC notes that in order to ensure an optimal physics program that takes full advantage of the new capabilities of RIA, the user community must play an active role in updating the scientific opportunities developed in 1997 and in making a strong and focused scientific case for the facility."

The present document updates the scientific case for the physics accessible with fast fragmentation beams separated in-flight by an advanced fragment separator. The document builds upon the 1994 NSCL White Paper, *The K500⊗K1200*, and includes new knowledge and insight gained in recent years with fast fragmentation beams of low intensity at the NSCL and other medium energy heavy-ion facilities in the world. It therefore augments the 1997 report on *Scientific Opportunities with an Advanced ISOL Facility*. Taken together, the two reports lay out the physics opportunities for the fully developed RIA facility.

The main attractive features of fast beams leading to enhanced sensitivity are summarized in the box below. As will be discussed in the body of this document, experiments with fast fragmentation beams will extend the range of accessible neutron-rich medium-mass and heavy nuclei by approximately 3–4 neutrons beyond that accessible by re-accelerated ISOL beams. One expects these nuclei to show more clearly the effects associated with neutron excess and to have a greater overlap with astrophysical element-creation processes such as the r-process.

In addition, many studies require beam energies significantly higher than attainable with the envisioned post-accelerator. In such cases, the direct use of fast fragmentation beams is the only economically viable option.

Fast beams will enhance the scientific reach of the proposed RIA facility and effectively address many key questions. Specifically, fast beams from RIA will allow enhanced sensitivity or novel experiments which explore explosive astrophysical processes and the origin of the elements, the properties of nuclei with unusual charge-to-mass ratios, the limits of nuclear existence, and the properties of neutron-rich nuclear matter.

Attractive features of experiments with fast beams:

- Economic production of medium-energy (E/A $\geq$ 50 MeV) beams of rare isotopes, without re-acceleration
- Increased luminosity from use of thick secondary targets (by up to a factor of 10,000)
- Reduced background from in-flight tracking and identification of individual isotopes in the beam on a particle-by-particle basis
- Efficient particle detection from strong forward focusing
- Short beam development times and low losses due to fast (sub-microsecond) and chemistry-independent separation and transport to experiment

# 2. EXTENDED REACH WITH FAST BEAMS

This section is a brief overview of the scientific reach provided by fast fragmentation beams at RIA. A more quantitative discussion of the intensities needed for selected experiments with fast beams is given in Appendix A.

RIA is designed to penetrate deep into the present *terra incognita* of the nuclear landscape and explore the limits of nuclear existence and the properties of nuclei with extreme neutron-to-proton ratios. This is the regime of the weakly bound states and resonances that play a crucial role in the formation of the elements in the astrophysical rapid neutron (r) and rapid proton (rp) capture processes. The physics opportunities made available with *low energy* beams from RIA have been discussed in detail in the 1997 report, *Scientific Opportunities with an Advanced ISOL Facility*. The present document will demonstrate that *fast fragmentation beams*, separated in flight, will complement the information obtained by re-accelerated low-energy beams, that they will enhance the scientific reach of RIA, and that they will make crucial contributions to our knowledge about nuclei very far from stability. In addition, fast fragmentation beams will provide new scientific opportunities as for instance the exploration of the equation of state in neutron-rich nuclear matter.

Some experiments, such as decay studies and lifetime measurements, involve stopping the isotopes of interest. We include in our discussion those experiments that utilize in-flight separation by means of a high-resolution fragment separator and subsequent ion-by-ion tracking and identification. Often, similar experiments can be performed by the standard ISOL technique of producing the isotopes of interest at rest in a thick target or by stopping the projectile fragments in an appropriate catcher, followed by extraction, low-energy isobar separation and transport to the experimental area. This latter technique has been discussed in the 1997 report, *Scientific Opportunities with an Advanced ISOL Facility*. The fast-beam approach discussed in the present document is particularly advantageous for studies of isotopes with low production yields and/or short lifetimes, in which extraction losses from a catcher must be avoided, and for experiments that can effectively utilize "cocktail" beams, i.e., beams containing several isotopes of very similar magnetic rigidity, with each isotope being identified and tagged on a particle-by-particle basis.

Experiments on very neutron-rich systems with fast fragmentation beams offer the advantages summarized in the box on page 8. For some applications these advantages are augmented by increased cross sections and sensitivity for reactions at higher beam energy.

Figure 2 illustrates the resulting scientific reach of fast beams. The stable nuclei are shown in white. The colors correspond to different beam intensities predicted for RIA.[*] nuclei in green ($>10^8$ particles/s) and blue ($10^4$–$10^8$ particles/s) will be available as beams with

[*] The yields are based on the fragmentation production mechanism. The production cross sections are taken from the EPAX2 formulation [sum99], and assume a 100 kW primary beam intensity and a $^7$Li production target thickness optimized for a 6% momentum acceptance fragment separator. In each case the primary beam is optimized to provide the highest fragment yields.

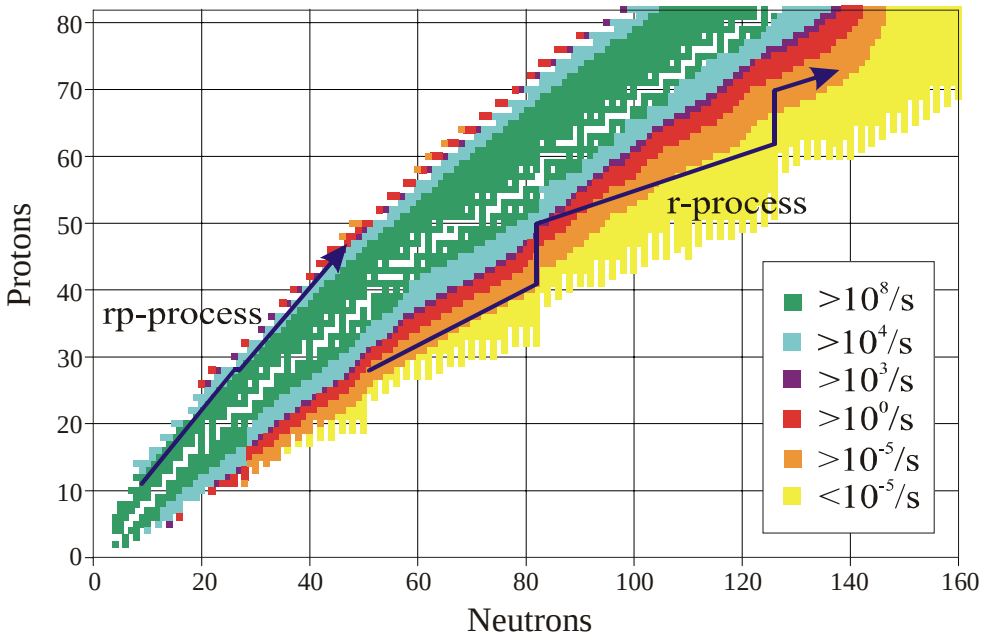


Figure 2: Chart of nuclei. Stable isotopes shown in white. Rare isotope production rates predicted for RIA (see footnote on page 9) shown in color with the color code given in the Figure. Experiments feasible with fast beams of various rates are discussed in this section and, in more depth, in Section 4. The minimum beam intensities needed for various types of experiments with fast beams are discussed in Appendix A.

sufficient intensity for many experiments with re-accelerated nuclei. As pointed out in the 1997 report *Scientific Opportunities with an Advanced ISOL Facility*, $10^3$ particles/s (purple) could be sufficient for selected experiments. Fast fragmentation beams will, in addition, allow selected experiments with nuclei shown in red (1–$10^3$ particles/s) and in some cases with nuclei shown in orange, corresponding to $10^{-5}$–1 particles/s. Meaningful information can be obtained with $10^{-5}$–1 particle/s as demonstrated recently at fragmentation facilities such as GANIL, GSI, NSCL, and RIKEN. Nuclei predicted to be particle stable, but still outside the experimental reach of RIA, are shown in yellow. With fast beams from RIA the neutron drip line may be reached for elements up to manganese (Z = 25), and maybe again at zirconium (Z = 40). For comparison, the heaviest known drip-line nucleus is $^{24}$O (Z = 8). Fast beams from the upgraded NSCL facility will make it possible to reach the drip line for all elements up to sulfur (Z = 16).

Even with very low intensities useful information can be obtained using fast beams. At the level of $10^{-5}$ particles/s the stability of an isotope (and hence in some cases the location of a drip line) can be determined and its half-life measured if the background is sufficiently low. At the level of 0.01 particles/s the total interaction cross section of the isotope can be determined, and information on its matter distribution can be deduced. Also at this level, modest-resolution mass measurements can be made. When the beam intensities reach 0.1 particles/s, nucleon knockout reaction measurements are possible. Recently, knockout reactions have proved to be an effective tool to learn about the structure of neutron- or

proton-rich nuclei. At about the same intensity it is possible to perform Coulomb excitation experiments to measure the energies of low-lying states and B(E2) values to obtain information about nuclear deformation.

In addition to the determination of basic nuclear properties, fast fragmentation beams can be used to excite giant resonances in exotic nuclei; these resonances are most effectively studied at high beam energies, and intensities above $10^6$ particles/s are needed. The giant monopole resonance provides an excellent measure of nuclear compressibility. Studies of neutron-rich nuclei are needed for reliable extrapolation of the compressibility to neutron-rich nuclear matter and to the matter of neutron stars. Measurements of collective flow to constrain the isospin dependence of the nuclear equation of state (EOS) require high beam energies and can be performed with neutron-rich fast fragmentation beams at RIA. The required intensities of about $10^4$ particles/s will be available at RIA for medium-mass nuclei ($A \approx 100$) with energies up to $E/A \approx 400$ MeV and neutron/proton ratios of $1 < N/Z < 1.7$. This will expand the range of N/Z values of medium-mass nuclei by nearly a factor of three over that accessible with stable beams.

Very neutron-rich and very proton-rich nuclei play important roles in astrophysical nucleosynthesis. The current advances in astrophysical observations and in computational capabilities for simulation require nuclear information of much higher precision than is presently available. Experiments with very short-lived isotopes are needed to establish the underlying nuclear physics with accuracy sufficient to allow meaningful interpretations of these new observations and to test models of stellar evolution and nucleosynthesis. Some of the most important cases involve hard-to-reach extremely neutron-rich r-process nuclei and very proton-rich rp-process nuclei, which typically are short-lived and are produced with very low intensities. Fast beams will allow the study of many neutron-rich nuclei that are beyond the reach of experiments with re-accelerated beams.

Historically, complementary information about the properties of nuclei has been obtained with stable beams of both low and intermediate energy. RIA will permit the continued use of this complementary approach: low-energy studies can be carried out with re-accelerated beams, and medium-energy studies can be carried out with fast beams produced by projectile fragmentation/fission and separation in flight. In many instances experiments with fast beams will have increased sensitivity, by several orders of magnitude, as compared to the alternative of stopping the fast isotopes in a suitable catcher, then extracting and re-accelerating them.[*] Thus, fast beams will permit studies of nuclei significantly closer to the neutron drip line, for which effects due to neutron excess are more pronounced and which are of enhanced astrophysical import. For instance, closed neutron-shell nuclei at $N = 126$ along the r-process path will become accessible.

[*] Note, however, that the conventional thick target ISOL technique can produce significantly higher yields, especially for non-refractory isotopes close to the valley of stability.

# 3. SCIENTIFIC MOTIVATION

## 3.1. Properties of Nuclei far from Stability

Nuclear Physics has strongly influenced the development of many-body theory. The atomic nucleus is a finite drop of a multi-component quantum Fermi liquid with strong interactions between the constituents. During the last decade nuclear concepts were successfully applied to other finite quantum systems of current interest: atomic and metal clusters, Fullerenes and other macro-molecules, quantum dots and solid state micro-devices, Bose condensates and Fermi gases in atomic traps. Nuclei very far from stability are open mesoscopic systems that are strongly coupled to the continuum. In contrast to open quantum dots and billiards, these loosely bound nuclear many-body systems are likely to exhibit entirely different many-body quantum features than their more strongly bound counterparts. This impact on other areas of many-body quantum physics is expected to continue with new ideas developed for nuclei far from stability; theoretical approaches and computational methods developed for nuclear physics will undoubtedly cross-fertilize other fields of physics. It is difficult to exaggerate the importance of nuclear experiments and theory for the understanding of nuclear matter in the Universe and its cosmological evolution.

Over the past few decades, nuclear models have been fine-tuned primarily to reproduce the properties of nuclei close to the valley of stability. RIA will allow the study of nuclei of vastly different composition. Experiments at RIA will provide an unprecedented wealth of new data in remote regions of the nuclear landscape that will challenge the best of nuclear models. Theoretical predictions become increasingly uncertain for nuclei far from stability. For very neutron-rich nuclei, the subtle interactions between weakly bound discrete states and slightly unbound continuum states will play an important, yet poorly understood role. At the very least, new numerical implementations of existing theoretical frameworks together with newly optimized sets of parameters will be needed. More likely, entirely new approaches to solving the many-body problem will be necessary. It is possible that different magic numbers are encountered far from stability and even that the basic premises of shell-model and mean-field descriptions become questionable.

Since exact solutions of the many-body problem can be obtained only for very light nuclei, the development of improved nuclear models will require detailed comparison between experimental data and theoretical predictions. In many instances, these comparisons will require a detailed understanding of the intricate interplay between nuclear structure and reaction mechanisms. In the past, these two aspects have often been treated as separate problems, partly because of limitations in computational power. With the growth in computational power, new and unifying approaches will become possible.

Such a unified description of nuclear structure and reaction mechanisms will require a solid understanding of the effective nucleon interactions governing both parts. Unusual N/Z ratios, encountered far from stability, can lead to effective in-medium forces different from those typically used near stability. Such differences can be particularly important for exchange and isospin-dependent forces. The presence of outer regions (skins or halos) with

an enhanced neutron concentration is of major significance for interpolation between in-medium effective forces and vacuum interactions. The components of nuclear forces responsible for pairing and α-particle clustering are very sensitive to continuum effects, which could require modification of the current approaches to pair correlations and cluster preformation. New types of cluster structures may be found at and perhaps even beyond the drip lines. The renormalization of weak interactions in the nuclear medium, essential for the quantitative description of nuclear decay and synthesis, can also differ for nuclei very far from stability as compared to nuclei near the valley of stability.

Mean-field approaches provide the global framework for understanding how single-particle properties, shell gaps, and nuclear shapes evolve towards the drip lines. At the next level, residual interactions within the shell structure determined by the mean field must be taken into account. The parameters of the effective Hamiltonian can be constrained by the properties of nuclei near stability, as demonstrated, for example, by the universal *sd*-shell Hamiltonian for nuclei in the region A = 16–40. In practice, this approach requires the diagonalization of increasingly large matrices. Monte-Carlo methods have recently been developed as an alternative approach for dealing with this increasing computational complexity. The theoretical description of nuclei very far from stability to be explored at RIA will drive major advances in the treatment of large-scale configuration mixing. Shell-model configuration mixing provides a complete set of predictions for nuclear properties, which can be tested experimentally. For heavy nuclei away from the closed shells, the deformed Hartree-Fock and group theoretical models, such as the Interacting Boson Model, provide predictions that will be tested by RIA.

We next address a few important issues for which major new insight will be obtained from experiments with fast beams of rare isotopes at RIA.

THE LIMITS OF NUCLEAR EXISTENCE. A major long-term experimental challenge for research with exotic beams is the exploration of the extremely neutron-rich regions of the nuclear chart. These regions are, for the most part, *terra incognita* – and for the heavier elements they are likely to remain so for a long time. For example, the heaviest stable isotope of tin found in nature is $^{124}$Sn, and the heaviest isotope identified in the laboratory is $^{134}$Sn, with a half-life of one second. Theoretical estimates range widely, but suggest that the heaviest particle-stable isotope could be $^{176}$Sn, 42 mass units further out, and beyond the range of any proposed accelerator. Since we cannot expect to study these nuclei directly, it is crucial to study nuclei that are as neutron rich as possible, so as to permit a more reliable extrapolation to the regions of astrophysical processes and to the neutron drip line where neutrons become unbound.

EXTENDED DISTRIBUTIONS OF NEUTRON MATTER. Experimentally, the properties of nuclei at or very close to the neutron drip line can only be explored for lighter elements. Several new phenomena have been observed in the most neutron-rich light elements. For example, the valence neutron(s) of the neutron-rich, weakly bound nuclei $^{11}$Li and $^{11}$Be have density distributions that extend far beyond the core. Such neutron halos present an exciting opportunity to study a variety of nuclear phenomena: diffuse neutron matter, new modes of excitation, and reaction mechanisms of weakly bound nuclei. The few nuclei studied so far give us a hint of what will happen as one closely approaches the drip lines. Since the

decreasing neutron binding energies result in extended and diffuse neutron matter distributions, surface effects and coupling to the particle continuum will strongly influence the properties of these nuclei. Pairing correlations will become increasingly important because the continuum provides an increased reservoir of states for scattered particles. New collective modes due to different proton and neutron deformations might appear, and the shell structure may change dramatically due to the strong pairing force at the surface and due to the expected decrease of the spin-orbit force. At present, $^{19}$C is the heaviest nucleus in which a one-neutron halo has been observed. Much heavier nuclei with extended multi-neutron distributions remain to be discovered and explored.

PROPERTIES OF NEUTRON-RICH BULK NUCLEAR MATTER. During a central collision of two nuclei at energies of E/A ≈ 200–400 MeV, nuclear matter densities approaching twice the saturation density of nuclear matter can be momentarily attained. The resulting hot and compressed reaction zone subsequently cools and expands to sub-nuclear density. Nuclear collision experiments offer the only terrestrial situation in which such densities can be achieved and experimentally investigated. Key issues already identified in the 1996 Long Range Plan for Nuclear Physics are the determination of the equation of state (EOS) and the investigation of the liquid-gas phase transition of nuclear matter. Such information is needed for nuclear systems of different N/Z composition to constrain extrapolations of the EOS to the neutron-rich matter relevant to Type II supernova explosions, to neutron-star mergers, and to the stability of neutron stars.

CAN HEAVY NEUTRON-RICH NUCLEI BE DEFORMED? It is widely assumed that the n-p residual forces are mostly responsible for the emergence of nuclear deformation. The arguments can be convincingly tested only when the systematics of nuclear shapes far from stability are firmly established. Important data are energies and transition probabilities to low-lying collective states obtained by Coulomb excitation. A new tool for determining the degree of deformation can be provided by the specific shape of the longitudinal momentum distribution of the core residue after particle removal reactions from deformed projectiles. The exotic nuclei may also reveal unusual symmetries related to deformations of higher multipolarities.

NEW MODES OF COLLECTIVE MOTION. Standard approaches, such as the random phase approximation, break down in the case of "Borromean" nuclei* whose excited states can only decay by emitting at least two (instead of one) particles. Available three-body methods, such as solving the Faddeev equation, usually consider the residual nucleus as an inert core. Such methods are to be supplemented by an improved treatment of microscopic dynamics and antisymmetrization. The strength functions of the collective response can be quite different from what is routinely seen in normal nuclei. Systematic studies of giant resonances and low-lying collective modes in loosely bound neutron-rich nuclei will allow one to establish exchange contributions to the classical sum rules, which express the general properties of nuclear matter in response to external fields. Such information may

* Three-body systems for which the two-body sub-systems have no bound states are often referred to as Borromean, after the three interlocked rings in the coat of arms of the Italian family of Borromeo.

further our understanding of collective motion in neutron matter, currently a hotly debated issue.

HOW DO MEAN-FIELD MODELS EVOLVE WITH N/Z? The basis of the nuclear shell model is that the mean field and its associated single-particle energies determine nuclear dynamics. Does this concept still apply to very neutron-rich nuclei near the drip lines? If so, what are the single-particle energies near the drip line and how well can they be extrapolated from the properties of nuclei near stability? Several specific mechanisms are important to quantify. As the neutron single-particle energies approach the Fermi surface and become loosely bound in neutron-rich nuclei, the orbitals become more closely spaced. This reduces the shell gap and sometimes allows shell inversion where the deformed configuration has a lower energy than the normal spherical configuration. This change in the shell structure has already been observed in nuclei near $^{11}$Be and $^{32}$Mg. It is not known whether such shell inversions exist in heavier nuclei. A possible change in the spin-orbit potential in a very neutron-rich environment is another factor that will influence shell gaps.

The neutron single-particle energies change slowly with neutron number, and thus the exact position of the neutron drip line is extremely sensitive to model parameters. The experimental determination of the single-particle energies of very neutron-rich nuclei will be crucial for describing the neutron drip line of heavier nuclei and the path of the astrophysical r-process (see also the following subsection).

Historically, nuclear physics has shown great discovery potential for new quantum phenomena, e.g., nuclear deformation and superdeformation, nuclear superfluidity and nuclear Meissner effect, new types of radioactivity, quantum chaos and development of periodic orbit theory, observation (and successful interpretation) of an unexpectedly large enhancement of weak interactions in compound states, and mesoscopic phase transitions seen via multifragmentation. With the unprecedented reach of RIA into a vast, yet uncharted terrain of nuclear physics, the large discovery potential for nuclear physics is assured for future years.

## 3.2. Nuclear Astrophysics

Nuclear processes underlie the creation of the elements and the evolution of stars. They define the successive stellar burning stages and drive the violent nova, supernova and X-ray bursts we observe in the Cosmos (see also the box on page 16). A recent summary of the role nuclear science plays in astronomy and astrophysics is given in *Opportunities in Nuclear Astrophysics*, a white paper based on a town meeting held at the University of Notre Dame in June 1999.[*] Specific experiments that provide information important for nuclear astrophysics are discussed in Section 4, Experimental Program, in which several topics of astrophysical interest are highlighted as sidebars. This section presents an overview of the important contributions of fast beams at RIA to nuclear astrophysics.

[*] http://www.nscl.msu.edu/~austin/nuclear-astrophysics.pdf

## Cataclysmic Binary Stars

Thermonuclear explosions in accreting binary star systems – novae, X-ray bursts and Type Ia supernovae – produce the most common explosive astrophysical events. At the conceptual level, the nature of the explosion mechanism seems reasonably well understood, but there are considerable discrepancies between the predicted observables and observations.

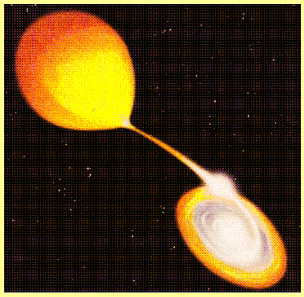

An understanding of the time evolution of energy generation and nucleosynthesis, and of the nature of mixing and convective processes, is necessary to explain the observed luminosities and the abundance distribution in the ejected material. The proposed mechanism involves binary systems with one or two degenerate objects, such as white dwarfs or neutron stars, and is characterized by the revival of a dormant object via mass flow from the binary companion.

The observed differences in the luminosity, time scale, and periodicity depend on the accretion rate and on the nature of the accreting object. These events involve nuclear processes at extreme temperatures and densities and synthesize a number of the important isotopes that make up our world.

Low accretion rates lead to a pileup of unburned hydrogen and the ignition of hydrogen burning via pp-chains in an environment supported by electron degeneracy pressure. Once a critical mass layer is attained there are large enhancements in the rates of the reactions. On white dwarfs this triggers nova events, and on neutron stars it results in X-ray bursts.

High accretion rates cause high temperatures in the accreted envelope and less degenerate conditions, and such rates usually result in stable H-burning or only weak flashes. High accretion rates on white dwarfs may cause Type Ia supernovae; high accretion rates on neutron stars may explain X-ray pulsars.

(Figure adapted from: http://violet.pha.jhu.edu/~wpb/cv_image.html Courtesy of Dana Berry and the Astronomical Visualization Laboratory at the Space Telescope Science Institute
Text from: “Opportunities in Nuclear Astrophysics: Origin of the elements”, Conclusions of a Town Meeting held at the University of Notre Dame, 7–8 June 1999)

There has been considerable progress toward understanding nuclear processes in the Cosmos. The reactions by which stars generate energy and synthesize the elements are known qualitatively, but many detailed predictions conflict with astronomical observations. Such discrepancies are not surprising, since many of the nuclear properties and reactions involved have not been measured, but have instead been extrapolated from available data or modeled theoretically. The RIA facility can address these discrepancies and will allow most of the astrophysically interesting nuclei to be produced and studied. This capability is now more important than ever since new observational, experimental and

theoretical tools are becoming available. Together, these promise to place key nuclear processes on a more solid footing than has previously been possible.

The timely nature of RIA is illustrated by the new results from space- and earth-based astronomical observatories. Several exciting new observations have a direct scientific link to nuclear astrophysics:

- The Hubble Space Telescope and large ground-based telescopes now provide greatly improved information on the element abundances produced in the primordial big bang, in the ejecta of individual explosive events, and as summed over the history of nucleosynthetic processes.
- The Compton Gamma Ray Observatory and other space observatories provide the cosmic abundances of exotic isotopes and a direct window on events near the cores of supernovae.
- Neutrino detectors provide information on reactions at the center of the Sun and on the role played by neutrinos in supernova explosions. They probe the nature of the neutrinos themselves.
- Presolar meteoritic grains formed in the ejecta of evolved stars provide the isotopic abundances of nuclei formed in individual events.
- The ROSAT X-ray telescope, the Rossi X-ray timing explorer, and most recently the new Chandra X-ray Observatory provide data on supernova ejecta, properties of X-ray bursters, X-ray pulsars, and neutron stars.

A deep understanding of these observations is only possible if one has the appropriate nuclear physics data. In the case of nova ejecta, for example, abundance measurements can tell us about the processes that take place during the nova outburst only if there are measurements (or reliable calculations) of the proton capture rates that produce the elements seen in the ejecta. In most cases, one needs nuclear reaction rates, nuclear masses, energy levels, or lifetimes for unstable nuclei that can only be reached via reactions with rare isotope beams. For such measurements, the RIA facility will provide an unparalleled arsenal of re-accelerated and fast fragmentation beams.

Other phenomena whose elucidation requires extensive new nuclear physics information obtainable at RIA include:

THE NATURE AND EVOLUTION OF SUPERNOVA EXPLOSIONS. Information on the rates of electron capture and β-decay in the hot, dense environments of stellar cores is of crucial importance. These rates affect the evolution of the stellar cores in Type II supernova explosions and (perhaps) the light curves of the Type Ia supernovae used to determine the nature of the cosmic expansion.

THE SITE OF THE R-PROCESS. About half of the heavy elements are made in the r-process, yet whether the r-process occurs in Type II supernovae, neutron star mergers, or in some other astrophysical environment is presently not known. Indeed, new abundance data for old metal-poor stars indicate that there may be more than one such site. The information on nuclei that participate in the r-process is currently not sufficient to accurately describe the

r-process and the elemental abundances it synthesizes, or to provide detailed information on the site of the r-process.

THE NATURE OF X-RAY BURSTS AND PULSARS. These events occur in binary stellar systems involving a matter-accreting neutron star. On the surface of the neutron star, hydrogen and helium burn via the rp- and αp-process powering bursts and synthesizing heavier elements that are incorporated into the crust of the neutron star and affect its observable behavior. The rp- and αp-processes proceed via proton and α-particle capture on proton-rich nuclei in combination with $\beta^+$-decays, but the rates of these processes and the masses of nuclei around the proton drip line are not known well enough to make accurate predictions of energy generation and nucleosynthesis. Electron capture rates on neutron-rich nuclei are needed to predict the composition change of the neutron star's crust in these scenarios.

THE NATURE OF NEUTRON-RICH MATTER FOUND IN NEUTRON STARS. Measurements of the isospin dependence of the nuclear compressibility will constrain the nuclear equation of state for neutron-rich matter.

THE ISOTOPIC DISTRIBUTION OF COSMIC RAYS ARRIVING AT EARTH. High-energy nuclear reaction data are needed to interpret this distribution which in turn will provide clues to the origin and generation of cosmic rays.

The opportunities for studies with fast fragmentation beams are manifold and represent a necessary complement to the direct reaction rate measurements possible with re-accelerated low energy beams. Sometimes high energy is essential for the science. For example, one can use (p,n) and (n,p)-like charge exchange reactions in inverse kinematics to determine weak interaction rates for unstable nuclei. In addition to the rates for electron capture and β decay, it should be possible to study the charged and neutral current reactions that lead to neutrino-induced breakup of abundant nuclei during supernova explosions. High-energy studies of the giant monopole and dipole resonances in very neutron-rich nuclei can determine how the nuclear incompressibility and the nuclear equation of state depend on the ratio of neutrons to protons in nuclei.

In other cases, fast fragmentation beams have a practical advantage – they make possible experiments with very weak secondary beams, simply because thick secondary targets can be used and because beam-particle identification can be done on a particle-by-particle basis. For example, the determination of nuclear deformation by Coulomb excitation or the determination of spectroscopic factors for calculations of capture rates can be carried out with beam rates of one particle per second or less. Masses, lifetimes, decay modes, and level densities are necessary for simulations of nucleosynthesis in the r-process or the rp-process; the ability to identify individual ions as they are implanted in position sensitive detectors greatly facilitates these measurements with weak beams. With fast fragmentation beams from RIA it will be possible, for example, to investigate r-process nuclei at the N = 126 neutron shell closure. Experimentally, this region has so far not been accessible, but it plays a crucial role in the synthesis of the heaviest nuclei found in nature. This is of special interest considering the possible use of heavy radioactive r-process nuclei as r-process chronometers.

Fast fragmentation beams can also be used to obtain information on low energy reaction rates that are important in many astrophysical processes. This is of importance in cases in which a direct measurement with low energy beams is not possible or direct measurements cannot be performed over the whole energy range of astrophysical interest because the cross sections are too small. If the reaction is dominated by resonances, fast beams can be used to determine resonance energies and widths. As the reaction rate depends exponentially on the resonance energy, this type of measurement may reduce the uncertainty of theoretically predicted reaction rates by orders of magnitude. In astrophysical scenarios such as the r- or the rp-process in which groups of nuclei are in equilibrium due to fast capture and photo-disintegration processes, the number and energy of all low-energy levels play an important role. Fast beam techniques involving neutron removal allow a determination of this information even for proton-unbound nuclei which play an important role in the rp-process and are too short-lived to be accessible with re-accelerated beams. Whether the reaction is non-resonant or resonant, an alternative to direct capture measurements, in some important cases, is the use of Coulomb breakup to measure the inverse reaction. The capture reaction rate can then be inferred using detailed balance. Application of this technique is limited to nuclei with a strong branch to the ground state in the capture reaction. Thick targets can be used, the inverse reaction yields a large phase space enhancement, and a beam passing a high-Z target experiences a large equivalent photon flux – these advantages make accurate measurements possible, even with low beam rates.

# 4. EXPERIMENTAL PROGRAM

This chapter illustrates experimental techniques and gives examples of specific measurements that can be performed with fast beams produced via projectile fragmentation or fission and then separated in flight. Pertinent references are given, but no attempt is made to be complete either in the number of research topics, or in the references to published work. While the material is organized according to main nuclear physics themes, the astrophysical impact of certain classes of measurements is discussed wherever appropriate and important astrophysical phenomena are highlighted in separate inserts.

## 4.1. Limits of Nuclear Existence

Many nuclei are stable against nucleon emission but unstable against radioactive decay – β-decay, electron capture, α-particle emission, or fission. The limits of nuclear stability against proton or neutron emission (the respective drip lines) remain largely unknown. For example, the neutron drip line, where nuclei become unbound against neutron emission, is only known for elements up to oxygen (Z = 8). Similarly, the largest number of protons that can be bound in a nucleus remains unknown. The quest for super-heavy elements has been a mainstay of low-energy heavy-ion research and has stimulated experiments of ever increasing sensitivity which culminated in the recent production and detection of a nucleus with Z = 118 [nin99]. Low-energy beams of neutron-rich isotopes will allow the synthesis of many new heavy isotopes and possibly even heavier elements. Fast beams, produced by projectile fragmentation or fission and then separated in flight, will be the technique of choice in exploring the most neutron-rich region of nuclear existence because they offer the advantage of very fast isotope separation and clean identification.

Fast beams from RIA offer the opportunity to reach the neutron drip line up to manganese (Z = 25) and potentially again at zirconium (Z = 40), but for heavier elements, the most neutron-rich regions of the nuclear chart will remain *terra incognita*; see Figure 2 on page 10. For these elements it is crucial to measure nuclei that are as neutron rich as possible. These data can then be used to improve models which are necessary to extrapolate toward the neutron drip line, particularly for nuclei which are important in astrophysical processes.

### Location of the Neutron Drip Line

The drip lines bound the territory of nuclei that are stable against nucleon decay. Theoretical predictions are uncertain, but suggest that 4000 to 7000 isotopes, most of them having very short half-lives, will lie within these bounds. Fewer than 300 isotopes are stable against β-decay.

The neutron drip line has been reached only up to oxygen (Z = 8) where the heaviest particle-stable isotope lies at A = 24. Figure 3 shows the results of the first experiment demonstrating that $^{26}$O is unbound [gui90]: If $^{26}$O were stable, more than 10 events should have been detected according to the cross section systematics, but not a single $^{26}$O nucleus was observed.

The properties of stable nuclei and those close to stability are the basis for extrapolations to the drip lines. Owing to Coulomb repulsion, the proton drip line lies relatively close to the valley of β-stability. As a consequence, mass predictions for nuclei close to the proton drip line are, at least for light nuclei, generally reliable. The predicted location of the neutron drip line, however, is highly uncertain, as illustrated in Figure 4 [naz99] which shows two-neutron separation energies $S_{2n}$ for the Sn isotopes calculated with some modern microscopic models. These models all describe the known data from N = 50–82 (left-hand side) rather well, but diverge for the unexplored region on the right-hand side. The drip line is uncertain by about eight neutrons. Experiments which pin down the mass and $S_{2n}$ values for the nuclei with N = 80–100 will greatly narrow the choice of viable models. Unknown nuclear deformations or as yet uncharacterized phenomena, such as the presence of neutron halos or neutron skins, make these predictions highly uncertain. Because of the inherently short lifetimes of nuclei far from the valley of β-stability, very neutron-rich nuclei must be studied by fast techniques. In-flight separation satisfies this requirement.

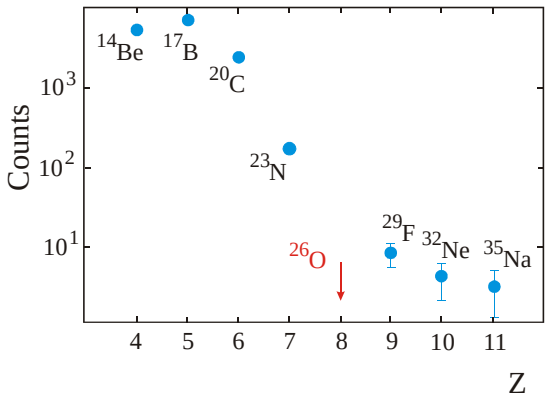


Figure 3: First evidence for the particle instability of $^{26}$O. The experiment was performed by fragmentation of a 44 MeV/nucleon $^{48}$Ca beam (adapted from [gui90]).

Since the neutron drip line lies further from the valley of stability, it is more difficult to access experimentally than the proton drip line. Fusion-evaporation reactions, commonly used to study proton-rich nuclei, cannot produce neutron-rich isotopes. However, the use of fast beams from projectile fragmentation or fission can extend studies of the neutron drip line to heavier elements. The transport time from the production target to the image of the fragment separator, where each ion is identified, is typically less than 1 μs – small compared to the shortest β-decay half-lives (≥ 1 ms). Hence, decay losses are negligible. Intensities of one particle per day are sufficient to establish the existence of an isotope.

The Coupled Cyclotron Facility at the NSCL is expected to double the number of elements that can be observed all the way out to the neutron drip line; sulfur (Z = 16) isotopes with masses around 50 will be detected. Depending on the model used, fast beams at RIA will be able to establish the drip line up to Z ≈ 25 (see Figure 2 on page 10) and may reach it again at Z = 40. The simple observation or non-observation of these extremely neutron-rich nuclei is crucial for evaluating and improving the predictive power of different mass models. The knowledge of nuclear binding energies far from stability (but inside the drip line) is crucial for an understanding of the astrophysical r-process (see page 54). Important parts of the r-process path will be available for study at RIA.

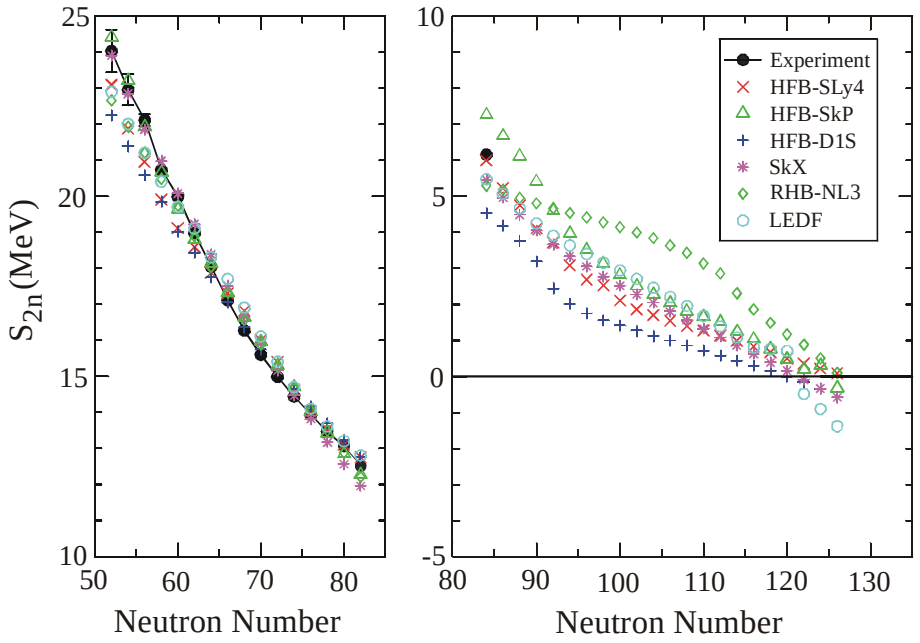


Figure 4: Predictions by six different microscopic models for the two-neutron separation energies of even-even Sn isotopes out to the drip line (adapted from Figs. 2 and 4 in [naz99]). The drop of ~7 MeV from the last point of the left-hand side to the first point of the right-hand side is due to the shell closure at N = 82. The references to the models are: HFB-SLy4 [cha97a], HFB-SkP [dob84], HFB-D1S [dec80], SkX (HF+BCS) [bro98a], RHB-NL3 [lal97], and LEDF [fay98].

## Neutron-Unbound States Near the Neutron Drip Line

Near the neutron drip line, sequences of odd-N isotopes are encountered that are neutron-unbound while the next heavier even-N isotope is neutron-bound, see Figure 2 on page 10. Investigations of these neutron-unbound nuclei can provide important insight into the nucleon-nucleus interaction far from stability and a better understanding of coupling to the continuum in neutron-rich systems and of the delicate structure of multi-nucleon halos or skins. The wavefunctions of these even-N nuclei are poorly known, and studies of adjacent neutron-unbound (odd-N) systems can yield single-particle information crucial to their characterization. Far from stability, neutron-unbound nuclei must be investigated via neutron-nucleus coincidence experiments. Fast beams have been proven to be particularly advantageous for such studies. In favorable cases, it is even possible to investigate the properties of isotopes beyond the drip line.

Studies of neutron-unbound ground states of nuclei far from stability have been performed only for light elements. The light nuclei of the N = 7 isotones, $^{10}$Li and $^{9}$He, are neutron unbound and have been studied with various methods: pion-induced double charge exchange [set87], multi-nucleon transfer reactions using stable beams [boh88, boh93, you93, cag99], and observations of final-state interactions in breakup reactions [kry93,

tho99, che00]. The measured Z-dependence of the energies for the low-lying spin ½ states for all N = 7 isotones is shown in Figure 29 on page 58, where single-particle properties are discussed in more detail.

Stable beams are not suited for studying low-lying unbound neutron states of heavier nuclei far from stability because of the large number of fragments and neutrons produced in the required reactions. These states are better produced and studied by breakup or, still better, by neutron or proton knockout from neighboring rare isotopes. Thus, far from stability, fast beams become the tool of choice. Typically, a neutron and a single charged fragment must be detected with good precision to allow reconstruction of the energies of the decaying states from the measured energies and angles of the decay products. Just as for normal transfer reactions, different channels offer complementary information, and both proton and neutron removal reactions are interesting and necessary.

For the example of $^{10}$Li, the resonance-like structure in the unbound two-body system has provided important information about the neutron-core interaction that is key to the understanding of the two-neutron halo of $^{11}$Li. As discussed in Section 4.2 on page 33, the theoretical treatment of this Borromean nucleus in a three-body picture requires knowledge of the interactions in both two-body subsystems (n-n and n-$^{9}$Li), and in particular the n-$^{9}$Li interactions in the $l$ = 0 and 1 channels. The left side of Figure 5 shows the relative velocity spectra of $^{9}$Li + n measured in breakup reactions with three different projectiles, $^{10,11,12}$Be [che00]. The data are normalized to the same number of incoming particles and clearly demonstrate that neutrons from the target make negligible contributions. Since the projectile $^{10}$Be cannot give rise to $^{9}$Li + n in a simple breakup picture, the small number of counts for this reaction confirms the selectivity of the experiment. The difference between the $^{9}$Li + n spectra for the $^{11}$Be and $^{12}$Be projectiles reflects the different population and binding of the valence neutrons. The narrow single peak in both spectra is due to the final

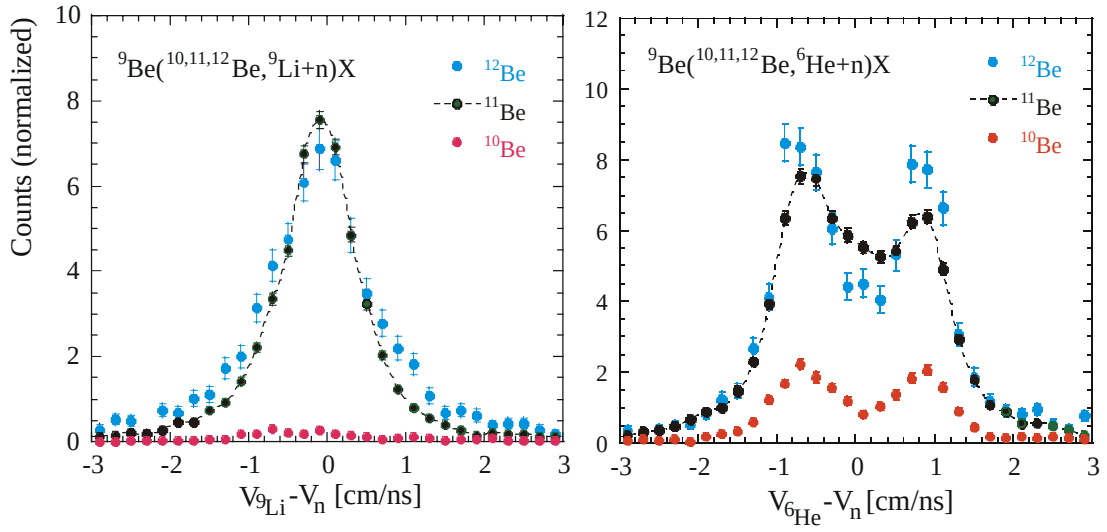


Figure 5: Relative velocity spectra of $^{9}$Li and an associated fast neutron (left) and the same for $^{6}$He (right). The difference in shapes reveals the dominant *s*- and *p*-wave nature, respectively, of the interaction in the two cases [che00].

state interaction corresponding to a very low decay energy, and it identifies the $^{10}$Li ground state as $l = 0$. A fit to the line shape yields an *s*-wave scattering length $a_S < -20$ fm and an excitation energy less than 50 keV above the $^{9}$Li + n threshold [tho99, che00].

For comparison, the right side of Figure 5 shows the decay of $^{7}$He which has an $l = 1$ ground state. The relative velocity spectra for $^{6}$He + n are shown for the reactions $^{9}$Be($^{10,11,12}$Be, $^{6}$He+n)X. The yield for $^{10}$Be $\rightarrow$ $^{6}$He + n is strongly suppressed because the breakup of $^{10}$Be is dominated by the decay to $^{6}$He and an α-particle. Again, the differences between $^{11}$Be and $^{12}$Be indicate the influence of the initial states, which has to be taken into account in the analysis. The overall shape with the minimum at zero relative velocity is consistent with the $l = 1$ ground state of $^{7}$He and determines the energy of the resonance as 440 ± 10 keV, in agreement with a previous measurement. Other work [kor99] using the pickup reaction p($^{8}$He, $^{6}$He+n)d has found evidence for an excited level at 2.9 MeV in $^{7}$He.

Recently, evidence for other unbound nuclei with $l = 0$ ground states have been found in relative velocity measurements. The line shape of the reaction $^{9}$Be($^{11}$Be, $^{8}$He+n)X indicates a dominant *s*-wave interaction in $^{9}$He corresponding to a level below 200 keV [che00], and a new experiment with $^{13}$Be has succeeded in crossing the neutron drip line for N = 9 [tho00]. Cases for N = 11 and beyond should come within reach at the NSCL Coupled Cyclotron Facility. The previously-mentioned many-body halos in heavier systems will depend critically on an understanding of the continuum states (resonances) of neighbouring unbound nuclei, and thus, the extension of these experiments to heavier drip-line nuclei is crucial. Beam intensities of $10^3$ particles/s are necessary, and nuclei up to magnesium (with N ~ 26) will be accessible with fast fragmentation beams from RIA. It is in principle possible to extend the techniques to nuclei in the three-body continuum. In this regard see the theoretical work [dan98] and also experiments [kor94] reporting a resonance interpreted as the ground state of $^{10}$He, unstable against the decay into $^{8}$He and two neutrons.

## Mass Measurements

The experimental proof of the existence of an isotope is of particular relevance for nuclei near the drip line where the nucleon separation energies are very small, and small effects determine whether a nucleus is stable against nucleon emission or not. At a more quantitative level, the mass (or binding energy) of an isotope is the most basic nuclear property of interest. While knowledge of the location of the drip lines can help to improve nuclear mass models, the masses themselves provide more important constraints not limited to nuclei near the drip lines. The identification of the general features of nuclear binding energies provided an early stimulus for the development of nuclear models. Precision mass measurements can provide important first indications of new regions of deformation or shell closures.

Existing models are well tuned to reproducing the masses of known nuclei, but predictions of binding energies far from the line of stability are distressingly uncertain. The variation among the predictions of several mass models was indicated in Figure 4 by the discordant positions of the neutron drip lines. Similarly, the theoretical predictions of the nuclear

masses very far from stability vary significantly, as illustrated in Figure 6 for xenon isotopes. Far from stability, the Figure shows the differences between the extended Thomas-Fermi model (ETFSI, purple) [abo95] and three other models: the extended Thomas-Fermi model with shell quenching (ETFSI-Q, blue) [pea96], the finite range droplet model (FRDM, green) [moe95], and the relativistic mean field model with the NL3 interaction (RMF-NL3, black) [lal99]. These differences underscore the limitations of existing nuclear models. Most of the models reproduce the experimentally known masses (red) within about 1 MeV, but their predictions diverge for more neutron-rich nuclei, where no experimental data are available. Mass measurements of nuclei far from stability are clearly needed.

For nuclei of sufficiently long lifetime (≥ 1 s), a number of precision techniques, most notably Penning ion trapping, have allowed accurate mass measurements to be made of nuclei essentially at rest in the laboratory. These measurements become increasingly difficult for shorter-lived nuclei produced at low rates. In such cases, time-of-flight measurements with fast beams from RIA will allow an extension of the reach of mass determinations 2–3 neutrons further from stability.

Mass measurements with fast beams can be performed with Schottky spectrometry in a storage ring [rad97]. Alternatively, one can combine high-resolution time-of-flight measurements and accurate momentum measurements in a spectrometer. This very fast and

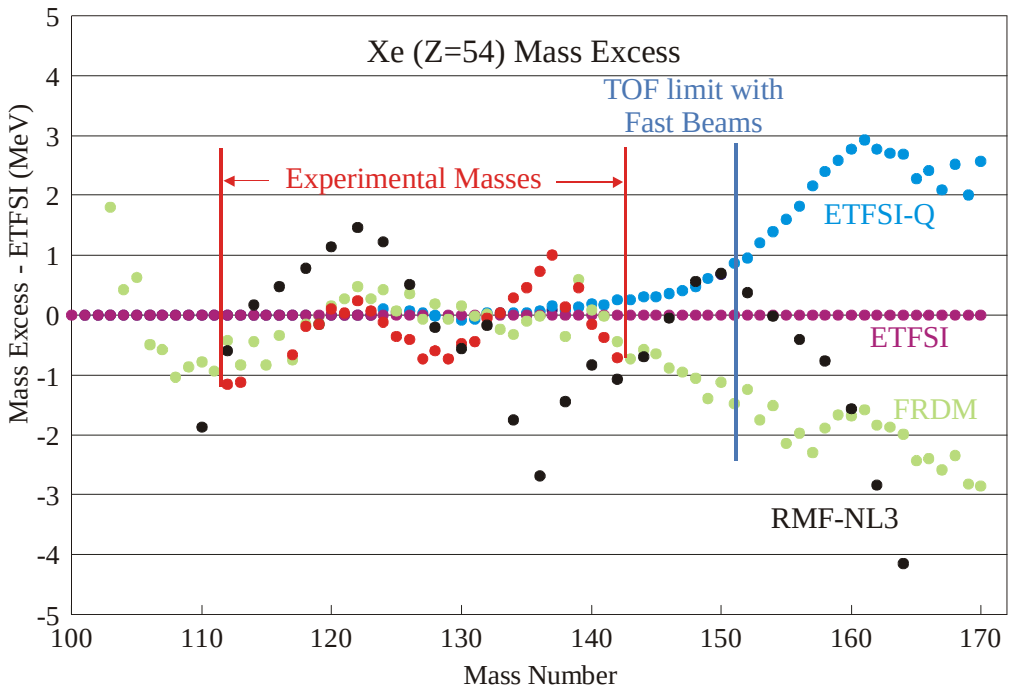


Figure 6: Differences between mass excesses predicted by the extended Thomas-Fermi model (ETFSI, purple) and measured masses (red) plus three other models: an extended Thomas-Fermi model with shell quenching (ETFSI-Q, blue), the finite range droplet model (FRDM, green), and the relativistic mean field model with the NL3 interaction (RMF-NL3, black) [man99].

direct method was advanced at GANIL [orr91] and requires a relatively long flight path to a high-resolution spectrometer. The technique has no significant lifetime limitation and can be employed down to intensities of 0.01 particle/s. With 1000 measured particles, uncertainties of the order of $3 \cdot 10^{-6}$ or 300 keV for $A \approx 100$ can be achieved. Since the mass predictions diverge to the level of 2.0–2.5 MeV at the limits of the experimentally accessible region shown in Figure 6, measurements at this level of accuracy will provide significant constraints.

For xenon isotopes, the limit ($A \approx 150$) for mass determinations with fast beams from RIA is indicated in Figure 6 – the astrophysical r-process path nuclei near $^{148}$Xe are within reach. Mass measurements with fast beams at RIA will be of particular astrophysical import because they can determine the masses of most of the important r-process nuclei between molybdenum and rhenium. Knowledge of these masses may help resolve one of the most vexing deficiencies of current r-process models: The use of present theoretical mass predictions for these nuclei in r-process nucleosynthesis calculations leads to a significant underproduction of $A \approx 120$–130 nuclei as compared to the measured r-process abundances. The reason for this large discrepancy is currently not understood. (See the discussion of shell quenching on page 56.)

Fast beams at RIA will also allow measurements of ground-state masses of proton-unbound nuclei important for the rp-process. These resonance states are so short lived that their masses cannot be determined by direct in-flight techniques. These mass measurements are discussed in the next section.

## Exploring the Proton Drip Line

Nuclei near the proton drip line are more readily produced than nuclei near the neutron drip line. This is due to the closer proximity of the proton drip line to the line of stability and to the curvature of the line of stability, which makes it easier to reach proton-rich nuclei by heavy-ion induced fusion-evaporation reactions. It is thus not surprising that much more is known about the proton drip line than about the neutron drip line. However, the study of the proton drip line is still interesting because it is possible to detect nuclei beyond the drip line. The Coulomb barrier increases the lifetime of nuclei which are only slightly proton unbound. These nuclei decay by tunneling of the unbound proton through the Coulomb barrier. If these nuclei are non-spherical, they provide interesting examples of quantum-mechanical tunneling through a deformed barrier [dav98]. Perhaps the most important aspect of nuclei near the proton drip line is their preeminent role in the astrophysical rp-process.

The properties of odd-Z nuclei along the proton drip line up to tin and possibly beyond are important for the understanding of the rp-process in X-ray bursters (see page 27) and X-ray pulsars (page 30). For rp-process calculations the mere knowledge of the location of the proton drip line is not sufficient: detailed properties of the nuclei at and just beyond the proton drip line are needed. For example, the time scale of the rp-process and therefore the observable time-dependence of X-ray bursts [sch98a, koi99] depend sensitively on the

## X-Ray Bursters

X-ray bursts are thought to result from thermonuclear runaways in the hydrogen-rich envelope of an accreting neutron star. Low accretion rates favor a sudden local ignition of the material with a subsequent rapid spread over the neutron star surface. Ignition of the triple-α reaction and breakout reactions from the hot CNO cycles trigger a thermonuclear runaway driven by the αp- and the rp-process. The αp-process is a sequence of (α,p) and (p,γ) reactions that convert the $^{14}$O and $^{18}$Ne ashes of the hot CNO cycles to isotopes in the $^{34}$Ar to $^{38}$Ca range. The rp-process is a sequence of rapid proton captures leading to the proton drip line, followed by β-decays of drip line nuclei that convert material from the Ar to Ca range into $^{56}$Ni.

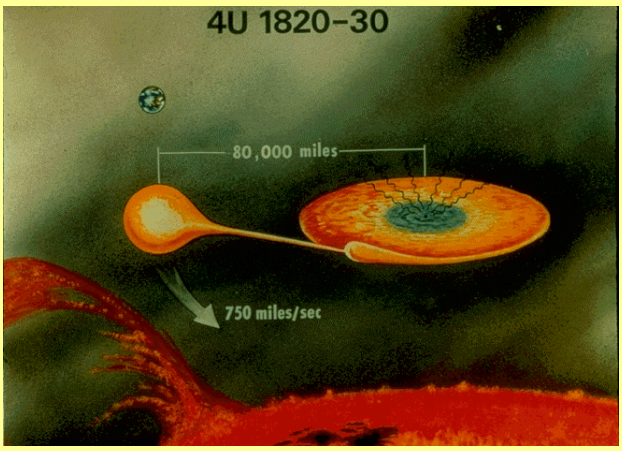


The runaway freezes out in thermal equilibrium at peak temperatures of around 2.0 to 3.0 billion Kelvin. Re-ignition takes place during the subsequent cooling phase of the explosion via the rp-process beyond $^{56}$Ni. The nucleo-synthesis in the cooling phase of the burst considerably alters the abundance distribution in the atmosphere, the ocean, and subsequently the crust of the neutron star. This may have a significant impact on the thermal structure of the neutron star surface and on the evolution of oscillations (waves) in the oceans.

Nuclear reaction and structure studies on the neutron deficient side of the valley of stability are essential for an understanding of these processes. Measurements of the breakout reactions will set stringent limits on the ignition conditions for the thermonuclear runaway; measurements of α-particle and proton capture on neutron deficient radioactive nuclei below $^{56}$Ni will set limits on the time scale for the runaway itself and on the hydrogen-to-seed ratio for the rp-process beyond $^{56}$Ni. Nuclear structure and nuclear reaction measurements near the double closed shell nucleus $^{56}$Ni determine the conditions for the re-ignition of the burst in its cooling phase. Information beyond $^{56}$Ni, especially in the Ge to Kr mass region, is needed to determine the final fate of the neutron star crust. The nuclear structure information needed to calculate the flow of nuclear reactions in X-ray bursts and the time dependence of the energy generation includes masses, β-decay lifetimes (also needed for isomeric or thermally populated excited states), level positions, and proton separation energies, especially in the Ge to Kr mass region. The rates of two-proton capture reactions that may bridge the drip line at waiting points are of special importance.

(Figure adapted from: http://heasarc.gsfc.nasa.gov/Images/exosat/slide_gifs/exosat18.gif
Text from: “Opportunities in Nuclear Astrophysics: Origin of the elements”)

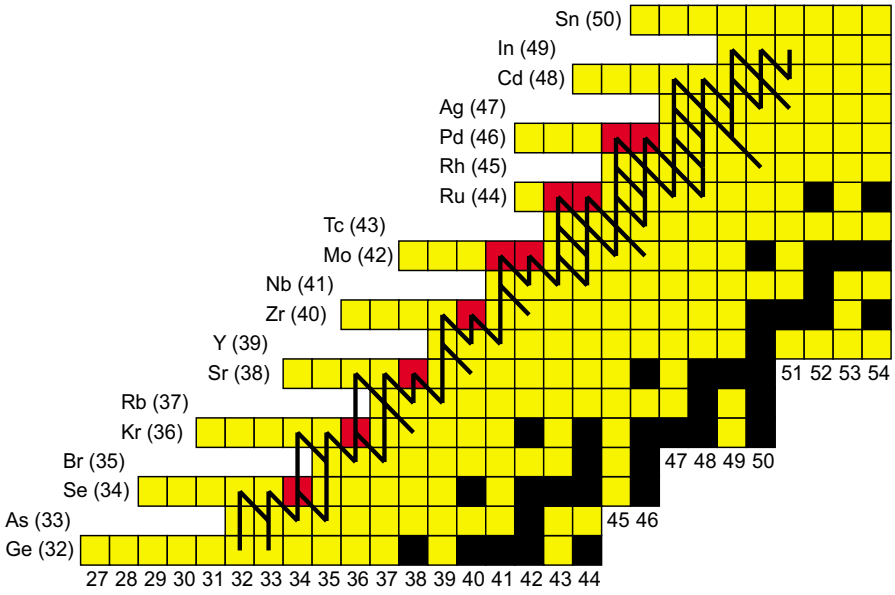


Figure 7: rp-process path predicted by network calculations. The waiting points are indicated in red, other proton-bound nuclei in yellow. Adapted from [sch98a].

masses of nuclei around the proton drip line above nickel. This has become important recently because a quantitative understanding of the origin of burst tails can provide a way to distinguish between pure helium burning and mixed hydrogen and helium burning in X-ray bursters. This distinction will give new insight on the accretion-rate dependence of nuclear burning and on how the accreted hydrogen and helium are distributed over the surface of the rapidly rotating neutron star [bil00].

Among the most important nuclei are the odd-Z nuclei between nickel and tin which lie just beyond the proton drip line. These nuclei are the intermediate steps in two-proton capture reactions [gor95, sch98a] that can bridge some of the long-lived waiting-point nuclei and accelerate the rp-process (Figure 7). What is needed are ground state masses and proton capture rates for these nuclei. In the rp-process these nuclei are in an equilibrium maintained by proton capture and proton decay. The equilibrium conditions are given by partition functions, which can be calculated from the energies and spins of all low lying excited states up to a few hundred keV. Most of the relevant nuclei have lifetimes below 10–100 ns, which are too short to be studied in traditional proton-radioactive decay experiments. The needed information can, however, be obtained using fast beam techniques described below. The techniques will complement reaction studies on longer-lived proton-radioactive nuclei that can be performed with re-accelerated beams.

The exploration of the proton drip line can be divided into three mass regions: $Z \leq 50$, $50 < Z \leq 83$, and $Z > 83$. Nuclei along the proton drip line in the lightest mass region have not been thoroughly explored because they do not decay by long-lived proton or $\alpha$-emission. The experiments concentrate on existence measurements [moh91, jan99] and $\beta$-delayed proton emission studies [muk98]. In addition, nuclei lighter than magnesium have been

studied using for example invariant mass measurements [kry95] transfer reactions [lep98] and elastic resonance scattering [axe96].

Recently, some exciting results in this mass region have been obtained with exotic beams delivered at fragmentation facilities [sum97, jan99, wef99], especially the observation of the doubly-magic nuclei $^{48}$Ni and $^{100}$Sn and their nearest neighbors. Figure 8 shows the first identified events of the doubly-magic proton-rich nucleus $^{48}$Ni. They were produced at GANIL by fragmentation of $^{58}$Ni [bla00].

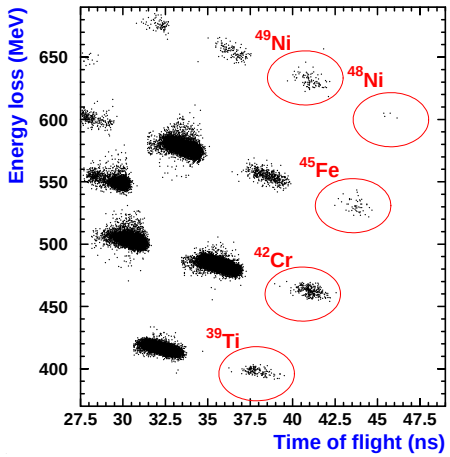


Figure 8: First observation of the doubly-magic nucleus $^{48}$Ni [bla00].

Odd-Z isotopes of nuclei beyond the proton drip line between tin (Z = 50) and bismuth (Z = 83) have been studied quite extensively by detecting decay protons [woo97, dav96]. Since these proton emitters are located several mass units beyond the proton drip line, they cannot give the exact position of the drip line or the exact binding energies in its vicinity, both of which are important for the rp-process. Recent measurements at GSI for proton-rich nuclei between Z = 60 and 84 have begun to fill in some of that information by providing mass data for the end points of α-decay chains leading beyond the proton drip line [rad97].

The heaviest mass region (Z > 83) is currently inaccessible because the fusion-fission cross section near the proton drip line is too high for proton decay to compete. Fragmentation reactions with high-intensity beams offer an alternative approach to probe this region of ground state proton radioactivity [sch99a]. In addition, fragmentation experiments will also contribute to the intermediate regions ($50 < Z \leq 83$) in cases where the high rate of fusion reaction products with the same A as the nucleus of interest limits fusion-evaporation reactions to a sensitivity of $\sigma \sim 1$ nb. The proposed RIA fragmentation facility would allow the comprehensive mapping of the proton drip line for odd-Z nuclei with the identification of all ground-state proton emitters up to Z = 93.

In the lighter mass region fast beams from fragmentation reactions will also be able to contribute to the exploration of the drip line by measuring properties of very short-lived proton-unbound nuclei.

Ground-state Q-values and energies of some excited levels of very short-lived proton emitters can be studied with neutron removal or (p,d) transfer reactions in inverse kinematics. The Q-values and the energies of the excited states can be kinematically reconstructed from the energies and angles of the decay products. Accuracies of ~20 keV or better can be achieved with improved detection systems. Figure 9 shows an example of a reconstructed invariant mass spectrum measured with an exotic beam produced in fragmentation. The $5/2^+$,$3/2^-$ doublet of $^{13}$N was populated in a one-neutron transfer reaction using a $^{12}$N beam [azh98].

## X-Ray Pulsars

X-ray pulsars are usually described as accreting neutron stars with high accretion rates. This leads to steady burning of the accreted material via the αp- and the rp-process on the surface of the neutron star. Detailed studies of the nucleosynthesis suggest that the accreted material is rapidly converted to heavier elements in the mass 80 to 100 range. This drastically changes the composition of the crust and the ocean of the neutron star; the original iron crust is replaced by a mixture of significantly more massive elements. As a result, the composition of the neutron star crust in a binary system is substantially different from that in an isolated neutron star. This composition change may have important effects on the thermal and electromagnetic conditions at the neutron star surface, and will affect the observed decay of the magnetic field of neutron stars. It will also change the sequence of electron captures in the deeper crust, which may affect the emission of gravitational radiation from the neutron star surface.

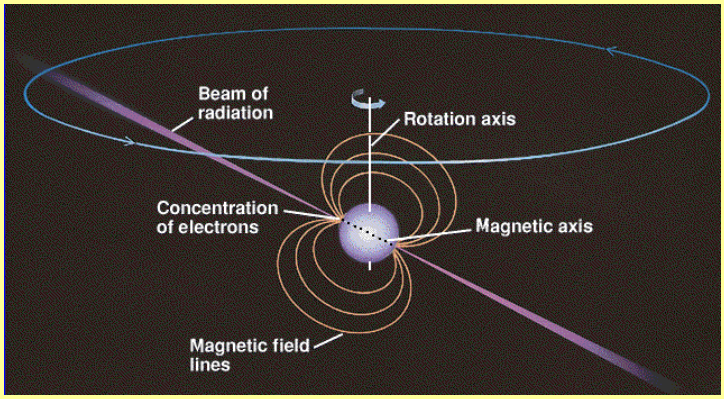


The final composition of the crust depends strongly on the nuclear physics associated with the rp-process and on the endpoint of the rp-process, which itself is directly correlated with the accretion rate. For experimental confirmation in the lower mass range, studies similar to those for the X-ray burst simulations are required. However, for large accretion rates the endpoint of the rp-process is expected to lie in the mass 150 range. This requires a new range of nuclear structure data near the limits of stability.

Of particular interest are β-decay lifetimes, and especially β-delayed proton and β-delayed α-particle decays. If these processes dominate, as is expected for the decay of very neutron deficient tellurium, iodine, and xenon isotopes, one reaches a natural halting point for the rp-process.

(Figure adapted from:
http://www.physics.fsu.edu/courses/fall98/ast1002/section4/neutronstars/pulsar/pulsar1.htm
Text from: “Opportunities in Nuclear Astrophysics: Origin of the elements”)

With the availability of intense fast beams from RIA it will be possible to extend these measurements for all of the proton unbound odd-Z nuclei that are important in the rp-process from $^{69}$Br up to $^{89}$Rh. In some cases, the high rates at RIA will allow one to extract information about level spins from angular distribution measurements. For example, the predicted fast beam intensity for $^{70}$Br is $8{\cdot}10^{7}$ particles/s, and fast beams with more than $10^{4}$ particles/s, which is a sufficient intensity, will be available for all odd Z, N = Z nuclei up to $^{90}$Rh.

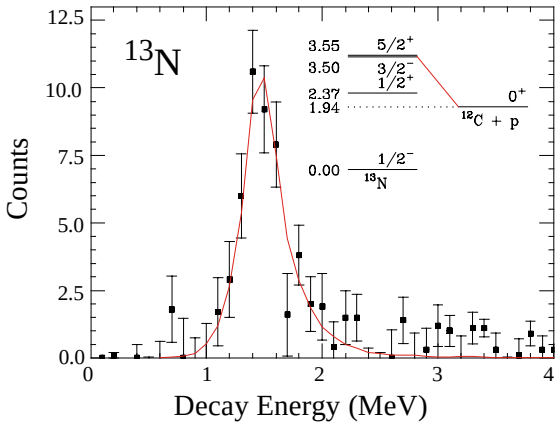


Figure 9: Invariant mass spectrum for $^{13}$N following neutron pickup by $^{12}$N projectiles from a fast fragmentation beam, adapted from [azh98].

Some of the proton capture rates important for the rp-process can be measured directly with re-accelerated beams, but capture on very short-lived proton-unbound nuclei are not accessible with this technique. They can, however, be determined by measuring the rate for the inverse process via Coulomb breakup of fast beams. The feasibility of such experiments has been demonstrated with the population and decay of excited states in $^{17}$Ne following its Coulomb excitation by a heavy target nucleus. The reaction $^{17}$Ne($\gamma$,2p)$^{15}$O could also be used to investigate the intermediary $^{16}$F(p,$\gamma$)$^{17}$Ne reaction. This reaction had been suggested as a possible breakout reaction from the hot CNO cycle, but the rate turned out to be too low to compete with the $^{15}$O($\alpha$,$\gamma$)$^{19}$Ne reaction [gor95]. With the intensities of fast beams at RIA it will be possible to determine the two-proton capture rates on nuclei between nickel and tin. For example, the proton capture rate on $^{69}$Br, which determines the rate of the two-proton capture reaction $^{68}$Se(2p,$\gamma$)$^{70}$Kr, could be explored using the reaction $^{70}$Kr($\gamma$,2p)$^{68}$Se. RIA is predicted to produce about $4{\cdot}10^{4}$ $^{70}$Kr nuclei/s, sufficient for Coulomb breakup measurements.

## Two-Proton Radioactivity

For years, ground-state two-proton radioactivity has been predicted to exist [gol60] for even-Z nuclei. It would be capable of providing a unique test of two-valence-proton wave functions and the proton-proton pairing interaction. Yet, this unusual decay mode has eluded experimental verification.

Traditional searches for long-lived ($T_{1/2} \geq 10$ μs) two-proton emitters have not been successful. Sequential emission of two protons has been observed following β-decay but no 2p-decay has been clearly identified [det91, muk98]. In these experiments, the proton-rich candidates were implanted in silicon detectors to observe their decay. The searches were concentrated on the medium-mass region where Coulomb and angular momentum barriers could potentially be large enough to allow for long lifetimes.

RIA offers the prospect of comprehensively mapping and studying the proton drip line. The search for lighter, very short-lived two-proton emitters can be pursued most efficiently with fast beams. In this technique, the potential two-proton emitter is produced via a transfer reaction and decays immediately in-flight. The strong forward focusing will allow efficient coincidence detection of all the three decay products (one fragment and two protons). The invariant mass of the system can then be reconstructed from the measured energies and angles of the three particles. For illustration, Figure 10 shows preliminary evidence for the observation of the direct two-proton emission from the first excited state of $^{17}$Ne [chr99]. This method is not limited to light nuclei and can be used to explore the drip line up to the mass region where the traditional searches for longer-lived two-proton emitters can be performed. With the intensities of RIA it will be possible to determine if two-proton emitters exist and, if so, to study their properties. Beam intensities of ~$10^4$ particles/s are sufficient for the studies of very short-lived two-proton emitters with fast beams.

RIA would also provide access to regions of much heavier even-Z nuclei which have longer lifetimes and which can be studied using the traditional implementation techniques. Up to now, the drip line for even-Z nuclei has been mapped only up to Z = 28 ($^{48}$Ni) and in heavier nuclei two-proton radioactivity should be a relatively common phenomenon. As with one-proton radioactivity, the higher Coulomb barrier in high-Z nuclei reduces the sensitivity of the tunneling rate to the decay energy such that most of these elements should have one isotope that is two-proton radioactive. It is notable that two-proton radioactivity should occur closer to stability than one-proton radioactivity in even-Z nuclei, although in many cases the system may be slightly one-proton unbound. These nuclei will allow true probes of the two-proton decay mechanism rather than sequential emission. For example $^{103}$Te, long predicted to decay by two-proton emission, could be produced with an intensity of 0.1 particles/s by fragmenting beams at RIA. Since implantation decay methods for the study of proton emitters can be performed with intensities as low as one particle per 10 hours (~$3\cdot10^{-5}$ particles/s), remarkable progress can thus be expected.

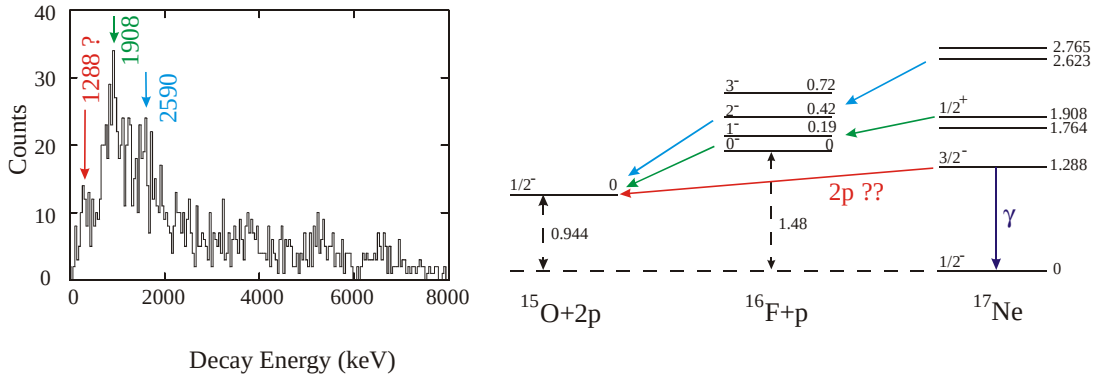


Figure 10: Decay energy spectrum of $^{17}$Ne. Expected contributions from excited states in $^{17}$Ne are marked by arrows and labeled by their excitation energies. Pertinent energy levels in the mass 17 system are shown on the right hand side. The first peak in the spectrum, at ~300 keV, could potentially correspond to the direct two-proton decay to $^{15}$O. Adapted from [chr99].

## 4.2. Extended and Unusual Distributions of Neutron Matter

### Nuclear Halos and Skins

Nuclei close to the neutron drip line can have properties dramatically different from those found near the line of stability. When the last few neutrons are weakly bound quantum mechanics allows them to penetrate far beyond the nuclear core, where it is outside the influence of the short-range attraction of the nuclear potential well. The result is that the nucleus develops a diffuse halo with one or a few neutrons distributed over a large volume.

The halos offer interesting analogies to other loosely bound structures encountered in atomic, molecular, and particle physics. These systems have in common with nuclear halos that they are bound by short-range forces which are weak and attractive. Certain molecules with large electric dipole moments can form the core of halo-like negative ions. It has been found experimentally that the electron is bound in an orbital as large as $10^{-6}$ cm in radius and with a binding energy of the order of a milli-electron volt [des94]. Another example is the hypertriton, which consists of a proton, a neutron and a $\Lambda$-particle. The $\Lambda$-particle is very weakly bound, and it may be viewed as circling the remainder (a deuteron) at a distance of the order of 20 fm [boh70]. With the advances of the techniques to study rare processes in nuclear physics, nuclear halos will often offer the best experimental opportunities for studying marginally bound quantum systems.

Because of their simplicity, halos can serve as test cases for developing new approaches in nuclear studies that can be extended to general nuclear systems. For example, the use of knockout reactions (discussed below) for identifying single-particle structures were initially thought to be specific to halos, but the technique has been shown to work also for deeply bound core states.

Another interesting feature of neutron-rich or proton-rich nuclei arises when the neutron and proton Fermi levels are very different. For such nuclei the proton and neutron density distributions may have a different radial extent, i.e., these nuclei may have a pronounced neutron (or proton) skin. For very neutron-rich nuclei these skins may be more than one Fermi thick.

In the following, we will focus on the discussion of nuclear halos for which many assumptions of traditional nuclear models must be questioned. Nuclei with pronounced neutron skins, however, may be appropriately described by mean field models. These nuclei will be discussed further in Sections 4.4 and 4.5, that discuss nuclear collective modes and excitations and the evolution of nuclear structure.

The most weakly bound nucleus studied so far is the two-neutron halo nucleus $^{11}$Li. The wave function for its last two neutrons has a root-mean-square (RMS) radius as large as the RMS radius of $^{208}$Pb; the probability of finding the valence nucleons outside the volume of a normal mass-11 system is greater than 80%. Even more interesting multi-nucleon halo nuclei may be produced and studied at RIA, opening up the unique prospect of exploring the quantum many-body problem in a completely new regime. For example, if $^{38}$Ne is

bound, it may consist of a core and a halo with eight neutrons and thus provide the chance to study the interaction of many neutrons in a diffuse, nearly proton-free environment.

At this stage one can only speculate about which nuclear models will be most appropriate for the description of halo nuclei. Three-body models have been used for the description of light two-neutron halo nuclei, but it is by no means clear that this is the most effective approach. Alternatively, the shell model has been rather successful in describing some of the observed properties of light halo nuclei. For the description of heavier nuclei with more complex halos, the effective interactions between the valence nucleons must be known accurately and incorporated appropriately. It is, however, quite likely that the expected strong coupling of the halo wave function to the particle-unbound continuum may eventually require the development of entirely different strategies than typically pursued in models of nuclei close to the valley of stability.

A nuclear halo was first identified in the case of $^{11}$Be [mil83] and soon after was detected as a more general phenomenon in measurements of interaction cross sections with radioactive beams [tan85]. Neutron and proton halos have since been encountered in a number of light nuclei and have attracted much interest in recent years [aus95, han95]. $^{11}$Be which has one weakly bound neutron is one of the simplest examples of a halo nucleus. In the extreme halo picture, $^{11}$Be is described as a $^{10}$Be core and an extended one-neutron wave function that does not affect the core. Experimental evidence suggests that this picture is mostly correct.

One of the most striking experimental manifestations of halos is their large cross section (with essentially single particle strength) for Coulomb dissociation on heavy targets via electric dipole transitions. Figure 11 compares the experimental cross sections for the ($^{11}$Be,$^{10}$Be) one-neutron removal reaction on targets of Be, Ti, and Au with calculations based on an extreme single-particle model combined with a simplified reaction theory [ann94]. A more realistic treatment of the reactions has been presented in [hen96]. The inclusion of a spectroscopic factor of about 0.8 [aum99] would further improve the agreement with the data. The conclusion offered from this and other experiments on Coulomb dissociation is that the dominant single-particle state associated with the neutron halo is decoupled from the giant resonance, which normally makes the E1 strengths at low energies extremely small. Or, in other words, the core-halo picture of $^{11}$Be is to a large extent justified.

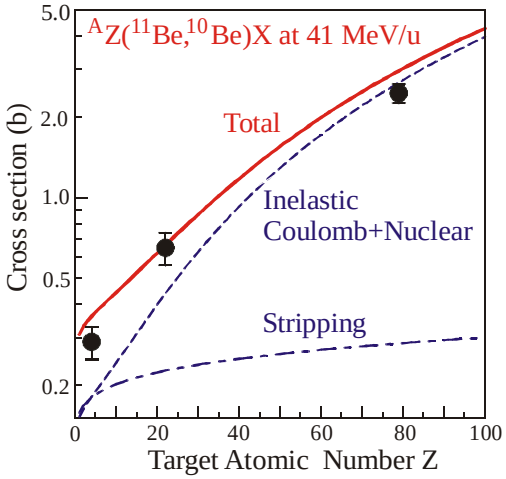


Figure 11: The one-neutron-removal cross sections for ($^{11}$Be,$^{10}$Be) on Be, Ti, and Au targets compared with simple theoretical estimates [ann94]. The strong Z dependence results from Coulomb dissociation of the halo characteristic of the $^{11}$Be ground state.

Other evidence for the halo nature of nuclei comes from the narrow momentum

distribution of the projectile residues in one-neutron removal reactions, as shown in Figure 12. Plotted are the relative probabilities of detecting the core after a halo nucleon removal as a function of core momentum along the beam direction. The distributions are sensitive to the wave function of the removed nucleon. A narrow distribution indicates a large spatial extent and is sensitive to the *l*-value of the removed nucleon. Results quite similar to those shown in Figure 12 were obtained for $^{11}$Be [aum99]. These distributions may be viewed qualitatively as a direct consequence of the Heisenberg uncertainty principle linking large sizes to narrow distributions of the momentum. The reaction calculations for $l = 0, 2$ clearly prove the $l = 0$ assignment and also reproduce the magnitude of the cross sections.

The large breakup cross sections and the sensitivity of knockout reactions to the halo structure provide a way to study the properties of halo nuclei even when they are produced at very low rates. The measurements discussed thus far can be performed with beam intensities as low as 0.01 particles/s. As an example of the sensitivity of knockout reactions, we show in the left panel of Figure 12 the momentum distribution for $^{19}$C, which has been identified as a new case of a halo nucleus [nak99, mad99]. The spin parity assignment, which was not known, is determined to be $1/2^+$, and the neutron separation energy, which has been inferred from coincidence data, is 0.6 MeV, comparable to that of $^{11}$Be. The intensity of the incident beam of $^{19}$C was of the order of one particle per second. Note that the measurements definitely exclude an $l = 2$ assignment, the other likely candidate in this region.

Proton halos are also possible, but owing to the strong influence of the Coulomb barrier they occur only in light elements ($Z \leq 20$), and they are less diffuse than neutron halos. Experimental evidence indicates that they are present in states such as the $l = 0$ first excited

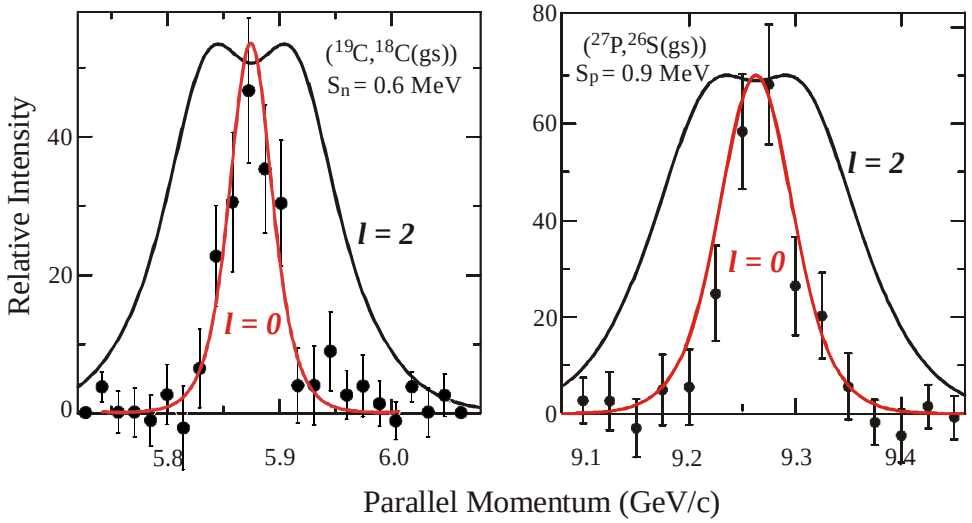


Figure 12: (Left) Parallel-momentum distribution of the charged fragment in the reaction $^{9}$Be($^{19}$C,$^{18}$C(gs))X. (Right) The same for the reaction $^{9}$Be($^{27}$P,$^{26}$Si(gs))X. (Adapted from [mad99] and [nav98]). Coincidences with γ rays were used to correct the data for broader components associated with excited levels contributing more than 50% of the cross section.

state of $^{17}$F and the $l$ = 1 ground state of $^{8}$B. The most developed halos are $s$ states ($l$ = 0), and the best candidates of this kind have turned out to be the proton-rich phosphorus isotopes $^{26,27,28}$P [bro96]. A recent experiment has shown that the odd valence protons of these three nuclei are in $1s_{½}$ states with spectroscopic factors of about 0.5, in good agreement with theory [nav98]. Owing to the relatively high charge of the silicon core (Z = 14), the halo character is not very pronounced. The right panel in Figure 12 [nav98] proves the $1/2^{+}$ assignment to $^{27}$P, which agrees with that of the mirror nucleus $^{27}$Mg.

Perhaps the most interesting halo states are those in which there are two or more neutrons in the halo. For these cases standard nuclear models may fail, as the interaction between the nucleons in the diffuse halo region, which is not included in traditional mean field models, will be important. It is immediately striking that the particle-stable most neutron-rich light nuclei all have an even number of neutrons. For example, the even-N nuclei $^{6,8}$He, $^{9,11}$Li, $^{15,17,19}$B are stable while the odd-N neighbors $^{5,7}$He, $^{10}$Li, $^{16,18}$B are unbound: the core binds two neutrons, but not one, and it binds four neutrons, but not three. This is a pairing effect, but the essential point here is that the binding cannot be calculated in a perturbative treatment; the properties of the combined system must be considered. The stability of these systems arises from the neutron-core and neutron-neutron interactions, which are both attractive, and which together provide the energy gain necessary to give a bound system. The most interesting candidate studied so far is $^{8}$He, which may be viewed as predominantly an α-particle coupled to a tetraneutron. The dominant β-decay process, leading to a neutron, a triton, and an α-particle, is possible experimental evidence for this assumed cluster structure [bor93] and for the importance of the n-n interactions outside of the α-particle core.

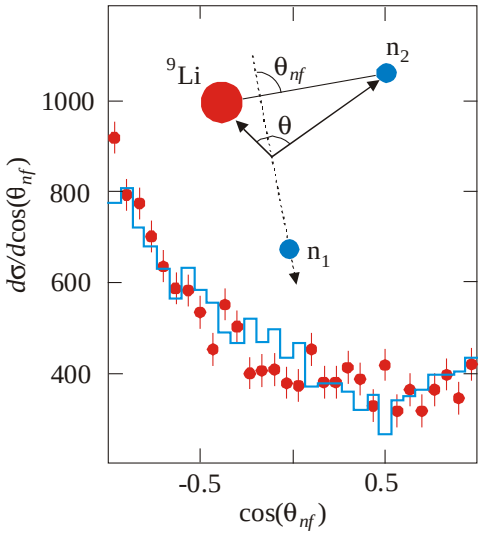


Figure 13: Angular distribution of the decay neutrons from $^{10}$Li following $^{11}$Li knockout reactions. The forward-backward asymmetry is interpreted as interference in the $l$ = 0,1 channels, adapted from [sim99].

Much has been learned about the two-neutron halo structure of the nucleus $^{11}$Li. A number of experiments suggested that the neutrons occupy the $1s_{½}$ and $0p_{½}$ orbitals with comparable amplitudes. This is an interesting result considering that $^{11}$Li has a N = 8 closed shell. For such a nucleus one would not expect a very mixed wave function. A recent experiment has observed an asymmetry (Figure 13) in the angular distribution of the decay of recoiling $^{10}$Li measured in a fast-beam experiment [sim99], see also [gar98]. The asymmetry is due to the interference of the $s$ and $p$ orbitals, and the relative phase can be determined from the measurement. The new technique opens a number of possibilities for angular-correlation studies in breakup reactions. The next generation of experiments will be able to investigate a number of interesting candidates: $^{17,19}$B, $^{20,22}$C, and beyond.

There are other interesting possibilities for extended multi-nucleon halo systems. Efimov very early [efi70] drew attention to a general aspect of the three-body problem with weak short-range attractive forces. Although it is usually believed that the three-body problem is too complex to be studied analytically, a rather wide class of tractable solutions exists for weakly bound quantum systems. Some marginally bound three-body systems can have one or even several bound excited states. The excited Efimov states will be near to the three-body threshold and of large spatial dimensions, for nuclear systems possibly on the order of 100 fm. The problem is also of interest in molecular physics. In this field, the van der Waals force is attractive and of short range and hence similar to the nuclear force. It has been shown experimentally that dimers and trimers of helium exist, see [sch94a]. The most interesting question, the possibility of excited levels, may however be too hard for the techniques of molecular physics to answer. It is most likely that nuclear physics will provide the best hunting ground in a search for Efimov states, which is an interesting option for the next generation of fragmentation facilities.

Detailed investigations of halo nuclei have been restricted to light nuclei, because these were the ones accessible at existing facilities. Fast beams at RIA offer the unique opportunity to produce and investigate extreme cases of multi-nucleon halos in heavier nuclei about which virtually nothing is known. Nuclei near the drip line should be available from RIA even up to mass 100, an order of magnitude increase over what is currently available.

## Reaction Cross Section Measurements

Measurements of interaction cross sections provide an effective means of searching for unusual features in nuclei, such as extended halo distributions. Indeed, a measurement of the interaction cross section of $^{11}$Li provided the first clear evidence of its extended matter distribution [tan85]. These measurements can be performed with beam intensities as low as 0.01 particles/s since interaction cross sections are of the order of barns and because thick targets can be used at energies of several hundred MeV/nucleon. Several successful theories can be used to interpret the data and extract matter distributions at high energy [hen96], where one starts from known nucleon-nucleon interaction cross sections $\sigma_{NN}$ and an assumed matter distribution [ber89]. The reaction probability is calculated in each volume element where projectile and target overlap, and it is integrated over the nuclear volumes, the trajectory, and all impact parameters. Improved models allow for correlations to be used rather than requiring static matter densities [alk96]. A remaining interesting question is whether in-medium modifications of nucleon-nucleon cross sections must be considered. The BUU transport model, for example, predicts that Pauli blocking reduces the in-medium $\sigma_{NN}$ to about 80% of that for free nucleons [xia98]. Measurements near E/A = 400 MeV should be ideal for addressing this question, since at this energy $\sigma_{NN}$ is near its minimum. As a consequence, collisions between light and medium-mass nuclei are partially transparent at all impact parameters, making the interaction cross section $\sigma_I$ sensitive to $\sigma_{NN}$. At much lower energies, $\sigma_{NN}$ is so large that the transparency is near zero for most impact parameters, and $\sigma_I$ is sensitive only to details at the nuclear surface.

Interaction cross sections have been measured at several laboratories. For example, experiments at GSI have probed the matter distribution over a wide range of light nuclei and demonstrated the presence of neutron skins in the heavy sodium isotopes [suz95]. At the NSCL, measurements of $\sigma_I$ have been made near E/A = 60 MeV, for both stable and exotic nuclei using a stack of Si detectors as a target [war96]. This technique has been extended to higher-Z targets by sandwiching Pb targets between the Si detectors [war00]. Reaction cross sections on Pb were measured for most bound isotopes of He, Li, and Be accurate to better than 5%. The generalization of this technique should allow measurements on all solid targets. Each target foil determines $\sigma_I$ for the energy range projectiles have in it, so the method can determine the energy dependence from high energies, where in-medium effects on $\sigma_{NN}$ are most readily observed, to lower energies where they cannot be.

The Si-stack method also allows the measurement of one-neutron ($\sigma_{-n}$) and two-neutron ($\sigma_{-2n}$) removal cross sections for one- and two-neutron halo nuclei, respectively. Because of the low beam intensities required, measurements will be possible for drip-line nuclei up to nickel. These measurements would provide the first tests of halo structures and of modifications to the core due to the halo neutrons. For example, successful microscopic predictions exist for $\sigma_{-2n}$ for $^6$He on both light and heavy targets, near both E/A = 50 and 800 MeV [war00, war97]. The intuitively appealing subtraction relationship, $\sigma_{-2n}(^6\text{He}) = \sigma_I(^6\text{He}) - \sigma_I(^4\text{He})$ [tan92], appears to be applicable at high, but not at low energies. A careful study of the energy dependence of $\sigma_{-2n}(^6\text{He})$ might reveal whether the failure at low energy [war00, neg96] results from second-order processes where knocked-out valence neutrons interact with the $^4$He core or from actual modifications of the $^4$He core.

A search for neutron avalanches from very neutron-rich projectiles is an additional exciting possibility [fuk93]. When one has heavier drip line nuclei available there could be closed shells of neutrons that may be removed in one step. Measurements of the probabilities of this type of removal would provide interesting information on correlations among the neutrons and the cluster structure of nuclei.

At RIA the measurements of interaction cross sections will allow a global exploration for unusual nuclear structures. It will also be one of the most sensitive tests (meaning that it can even provide a measurement with weak beams) to search for the development of nuclear halos and skins. The high energy of the fast beams is essential to allow the inner parts of the nucleus to be explored, to take advantage of reaction models valid at higher energy, and to allow very thick targets to be used. Since beam intensities as low as 0.01 particles/s can be used, one may be able to explore drip line nuclei up to perhaps $^{110}$Zr and search for neutron skins in $^{150}$Sn and beyond.

## 4.3. Properties of Bulk Nuclear Matter

### The Equation of State of Neutron-Rich Nuclear Matter

#### *Nuclear Equation of State at High Density*

During a central collision of two nuclei at energies of E/A = 200–400 MeV, nuclear matter densities approaching twice the saturation density of nuclear matter can be momentarily attained. Such collisions provide the only terrestrial situation in which such densities can be achieved and investigated experimentally to extract the equation of state (EOS) and other properties of dense nuclear matter.

Present experiments, aimed at determining the EOS, do not explore its dependence on the neutron-to-proton ratio. This information must be known for extrapolating the EOS towards the limit of neutron matter, which is an important nuclear property needed for the theoretical modeling of Type II supernova explosions, neutron star mergers, and the stability of neutron stars (see page 40).

The development of fast fragmentation beams at RIA will provide intensities greater than about $10^4$ particles/s for A ≈ 100 nuclei for energies up to E/A ≈ 400 MeV and neutron/proton ratios approximately spanning the range 1 < N/Z < 1.7. This will expand the range of N/Z values for beams in this mass range by nearly a factor of three over that accessible with stable beams and facilitate explorations of the isospin dependence of the EOS. To illustrate existing uncertainties in this isospin dependence, the blue dashed and red solid lines in Figure 14 show the relationship between the density and the energy per nucleon for a neutron-rich system (N = 2Z) for two simple formulations of the isospin dependence of the EOS [col98]. For symmetric (N = Z) nuclear matter, these two formulations reduce to the soft EOS, shown by the dotted line, with an incompressibility constant K = 200 MeV.

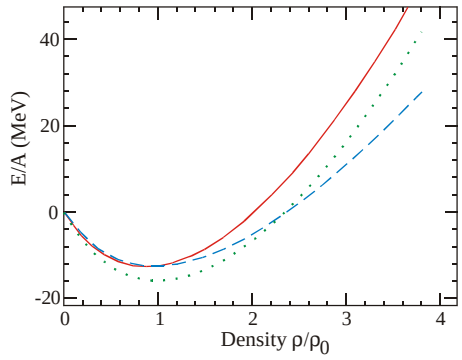


Figure 14: Energy-density relationship from which the nuclear equation of state can be derived, at zero temperature, for symmetric nuclear matter (dotted line) and for nuclear matter with asymmetry constant (N – Z)/A = 1/3 assuming a soft (blue dashed line) and a stiff (red solid line) isospin dependent compressibility, adapted from [col98].

Important information about the nuclear mean field that governs the EOS can be obtained from the study of collective flow, a set of observables related to the mean nucleonic velocity field at breakup. A rich variety of non-equilibrium phenomena is manifested by this velocity field that provides a battery of constraints on the EOS through comparisons to transport theory. In the following subsections, we discuss both experimental measurements of sideward-directed flow in the reaction plane and “squeeze-out” flow

## Neutron Stars

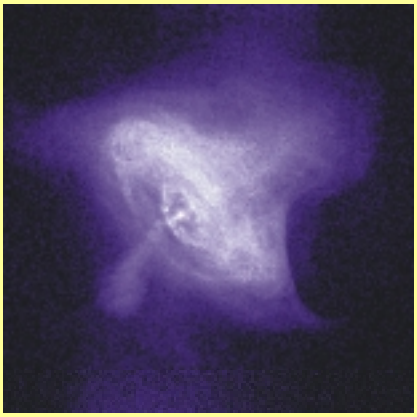

At the end of the life of a massive star, its iron-like core collapses and the resulting supernova explosion disperses the outer part of the star into the interstellar medium. In most cases the explosion leaves behind a part of the core, an extraordinarily dense object, a neutron star with a typical mass 1.5 times that of the sun and a radius of about 10 km. Intense gravitational forces compress the star, which at its center has a density $10^{15}$ times that of water. Going from a neutrons star's surface toward its center, the environment changes from an iron-like solid crust to a region whose ratio of neutrons to protons increases and then to a region where weakly charged nuclei may have linear or sheet-like shapes and are imbedded in a neutron fluid. About one kilometer below the surface, neutron star matter consists of a nuclear fluid composed mostly of neutrons and only trace amounts of protons and electrons. At higher densities, nearer to the stellar center, the environment is more or less unknown and may contain muons, other heavy relatives of electrons, pions, kaons, lambda and sigma baryons, or even quark matter or quark-matter droplets. It appears that large parts of a neutron star could exist in a mixed phase, for example, a mixture of ordinary hadronic matter and quark matter.

The experimental and theoretical exploration of the structure of neutron-star matter and the determination of the equation of state (EOS) associated with such high-density matter is of key importance for understanding the physics of neutron stars and supernova explosions.

(Figure of the crab nebula adapted from:
http://chandra.harvard.edu/photo/0052/0052_xray_lg.jpg
Text from: "Opportunities in Nuclear Astrophysics: Origin of the elements")

perpendicular to the reaction plane. (The latter is sometimes discussed in work at higher energies in the context of "elliptical flow." This is one of many techniques that have been applied across energy domains to address similar challenges.)

***Sideward-Directed Flow***

Sideward-directed flow is an ordered motion of nuclear matter in the reaction plane. The collective motion of particles in this plane is influenced by the Coulomb and nuclear mean field potentials and by the kinetic pressure from nucleon-nucleon collisions via the residual interaction.

The reaction plane is defined by the direction of the beam (chosen as the z-direction) and by the impact-parameter vector (chosen as the x-direction). The average transverse

momentum per nucleon can be projected on the reaction plane to obtain $\langle p_x/A \rangle$ [dan85]. This quantity can be determined as a function of the rapidity,* $y$, and is defined to be positive for forward emitted projectile remnants at large positive $y$. Values for $\langle p_x/A \rangle$ near mid-rapidity ($y = 0$) increase monotonically with $y$. The slope $F = d\langle p_x/A \rangle/dy$ at $y = 0$ provides a convenient observable known as the directed transverse flow $F$. Figure 15 shows a comparison between measured $\langle p_x/A \rangle$ values for protons and beryllium fragments for Kr + Au collisions at E/A = 200 MeV [hua96]. The larger slope (and larger flow $F$) for the beryllium fragments, relative to protons, is due to the interplay of the collective flow velocity (which is independent of fragment mass $M_F$) and the randomly oriented thermal velocity (which is inversely proportional to $M_F$). The flow velocity is governed by the mean field and is sensitive to the EOS, while the thermal velocity is governed by effective nucleon-nucleon cross sections, which are modified from their free values by the nuclear medium.

Because of the interplay between mean field and nucleon-nucleon collision dynamics, values for $F$ depend strongly on the incident energy. At low energies, E/A ≈ 10 MeV, the Pauli exclusion principle blocks most nucleon-nucleon collisions and the attraction of the mean field dictates largely attractive momentum transfers (negative deflection angles) to the emitted particles. At higher incident energies, E/A ≈ 200 MeV, nucleon-nucleon collisions are less blocked, leading to predominantly repulsive momentum transfers (positive deflection angles). The interplay between the attractive mean field and the repulsion from nucleon-nucleon collisions leads to the disappearance of sideward-directed flow at a value for the incident energy called the balance energy, $E_{bal}$. At incident energies of E/A = 150–400 MeV, well above the balance energy, nuclear matter densities of approximately twice the saturation density of nuclear matter can be momentarily attained. It is at these beam energies, and at the resulting densities, that collective flow observables are most sensitive to the compressibility of the nuclear EOS. The compressibility at high density is important to nuclear dynamics and to astrophysical phenomena. Using fast fragmentation beams from RIA at a range of incident energies, one can explore the isospin dependence of the EOS at a range of densities.

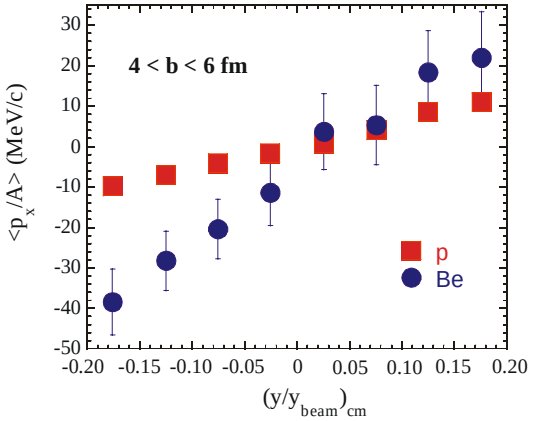


Figure 15: Average transverse momentum per nucleon for protons (red solid squares) and beryllium fragments (blue solid points) measured for Kr + Au collisions at E/A = 200 MeV; from [hua96].

* The rapidity $y$ is defined by: $y = ln[(E + p_{//} c)/E - p_{//} c)]/2$, where $c$ is the speed of light, $p_{//}$ is the momentum component parallel to the beam axis and $E$ is the energy of the particle. The rapidity is additive under Lorentz transformations and, for small $y$, reduces to the velocity component parallel to the beam.

### *Balance Energy*

Experimentally it is easier to determine the balance energy at which the transverse flow vanishes than it is to measure or theoretically calculate small flow values. Values for the balance energy, $E_{bal}$, have therefore been extracted for a variety of systems, testing our understanding of the momentum dependence of the mean field and of the density and isospin dependencies of the in-medium nucleon-nucleon cross section. As an example, Figure 16 shows the impact parameter dependence of $E_{bal}$ extracted for $^{58}$Fe + $^{58}$Fe and $^{58}$Ni + $^{58}$Ni collisions [pak97]. Larger values of $E_{bal}$ are observed for the more neutron-rich $^{58}$Fe collisions than for those with $^{58}$Ni, for which N/Z is closer to unity.

Different values of $E_{bal}$ for the two systems are, indeed, predicted by calculations with the Boltzmann-Uehling-Uhlenbeck equation using free nucleon-nucleon cross sections (open circles and squares), and result from the isospin dependence of the nucleon-nucleon cross sections ($\sigma_{np} > \sigma_{pp}$ , $\sigma_{nn}$ ). However, the overall magnitude of the balance energy is clearly underestimated. Improved fits to the data can be obtained by reducing the in-medium cross sections, but the nature of the needed reduction is presently not known. It could be isospin dependent, but the current data are insufficient to determine this.

When the density dependence of the symmetry term of the EOS is varied, and a stiff density dependence is assumed for the symmetry term, similar balance energies for the two systems are obtained at one impact parameter, $b/b_{max}$ = 0.45 [sca99]. These calculations are shown by the triangles in Figure 16. From more detailed examinations of the calculations it was concluded that at densities greater than saturation density sideward-directed flow is sensitive mainly to the density dependence of the symmetry term of the EOS [sca99]. This sensitivity grows with incident energy because higher densities are attained at higher energies. Additional sensitivity to the symmetry term is predicted when flow values for neutrons and protons (or $^{3}$H and $^{3}$He nuclei) are compared, because the forces due to the symmetry term have opposite signs for neutrons and protons.

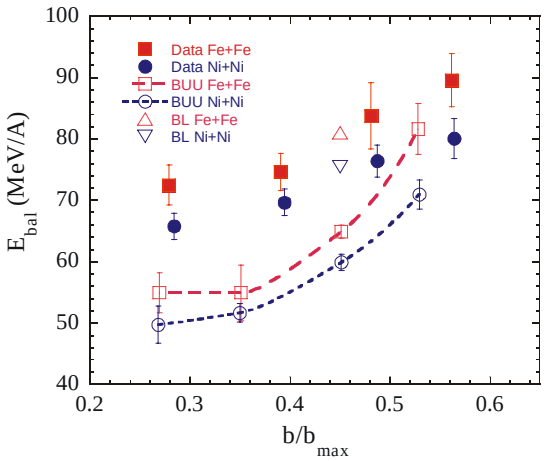


Figure 16: The impact parameter dependence of the measured balance energy is shown for $^{58}$Fe + $^{58}$Fe (red solid squares) and $^{58}$Ni + $^{58}$Ni (blue solid circles) collisions. The open red squares and blue circles indicate the corresponding calculated points assuming free nucleon-nucleon cross sections. The red and blue triangles are calculations for the balance energies of protons assuming an EOS with a stiff isospin dependence. Adapted from [pak97].

Investigations of such isospin dependencies will become increasingly sensitive for systems that differ more significantly in N/Z than those presently accessible with stable beams. Intense fast fragmentation beams of rare isotopes at

RIA would provide the capability to compare systems of fixed mass (N + Z), but greatly different N/Z. Such comparisons would provide unprecedented opportunities to examine isospin dependencies of the in-medium cross sections and the nuclear mean field at high density. These studies can be performed with beam intensities as low as $10^4$ particles/s. For the mass 58 system, for example, one can compare $^{58}$Ti + $^{58}$Fe collisions to $^{58}$Zn + $^{58}$Ni collisions and thus extend the range of the asymmetry parameter (N – Z)/A by 250%. Comparable studies can be performed in the mass 100 range (e.g. $^{106}$Zr + $^{106}$Pd and $^{106}$Sb + $^{106}$Cd) and for higher mass systems as well.

***Isospin Dependence of the EOS at Higher Energy***

The symmetry energy of nuclear matter describes the dependence of the energy per nucleon on the relative numbers of neutrons and protons. It reflects the fact that strongly bound states of relative motion are available for the neutron and proton system, which are forbidden to the two-neutron or two-proton systems by the Pauli principle. In addition to its relevance to nuclear physics, the symmetry energy is of great importance for studies of neutron stars, nucleosynthesis, and supernovae. It affects the collapse of massive stars, neutrino emission rates, kaon condensation in neutron stars, magnetic properties of neutron stars, the cooling rates of proto-neutron stars, and the predicted correlation between the radius of a neutron star and the pressure of neutron-star matter near normal nuclear densities.

Both the magnitude and the density dependence of the symmetry energy are poorly known. Current studies of the EOS and the related compressibility of nuclear matter have been limited to projectile and target nuclei close to the line of β stability with little freedom of varying the N/Z ratio (at fixed mass numbers). In dense astrophysical environments, the neutron-to-proton ratio can approach N/Z ≈ 7, and densities ranging from a fraction to several times that of normal nuclear matter are encountered. Because the symmetry energy increases with density, measurements that can constrain this density dependence are particularly valuable.

As already mentioned, the momentary attainment of high densities in central heavy ion collisions at E/A > 200 MeV permits experimental investigations of the nuclear EOS at such densities. Theoretical analyses indicate that measurements of directed transverse flow and squeeze-out flow are sensitive to the compressibility of nuclear matter. The theoretical modeling of these reactions is made ambiguous, however, by uncertainties in the in-medium nucleon-nucleon cross sections and in the momentum dependence of the nuclear mean field. The latter sensitivity is illustrated in the left panel of Figure 17. Here similar flow values are obtained for two different forms of the EOS, one soft with a momentum dependent mean field and one stiff without momentum dependence [pan93]. This ambiguity can be resolved if a similar analysis is performed for the mass-asymmetric Ar + Pb system at E/A = 400 MeV; see the right panel of the Figure [pan93]. This illustrates the importance of measuring a broad range of systems, including ones with similar entrance channel masses, but significantly different neutron-to-proton compositions.

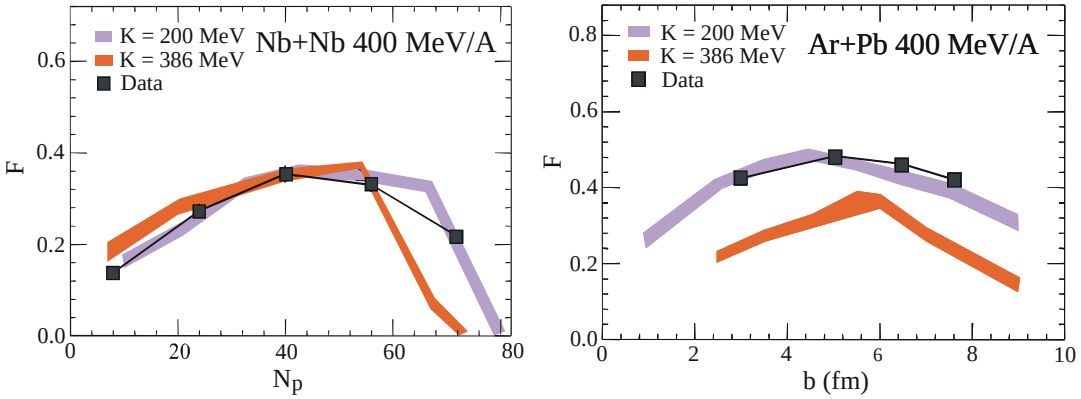


Figure 17: Left Panel: Comparison of measured (solid points) and calculated (shaded regions) values for the directed collective flow in Nb + Nb collisions as a function of the observed proton multiplicity. Calculations in violet correspond to a momentum dependent mean field with a soft EOS (K = 200 MeV); calculations in red correspond to a momentum independent mean field with a stiff EOS (K = 386 MeV). Right Panel: A corresponding comparison of measured (solid points) and calculated values (shaded regions) for the directed collective flow in Ar + Pb collisions as a function of deduced impact parameter. From [pan93].

While a preference for a soft EOS is indicated, this analysis assumed a specific density dependence of the symmetry term of the EOS; the conclusions could be changed if the assumed density dependence of the symmetry term were wrong. With fragmentation beams of rare isotopes at E/A > 200 MeV, the density dependence of the symmetry term of the EOS can be explored by comparing mass-symmetric systems such as $^{58}$Ti + $^{58}$Fe, $^{58}$Zn + $^{58}$Ni, $^{106}$Zr + $^{106}$Pd, and $^{106}$Sb + $^{106}$Cd to asymmetric systems such as $^{58}$Ti + $^{106}$Pd and $^{58}$Zn + $^{106}$Cd. Additional information can be obtained from measurements of these reactions by comparing emission out of the reaction plane to that in the reaction plane and thereby extracting the squeeze-out flow effect.

Another technique for analyzing collective flow involves diagonalizing the flow tensor and comparing the principal axes $\lambda_1 < \lambda_2 < \lambda_3$ to each other. The usefulness of this is illustrated in the left panel of Figure 18, where predictions for the ratio $R_{21} = \lambda_2/\lambda_1$ for central Au + Au collisions at E/A = 400 MeV are shown. The ratio involves the principal axis, $\lambda_2$ (out of the reaction plane), and the shorter of the two in-plane principal axes, $\lambda_1$. The different predictions depend strongly on the EOS, a sensitivity that has not been adequately exploited in the past. The right panel of Figure 18 shows a comparison between predicted and measured values for a similar quantity, the out-of-plane to in-plane yield ratio, $R_N$, derived from the measured azimuthal distribution as a function of the transverse momentum. It shows a strong sensitivity to the momentum dependence of the mean field. Similar techniques are being applied at higher incident energies to search for the softening of the EOS due to the transition to the quark-gluon plasma at high density.

The symmetry term of the EOS generates a force that has an opposite sign for protons and neutrons, providing additional sensitivity to the isospin effects; it would be useful to

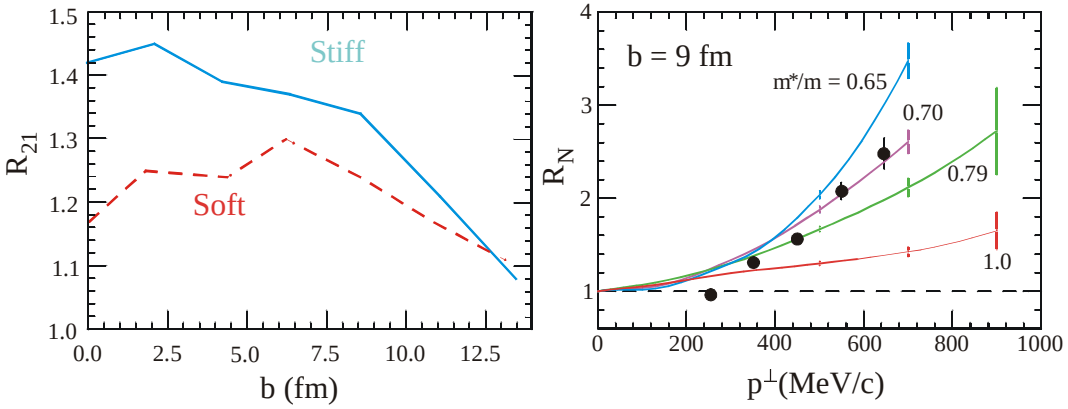


Figure 18: Left Panel: Comparison of calculated values for the ratio $R_{21} = \lambda_2/\lambda_1$ of the principal axes (where $\lambda_1 < \lambda_2 < \lambda_3$) of the flow tensor as a function of the impact parameter for $^{197}$Au + $^{197}$Au collisions at E/A = 400 MeV. The red dashed and blue solid lines correspond to calculations with a soft (K = 200 MeV) and stiff (K = 386 MeV) EOS, respectively. Right Panel: Comparison of calculated (lines) and measured (solid points) out-of-plane to in-plane yield ratio $R_N$ as a function of the transverse momenta of emitted protons for peripheral (b = 9 fm) Bi + Bi collisions at E/A = 400 MeV. The various calculated curves are labeled by the effective mass ratio m*/m of the momentum dependent mean field (with a soft EOS) used in the calculation. From [dan98a].

compare the flow for different isobars like $^3$H and $^3$He or p and n. For this reason, some flow measurements of neutrons would be useful.

The degree to which projectile and target nucleons are mixed within the overlap region is a key question for such investigations. Careful tests of the predictions of transport theory for this mixing are necessary to establish the isospin composition of the dense regions where the pressure develops that generates the observed flow. Such predictions can be tested by measurements of the flow of the emitted light particles as a function of their isospin. The sensitivity of such tests can be optimized by studying the collisions of isospin asymmetric exotic systems such as $^{106}$Zr + $^{106}$Cd and $^{106}$Sb + $^{106}$Pd using fast fragmentation beams at RIA.

Experiments of this nature can be performed with thick targets, enabling investigations of the density dependence of the symmetry term of the nuclear EOS to be undertaken with beams of intensities as low as $10^3$ particles/s if the detection of neutrons is not required. Beam intensities of at least $10^5$ particles/s would be required for flow measurements of neutrons.

## The Liquid-Gas Phase Transition in Neutron-Rich Matter

Theoretically, there is little doubt that nuclear matter has a phase transition at sub-nuclear density between a Fermi liquid, characteristic of nuclear matter at low excitation, and a nucleonic gas. This constitutes one of two bulk phase transitions of strongly interacting matter; the other is the transition from a hadronic gas to a plasma of quarks and gluons. Both phase transitions can be experimentally studied by heavy-ion collisions. In such

experiments, finite size effects are expected to modify the properties of the nuclear liquid-gas phase transition. Analogous finite size modifications have been observed for the solid-liquid phase transition in metallic clusters and may play a role in the deconfinement transition to the quark-gluon plasma at higher incident energies. The investigation of phase transitions in finite systems is an important issue in many-body physics.

Copious emission of intermediate mass fragments (IMF: $3 \leq Z_{IMF} \leq 30$) is one predicted consequence of the liquid-gas phase transition of nuclear matter. Experiments have identified such multifragmentation processes in both central and peripheral heavy ion collisions. The left panel of Figure 19 shows the incident energy dependence of the IMF multiplicity detected in central Kr + Au collisions [pea94]. For central collisions, multifragmentation events are observed for incident energies in the range of E/A = 35–400 MeV, and maximum fragment production occurs at E/A ≈ 100 MeV. The right panel shows the impact parameter dependence for the fragmentation of Au projectiles at higher incident energies [sch96], where mid impact-parameter collisions lead to multifragmentation events and central collisions lead to vaporization events with few IMF's and many light particles. In both cases, fragment multiplicities increase to a maximum with increasing energy deposition (increasing incident energy for central collisions or decreasing impact parameter for peripheral collisions). Then the fragment multiplicity declines with energy deposition as the system begins to vaporize completely into nucleons and light particles.

Large fragment multiplicities like those in Figure 19 have been reproduced via the Expanding Evaporating Source (EES) model [fri90], or via multiparticle phase space models like the Statistical Multifragmentation Model (SMM) [bon95] and the Microcanonical Metropolis Monte Carlo (MMMC) model [gro97], which assume that

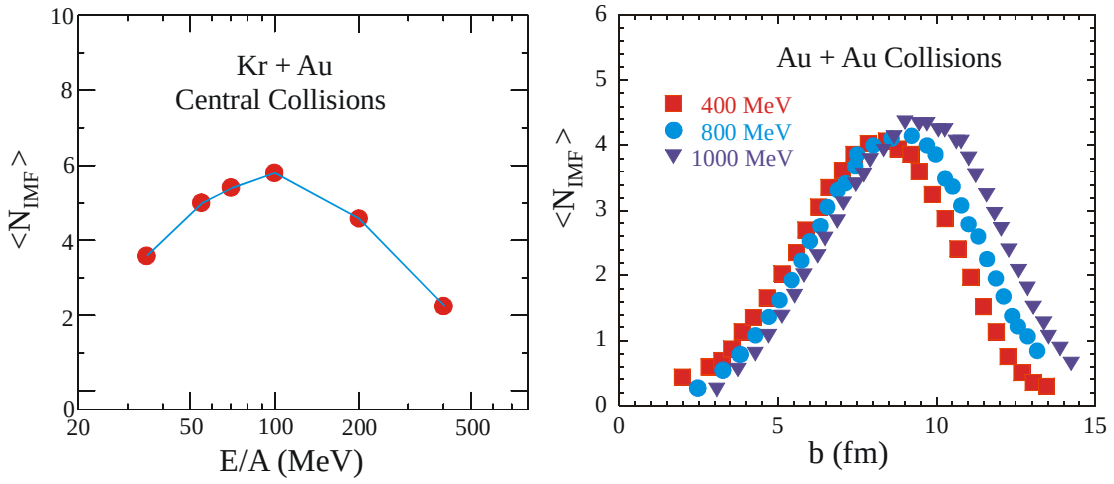


Figure 19: Left panel: Measured mean intermediate mass fragment multiplicities (solid points) and corresponding SMM calculations (solid line for central Kr + Au collisions (b < 0.25) as a function of incident energy. Right panel: Mean multiplicity of intermediate-mass fragments $<N_{IMF}>$ as a function of impact parameter for the reaction $^{197}Au + ^{197}Au$ at E/A = 400, 800, and 1000 MeV. Adapted from [pea94, sch96].

multifragmentation occurs at low density. These models associate this behavior with low-density phase transitions similar to the liquid-gas phase transition of nuclear matter. In contrast, conventional compound nuclear fission or evaporation models, which assume the system remains near saturation density, typically produce IMF multiplicities of the order of unity, making such models unsuitable for the description of multifragmentation. As an example of how well statistical multifragmentation models reproduce the experimental multifragmentation data, Figure 20 shows a comparison between the measured charge distributions for central Au + Au collisions at E/A = 35 MeV and corresponding SMM calculations [dag96]. Similar results can also be obtained for peripheral collisions at much higher incident energies, indicating that both peripheral heavy ion collisions at E/A $\geq$ 400 MeV and mass-symmetric central heavy collisions at E/A $\approx$ 30–200 MeV offer optimal conditions for the investigation of statistical multifragmentation. In the following, measurements of peripheral collisions using fast fragmentation beams from RIA are proposed to investigate the isospin dependence of the nuclear liquid-gas phase transition.

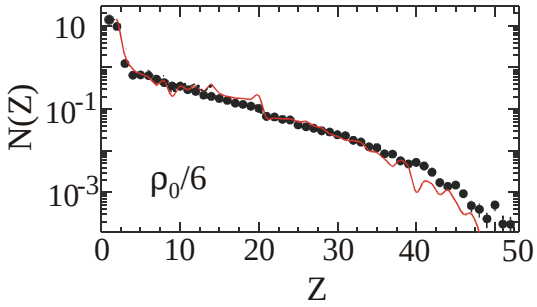


Figure 20: Charge distribution N(Z). The points show experimental data and the line shows results of efficiency corrected SMM calculations for a source of $A_{source}$ = 315 and $Z_{source}$ = 126, excitation energy of $E^*_{source}/A$ = 4.8MeV and collective expansion energy of $\langle E_{coll}/A \rangle$ = 0.8 MeV that breaks up at a density of $\rho_{source} = \rho_o/6$ [dag96].

***Isospin Dependence of Statistical Multifragmentation***

The symmetry term in the nuclear matter EOS is anticipated to be the principal source of the isospin dependence of the nuclear liquid-gas phase transition. Pure neutron matter is probably unbound and does not exist in the liquid phase. Due to the weak binding of neutron-rich matter, the region of mixed phase equilibrium is expected to shrink with increasing neutron excess. Models for the liquid-gas phase transition in two-component (neutron and proton) nuclear matter, for example, predict the critical temperature to decrease and the phase transition to change from first to second order as a consequence of non-zero isospin asymmetry. These models also predict that the coexistence region for neutron-rich matter will display fractionation effects wherein the gas is significantly more neutron-rich than the liquid. Even more dramatic situations may be encountered in the inner crusts of neutron stars where a few protons can serve to bind nuclei (with masses up to A ~ 1000 and sometimes with planar or rod-like shapes) which reside in a nearly pure neutron gas.

Fast fragmentation beams of rare isotopes offer the unique opportunity to explore the isospin dependence of multifragmentation and the liquid-gas phase transition. Ideally, such experiments would be performed in inverse kinematics by fragmenting rare isotopes from

the beam. Fast fragmentation beams from RIA with energies of E/A > 200 MeV and intensities of $10^4$ particles/s, or more, are ideal for this purpose. For example, one can compare the projectile multifragmentation of $^{106}$Zr (N/Z ≈ 1.7) to that of $^{106}$Sb (N/Z ≈ 1.1). The kinematics of projectile fragmentation also has the advantage of reducing the solid angle coverage needed in the laboratory frame and lowering the detection thresholds in the rest frame of the emitting source.

Expected enhancements of the isospin asymmetry of the gas can be explored via measurements of quantities like the t–$^3$He yield ratio, which is less influenced by secondary decay of particle unstable fragments than the n-p ratio. The left panel of Figure 21 shows the temperature dependence of the t–$^3$He ratio predicted for a nuclear system undergoing a phase transition within a lattice gas model [cho99]. Calculations that neglect the symmetry term in the nuclear EOS are denoted by the blue square points, which deviate little from the N/Z value (≈1.7) of the combined system. Calculations that incorporate the symmetry term in the nuclear EOS display a considerable amplification of the isospin asymmetry of the gas phase and enhanced t–$^3$He ratios (red circular points) which attain values in excess of 50 at T ≈ 2.4 MeV. Experimental t–$^3$He yield ratios obtained for central $^{112}$Sn + $^{112}$Sn, $^{112}$Sn + $^{124}$Sn, and $^{124}$Sn + $^{124}$Sn collisions [xu99], shown in the right panel of Figure 21, increase rapidly with the N/Z of the system, thus supporting the idea that light particles (which contribute to the gas phase) are proportionately more neutron-rich than the overall system.

Besides these fractionation effects, it will be important to investigate the sensitivity of the fragment multiplicities and charge distributions to the isospin of the system. As an example, Figure 22 compares IMF multiplicities predicted by equilibrium MMMC statistical calculations for the decay of hot $^{180}$Pb and $^{180}$Yb nuclei [llo99]. These calculations predict a shift of 1 MeV/nucleon for the threshold of multifragmentation. To

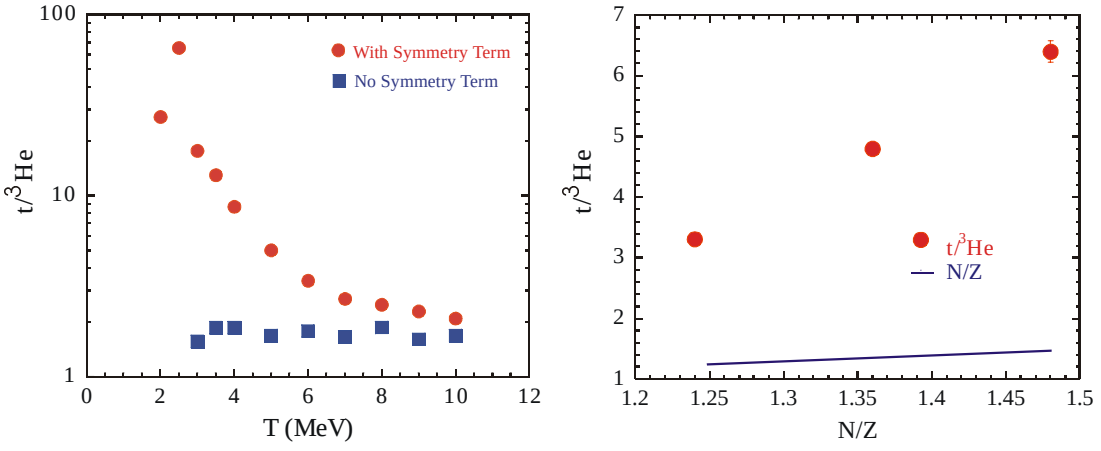


Figure 21: Left panel: Ratios of triton and $^3$He yields calculated via the lattice gas model with (red circles) and without (blue squares) the symmetry term in the nuclear mean field potential [cho99]. Right panel: Measured dependence of the ratio of t and $^3$He yields as a function of the N/Z of the total system of projectile plus target. The N/Z ratio of the combined system is plotted as the blue solid line [xu99].

make the expected differences as large as possible, the corresponding measurements should be performed with beams that have the widest range of N/Z values possible. Energies of E/A > 200 MeV and intensities of $10^4$ particles/s or more are ideal for these measurements. It should be possible to test these effects by comparing the fragmentation of projectiles at N/Z values over the range 1 < N/Z < 1.7 using fast fragmentation beams of RIA.

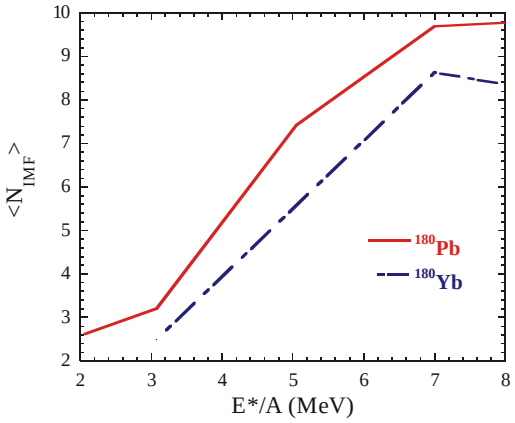


Figure 22: Fragment multiplicity predicted by the statistical fragmentation model of [gro97] for hot $^{180}$Pb (solid) and $^{180}$Yb (dashed) nuclei. Adapted from [llo99].

### *Isospin Dependence of Dynamic Fragmentation and Multifragmentation*

Another opportunity to examine the isospin dependence of the EOS, this time at low densities, is afforded by the study of dynamical fragmentation. The low-density region of the EOS is relevant to the liquid-gas phase transition. It may also be relevant to the mass ejection during and after the merging of neutron stars and the associated ejection of nucleosynthesis products into interstellar space. This could help answer the question whether neutron star mergers are possible sites for the astrophysical rapid neutron capture process (r-process).

Subnuclear densities can be attained in central collisions at higher energies. In such collisions, the nuclear matter is compressed initially, and a collective expansion to low densities sets in subsequently. Such a collective expansion can enhance multifragmentation because it rapidly carries the highly excited system to low density before its excitation energy can be radiated away by light particle evaporation. Transport model calculations predict that the system may undergo spinodal decomposition when the density of the system approaches one third that of normal nuclear matter, i.e., the system becomes adiabatically unstable and density fluctuations grow exponentially. Some of the denser regions become fragments and the more dilute regions develop gaps filled by nucleons and light particles. Subsequently, the system may thermalize or disintegrate without achieving equilibrium between the liquid and gaseous phases if the expansion velocity is sufficiently rapid.

The threshold of dynamical multifragmentation is predicted to be sensitive to the low density EOS. For neutron-rich fast fragmentation beams, the asymmetry term in the nuclear EOS makes an important contribution to the incompressibility and will therefore influence whether or not multifragmentation occurs [col98]. For an EOS with a soft compressibility, calculations at E/A = 50 MeV predict that the system expands and undergoes multifragmentation. For an EOS with a stiff compressibility at low density, corresponding calculations predict that the system recontracts to a dense residue [col98].

Measurements of fragment multiplicity and collective expansion velocity in central collisions near the multifragmentation threshold can therefore provide information about

the symmetry term of the EOS at low density. For this purpose, systems with very different N/Z ratios are needed. Comparisons of $^{52}$Ca + $^{48}$Ca collisions (N/Z = 1.5) to $^{50}$Fe + $^{50}$Cr collisions (N/Z = 1), for example, can be performed at E/A = 50 MeV with fast fragmentation beams of rare isotopes. Since the detection of slow IMF's requires the use of thinner (5 mg/cm$^2$) targets, these experiments require higher beam intensities than do measurements of sideward directed flow. Intensities of the order of $10^5$ particles/second should be sufficient for such investigations.

Subnuclear densities can also be attained in peripheral collisions. In some respects, peripheral collisions may be even more sensitive to the isospin dependence because, for sufficiently neutron-rich nuclei, the N/Z ratio is enhanced at the nuclear surface. The mean-field attraction between target and projectile at approximately touching distances is dominated by surface interactions. For touching collisions, surface interactions strongly influence whether the two nuclei fuse or not. This qualitative argument is supported by transport model calculations [col98] which predict that the cross section for incomplete fusion is sensitive to the nuclear equation of state in the surface region and, in particular, to the density dependence of the symmetry term. The model predictions can, for example, be tested by measuring the energy dependence of incomplete fusion cross sections for reactions like $^{56}$Ca + $^{238}$U. As the cross section for incomplete fusion is of the order of a barn, such experiments can be performed with intensities as low as $10^5$ particles/s.

In peripheral collisions with large projectile- and target-like residues in the exit channel, the flow of nucleons between these binary partners is influenced by the mean field, which supplies a driving force that distributes neutrons and protons differently so as to minimize the symmetry energy. At lower energies, E/A < 20 MeV, this can lead to a preferred direction for the flow of neutrons between binary reaction partners of different N/Z ratio from the neutron-rich to the neutron-deficient nucleus. This could be explored by measuring the mass and charge distributions of the projectile-like fragments as a function of the projectile energy loss. The total cross sections for such processes are of the order of barns but are distributed over many isotopes. The use of thick targets of the order 10–20 mg/cm$^2$ will permit such experiments to be performed with intensities of $10^5$ particles/s, given efficient detection arrays. Some of this work can be performed with re-accelerated beams at RIA, but at the higher incident energies, fast fragmentation beams will be needed.

In peripheral collisions below E/A ≈ 80 MeV, projectile and target nuclei are often joined by a neck that may persist for about 100 fm/c. Transport model calculations predict this neck to be more neutron-rich than the projectile- and target-like residues. This occurs because the neck is, on the average, at a lower density than the residues and because the symmetry term decreases with density. Thus, increasing the asymmetry of the more dilute neck and minimizing the asymmetry of the denser residues can reduce the overall symmetry energy.

Boltzmann-Langevin transport calculations predict that formation and rupture of the neck are sensitive to the density dependence of the symmetry term of the EOS [col98]. Figure 23 shows the projection of the matter density for $^{60}$Ca + $^{60}$Ca collisions at E/A = 50 MeV on the reaction plane, 90 fm/c after the rupture of the neck between the projectile and target residues. For calculations assuming a mean field with a symmetry term yielding a

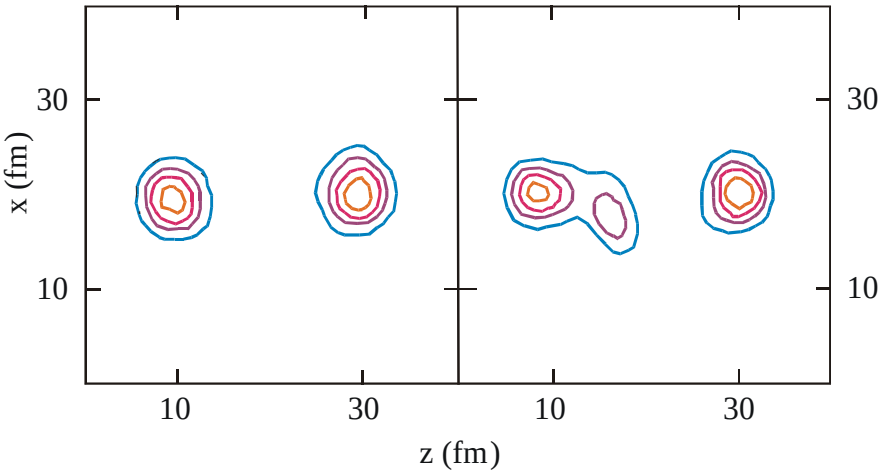


Figure 23: Contour diagrams depicting the density projected on the reaction plane 90 fm/c after the rupture of the neck connecting projectile and target residues produced in $^{60}$Ca + $^{60}$Ca collisions at E/A = 50 MeV. The left (right) panel shows the predictions for a mean field with a symmetry term with a stiff (soft) EOS. Adapted from [col98].

soft EOS (right panel), the matter in the neck region forms an elongated structure close to the left residue. This structure will ultimately separate as a fragment and be repelled from the residue by the Coulomb interaction. No such structure is formed for calculations with the mean field with a symmetry term yielding a stiff EOS (left panel). Measurements of neck-fragment cross sections for projectiles of different N/Z ratio will therefore help determine the density dependence of the symmetry term in the EOS at sub-saturation densities. The cross sections for such processes are of the order of several hundred mb; experiments using fast fragmentation beams at RIA with beam intensities of $10^5$ particles per second are feasible with thick targets of the order of 40 mg/cm$^2$.

## 4.4. Collective Oscillations

Collective excitations of nuclei can probe both global and specific nuclear properties, for example the compressibility of nuclear matter, nuclear size and shape, the neutron and proton distributions within nuclei, and properties of individual nuclear species seen via their response to an external field. Moreover, similarities and differences of collective excitations in various finite quantum systems, for instance, nuclei and atomic clusters, can provide a deeper understanding of mesoscopic physics in general. The coherent nature of collective modes and the physics of their damping and decay characterize the self-organization and quantum decoherence in a system. The two-component character of nuclear Fermi liquids gives an additional important possibility to study the dependence of those processes on the proton-neutron composition.

A large excess of neutrons in a nucleus could potentially yield different properties of the neutron and proton liquids, which will significantly influence the collective motion in the nucleus. The nuclear composition also changes the role of exchange forces in collective

motion and the exchange contribution to the classical sum rules, which are not yet well understood even though exchange is important for the extrapolation to neutron matter. On the other hand, nuclear deformation is driven by single-particle shell structure, and that can be very different in neutron-rich matter from what it is in nuclei near stability. The proximity of the continuum with different evaporative rates for neutrons and protons can change the dissipative properties and decay of the collective modes, and therefore their strength functions and widths.

Giant resonance experiments can address these questions. However, short lived nuclei can only be studied in inverse kinematics in which the projectile has to be excited. The cross sections for exciting giant resonances are strong functions of the beam energy, and energies of ~100 MeV/nucleon are necessary. The giant dipole resonance (GDR) and the giant monopole resonance (GMR) are the two most important resonances in exotic nuclei that are accessible with RIA.

## Giant Dipole Resonance

The giant dipole resonance (GDR) is a sensitive tool for studying non-uniform charge distributions in nuclei. For example, the halo structure in neutron-rich light nuclei could result in a completely different electromagnetic response as compared to stable nuclei [bra99]. A vibration of the neutron halo or skin with respect to the core would shift strength from the normal giant resonance region (~22 MeV) to much lower energies of about 1 MeV. A shift of GDR strength towards lower energies is also predicted to occur for heavier nuclei as one approaches the neutron drip line [bra99]. The GDR strength will be strongly fragmented (Landau damping). This loss of collectivity is due to the modification of the mean field as a function of the N/Z ratio. Measuring the response of these extreme systems will help us understand the collective motion of these neutron-rich nuclei and extrapolate to the collective motion of neutron matter.

The existence and strength of a low energy or soft component of the GDR in neutron-rich nuclei can potentially have a large influence on the path of the r-process (see page 54). During much of the r-process, photodisintegration ($\gamma$,n) and radiative capture (n,$\gamma$) are in equilibrium. However, these reactions fall out of equilibrium as the temperature and neutron density decrease at the end of the neutron-producing event. In this situation, nucleosynthesis depends on the absolute rates of the (n,$\gamma$) and ($\gamma$,n) processes. These in turn depend on the GDR strength function. Figure 24 shows the measured relative abundances of elements (red circles) compared to r-process calculations with the normal GDR strength function (blue line) and a GDR strength function of abundances having significant strength shifted towards lower energy (green line) [gor98]. The normalization is arbitrary and only the shapes of the abundance distributions should be compared to the data. It is apparent that the shape of the GDR strength function has a significant impact on the relative abundances produced in the r-process.

The study of the GDR in exotic nuclei relies on its large excitation cross-section and a clean separation and/or identification from other giant resonances. Two important factors are necessary to excite the GDR strongly in the projectiles: High beam energies and high-Z

targets. At high beam energies GDR formation is dominated by Coulomb excitation which is proportional to $Z^2$ of the target. Coulomb excitation can be viewed as an exchange of virtual photons and the virtual photon spectrum is a strong function of the beam energy. As an example of the energy dependence, Figure 25 shows the excitation probability of the GDR in projectiles of $^{11}$Li, $^{40}$Ar, and $^{86}$Rb on a Pb target. The cross section increases dramatically up to 200 MeV/nucleon. This energy will be readily available for fast beams of rare isotopes from RIA.

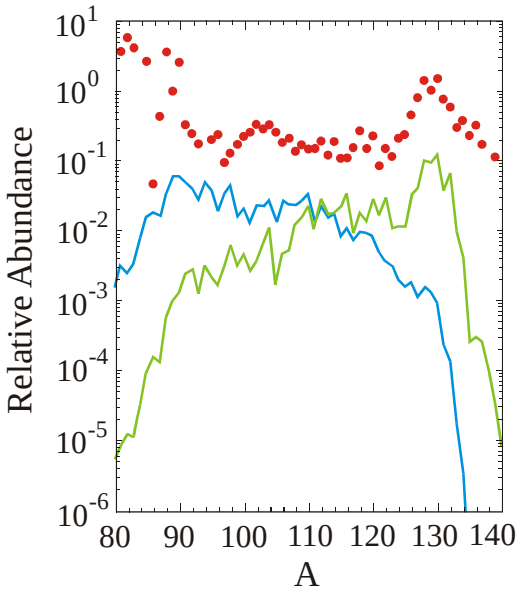


Figure 24: Influence of the normal GDR (blue) and a GDR which includes low energy dipole contributions (green) on the r-process nuclear abundances. The normalization to the measured abundances (red) are arbitrary, adapted from [gor98].

The GDR is located above the particle evaporation threshold, and thus the excited projectiles will break up in flight. Two possible experimental techniques that can be applied to reconstruct the excitation function of the projectile have recently been applied for the first time in the study of the GDR in $^{11}$Be and $^{20}$O. In the method of virtual photon scattering the γ-ray decay back to the ground state is detected [var99]. In virtual photon absorption the excitation energy is reconstructed from the break-up fragment and the neutron(s) [aum99a, aum99b]. Both experiments demonstrated the feasibility of the methods and the great opportunities with fast beams at RIA.

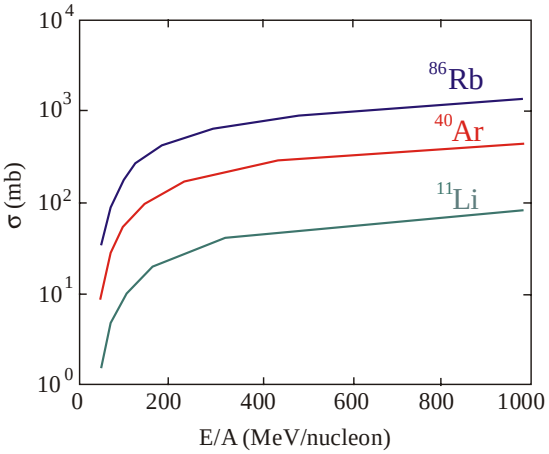


Figure 25: GDR excitation function for three isotopes.

A beam intensity of at least $10^6$ particles/s is needed to make these studies feasible. For heavier beams somewhat smaller intensities should be sufficient because the excitation cross section scales with NZ/A yielding a factor of > 10 between $^{11}$Li and $^{86}$Rb (see Figure 25). With fast beams from RIA a large range of nuclei will be available for study where up to now only the narrow range of stable nuclei can be explored.

The most interesting mass range is the region around the closed shell nucleus $^{132}$Sn. Several important waiting points in the r-process path are only 1–2 mass units away from $^{132}$Sn towards more neutron-rich nuclei. With fast beams from RIA it will be possible to

## The r-process

The r-process takes place in an environment of high temperature, exceeding $10^9$ Kelvin, and high neutron density, greater than $10^{20}/cm^3$, in an event lasting several seconds. In this circumstance, the time interval between neutron captures is much shorter than the lifetime for β-decay. A rapid succession of neutron captures on a seed nucleus finally produces a nucleus with a neutron binding energy sufficiently small that the rate of capture is balanced by the rate of photodisintegration induced by the ambient blackbody photons. After some time at this waiting point, a β-decay occurs and the capture process can begin again. As a result, nuclei tend to pile up at the waiting points. In this equilibrium approximation, the abundance of a nucleus is proportional to its half-life. A special case, where pile-up is large, occurs near neutron shell closures, because β-decay lifetimes are long and because waiting points recur after only a single neutron capture. At the end of the r-process event, the radioactive products decay back toward the valley of stability, sometimes emitting neutrons in the process. The resulting abundance peaks, occurring on the low-mass side of the s-process peaks, are the signature of the r-process.

At present the astrophysical site of the r-process is under debate. The neutrino-heated bubble outside the protoneutron-star in a supernova is in many ways an ideal site. Since r-process abundances appear to be independent of the preexisting heavy-element enrichment of the star, the r-process site must produce its own seeds – the hot-bubble site seems to do so.

However, some models suggest that the entropy in this bubble is too small to reproduce the observed abundance distribution. Consideration of general relativistic effects may resolve this problem. Or, it may be necessary to consider other sites such as merging neutron stars.

Despite these uncertainties, the general features of the r-process outlined above determine what nuclear information is required. The path of the r-process flow is through neutron-rich nuclei, far from the valley of stability. It passes through nuclei with neutron binding energies of about 1–4 MeV, depending upon parameters such as neutron flux and temperature.

("Opportunities in Nuclear Astrophysics: Origin of the elements")

study the GDR in nuclei along the r-process path in this region. The predicted intensities are sufficient to follow the r-process from cadmium to antimony. For other regions ($28 < Z < 47$ and $Z > 52$) measurements of the GDR parameters of neutron-rich nuclei will provide benchmark data which will facilitate reliable extrapolations to the nuclei along the r-process path. For example, nickel isotopes can be measured up to $^{74}$Ni while the r-process is believed to proceed through $^{78}$Ni.

It might also be possible to measure the relative spatial distribution of neutrons and protons. The neutron skin in stable isotopes has been measured with inelastic scattering of isoscalar beams [kra94a]. For the studies of rare isotopes, isoscalar targets will be necessary and these experiments will be very difficult (see the following section). It also appears possible to excite the spin dipole resonance in (t,$^3$He) charge exchange reactions

[kra99]. These reactions are discussed in the section on Gamow Teller transitions (see page 65).

## Giant Monopole Resonance

The compressibility of a nucleus is determined by the effective interaction between the nucleons in their many-body environment. The isovector properties of this interaction determine the dependence of the compressibility on neutron number. Consequently, the measurements of the giant monopole resonance in neutron-rich nuclei will shed light on fundamental properties of the effective force, and on the nuclear compressibility.

The experimental and theoretical exploration of the properties of neutron-star matter and the determination of the equation of state (EOS) associated with such high-density matter are of key importance for understanding the physics of neutron stars and supernova explosions. Since the properties of a neutron star depend on the nuclear equation of state, and hence on the compressibility and symmetry energy of nuclear matter, it is important to determine these quantities.

For small-amplitude density oscillations, the compressibility of nuclear matter of normal density can be obtained from the frequencies and strengths of nuclear vibrations that involve the compression of nuclear material, the isoscalar monopole and isoscalar dipole resonances [bla80]. In order to extract the compressibility of infinite nuclear matter from the measured giant monopole resonance (GMR) energy, it is necessary to understand the correction factors due to surface effects in finite nuclei [far97]. The dependence on isospin is presently not well understood because the current data are limited to stable nuclei [you97, you99]. The most recent value of the nuclear incompressibility extracted from the GMR is 231 ± 5 MeV [you99], but this precise value applies only to stable nuclei. Calculations predict significant differences of the GMR strength distribution in very neutron-rich nuclei compared to stable nuclei. Figure 26 shows calculations for the isoscalar monopole strength in calcium isotopes. $^{60}$Ca exhibits a shift of the centroid energy and significant strength at substantially lower energies [sag98].

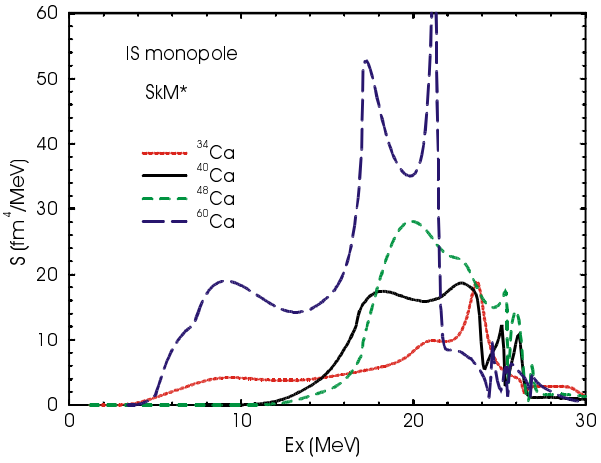


Figure 26: Predicted isoscalar monopole strength distribution for calcium isotopes; adapted from [sag98].

The GMR in exotic nuclei can be excited by inelastic deuteron or α-particle scattering in inverse kinematics. So far no attempts have been made to perform these extremely difficult measurements for which fast fragmentation beams are absolutely essential. For medium mass nuclei and a beam

energy of 150 MeV/nucleon, the α-particle scattering angle for the excitation energy range of interest (10–20 MeV) is 1°–3° in the center-of-mass (50°–80° in the laboratory frame). The cross section for the excitation of the monopole is about 100 mb/sr and peaks at 0º. It can be distinguished from the giant quadrupole resonance only at angles less than 2º. The GMR is located above the particle threshold and the projectile will break up in flight. Thus it will be necessary to detect the scattered deuterons or α particles, which will be extremely difficult because of their low energies (less than ~1 MeV).

Beam intensities larger than $10^7$ particles/s are necessary for these experiments. This will, for example, allow the measurement of the GMR with fast beams from RIA in nickel over a range of 20 isotopes. Up to now the GMR has been measured in only two nickel isotopes, $^{58}$Ni [you96] and $^{60}$Ni [bue84], which have isospins of $T_z$ = 1 and 2, respectively. RIA would extend the coverage by an order of magnitude of $T_z$ = –1.5 to 8.5 ($^{53}$Ni to $^{73}$Ni). For the tin isotopes, the neutron-rich limit is $^{134}$Sn corresponding to $T_z$ = 17. The measurement of the GMR in $^{132}$Sn should help considerably in determining the value of the compressibility of infinite (neutral) nuclear matter [pea92].

## 4.5. Evolution of Nuclear Properties Towards the Drip Lines

Our understanding of the evolution of nuclear properties towards the neutron drip line depends upon two key questions: How does the shell structure change in neutron-rich matter? What are the collective properties of neutron-rich matter?

Magic numbers in neutron-rich nuclei near the drip line may be very different from those near the valley of stability [dob94, dob96]. Figure 27 illustrates some possibilities [dob96].

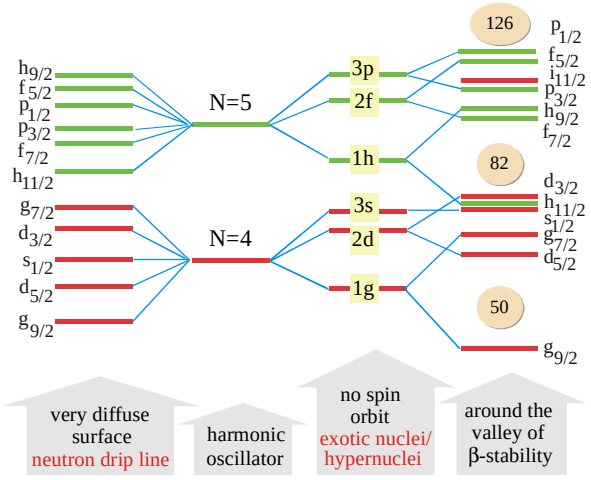


Figure 27: Single-particle spectrum for different nuclear potentials [dob96]. The shell structure characteristic of nuclei close to stability, shown in the column on the right, appears modified for neutron-rich nuclei due to the weak binding energy and the strong pairing force, as shown in the column on the left.

The increase in pairing correlations together with the shallow single-particle potentials that might occur in nuclei near the drip lines could result in a rather uniformly spaced spectrum of single-particle states as illustrated on the left-hand side of Figure 27. Such a uniform distribution of nuclear levels would be very different from the known properties of nuclei near the valley of stability, which typically have a bunched spectrum with large gaps as shown on the right-hand side of Figure 27. The large gaps in the single-particle spectrum at N = 50 and 82 are responsible for the extra stability of the nuclei with these magic numbers. The uncertainties associated with extrapolating the spin-orbit interaction from the valley of stability to neutron matter are considerable [pud96].

Experiments at existing rare isotope beam facilities have provided firm evidence that in neutron-rich nuclei the shell closures at N = 8, 20, and 28 are much less pronounced than they are in nuclei close to the valley of stability. The loss of magic properties for neutron-rich N = 8 and 20 nuclei is associated with a weakening of the shell gap, together with a change in shape to a deformed configuration that becomes the ground state. The conditions for this drastic change in structure may also be present in the regions of nuclei around $^{62}$Ti (N = 40), $^{80}$Ni (N = 50), and $^{126}$Ru (N = 82).

The rapid neutron capture process (r-process) depends on the properties of nuclei near the neutron drip line. Most of these properties are not known experimentally; input to the r-process models is largely based upon a theoretical extrapolation from the properties of nuclei near the valley of stability to those involved in the r-process. These properties determine the path along N and Z and the time scale for the r-process. The path determines the elements and their abundances that result from the r-process. The r-process passes through nuclei with neutron binding energies of about 1–4 MeV, depending upon the neutron flux and temperature. Quantitative r-process network calculations require knowledge of nuclear masses with an accuracy of the order of ideally 100 keV or better, β-decay lifetimes, and the number of neutrons emitted in the β-decay chain leading back to the valley of stability.

As shown in Figure 28, a weakening of the shell gap reduces the discrepancies between the calculated and measured r-process abundances at the N = 50 and N = 82 shell closures [pfe97]. However, it remains to be experimentally determined whether heavy nuclei near the neutron drip line show this effect or whether other effects account for the measured abundances.

Near the proton drip line, the large Coulomb barrier probably makes the general shell structure similar to that observed in nuclei near the valley of stability. This can be tested by studying the proton-rich nuclei below Z = 28 that are mirrors (nuclei with N and Z interchanged) of well-known neutron-rich nuclei. The mirror pair with the most proton-rich nucleus is $^{48}$Ca/$^{48}$Ni [bla00]. Above Z = 28, the proton drip line lies close to N = Z; little is known about single-particle structure in this region. Most nuclei near the proton drip line will be within reach of current facilities and those which will be online in the next few years. However, the great increase in the beam intensities available with RIA will allow for much more precise measurements. The rp-process depends upon the detailed properties of the nuclei near N = Z, whose measurement will require the high beam intensities available at RIA.

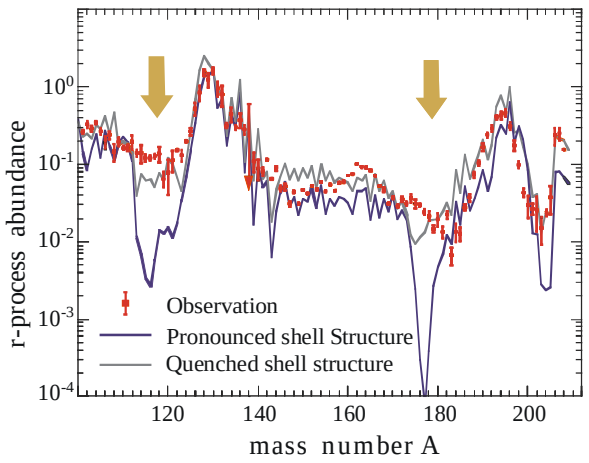


Figure 28: Influence of the shell gap on the r-process abundances, adapted from [pfe97].

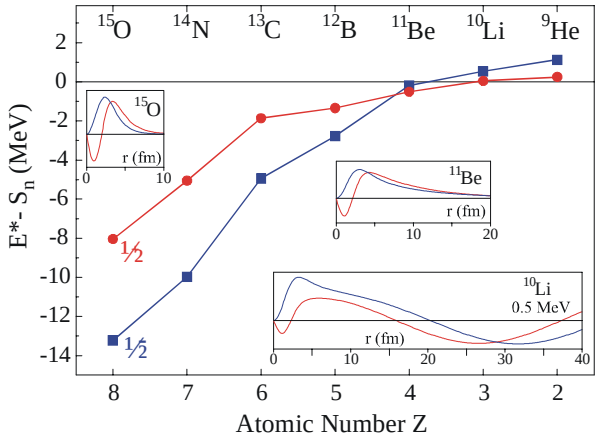


Figure 29: The observed eigenenergy (i.e. the difference between the nuclear excitation energy and the ground state neutron separation energy) is shown for N = 7 isotones as a function of the proton number. For the odd-odd nuclei the energy is the center of gravity of the appropriate multiplet. The insets show *s* and *p* wave functions [han99] calculated for a Woods-Saxon potential.

The last few years have seen the development of experimental techniques, based on fragmentation beams, that can determine the single-particle and collective aspects of nuclei with high sensitivity. Results for neutron-rich nuclei with Z = 2–8 illustrate the power of and prospects for these new methods. Figure 29 shows the evolution of the lowest ½$^-$ (blue) and ½$^+$ (red) states for the N = 7 isotones from the region of nuclear stability to the neutron drip line and beyond. In $^{15}$O, the ½$^+$ (*s*) state belonging to the next (*sd*) shell is 5 MeV above the ½$^-$ (*p*) ground state. This spacing is typical of the normal shell gap between the *p* and *s* states at N = 8. If interpreted as single-particle states (they are actually known to be more complex [sag93]), both are deeply bound with spatially well-localized wave functions shown as $\chi(r) = r\,R(r)$ in the insets of Figure 29, calculated for a Woods-Saxon potential. The two states approach each other with decreasing proton number, and in $^{11}$Be they have crossed [tal60, sag93] so that the ½$^+$ intruder becomes the ground state, and N = 8 is no longer a magic number. The ½$^+$ and ½$^-$ states are bound by only 0.50 and 0.18 MeV, respectively, and both are halos with RMS radii close to 7 fm (the core radius is 2.3 fm). The same states have been observed as resonances in the unbound systems $^{10}$Li and $^{9}$He, see [set87, boh88, boh93, you93, tho99, cag99, che00]. These data represent the first completed systematic exploration of nuclear structure two steps beyond the drip line.

In the following three subsections, we discuss experimental techniques that can be used with fast fragmentation beams. The conventional nuclear models are based on single-particle degrees of freedom, and knockout reactions are especially well suited for studying this feature. The Coulomb excitation of excited states will enable one to determine the deformation in nuclei near the neutron and proton drip lines. Finally, reactions which involve the strong-interaction excitation of the neutron and proton degrees of freedom will be discussed.

In the final subsections we discuss electron capture and β decay. Electron capture plays a crucial role in stellar evolution, and β decay of neutron-rich nuclei is important for the r-process. Theoretical models of electron capture and β decay must be based upon a solid foundation of single-particle and collective properties of nuclei.

## Knockout Reactions

Direct reactions with fast beams are a powerful tool that allows the determination of orbital angular momentum quantum numbers and spectroscopic factors for reactions leading to individual excited states. Special promise is shown by single-nucleon knockout reactions [nav98, tos99]. They have been used to extract spectroscopic factors, which have been compared with the results from large-basis shell-model calculations [bro88]. Measuring the longitudinal momentum distribution provides the basic information about the shell structure of the occupied states. With γ-ray coincidences, the method has been successfully extended to excited-state spectroscopy. The left-hand side of Figure 30 displays the γ-ray spectrum for the reaction $^{9}$Be($^{11}$Be,$^{10}$Be*)X. The right-hand side shows the absolute cross sections obtained by apportioning the total stripping cross section according to the measured absolute branching ratios [aum99]. The total calculated cross section (solid) consists mainly of contributions from removal by neutron knockout (dashed) and diffraction dissociation (dot-dashed) and is in good agreement with data. The momentum distribution $d\sigma_0/dp_z$ for the cross section to the ground state, similar to the cases shown in Figure 12, clearly identifies these knockout reactions as having $l = 0$. The observation of the knockout cross section to the excited $2^+$ state of $^{10}$Be shows that the ground-state of $^{11}$Be contains components coupled to this $2^+$ state. This is direct evidence for a deformed component of the $^{11}$Be ground state which is essential for a complete understanding of the change in the shell structure at Z = 4.

Knockout reactions can be used to study states that are reached by removing a nucleon from any projectile produced by the fast fragmentation method. Although the initial

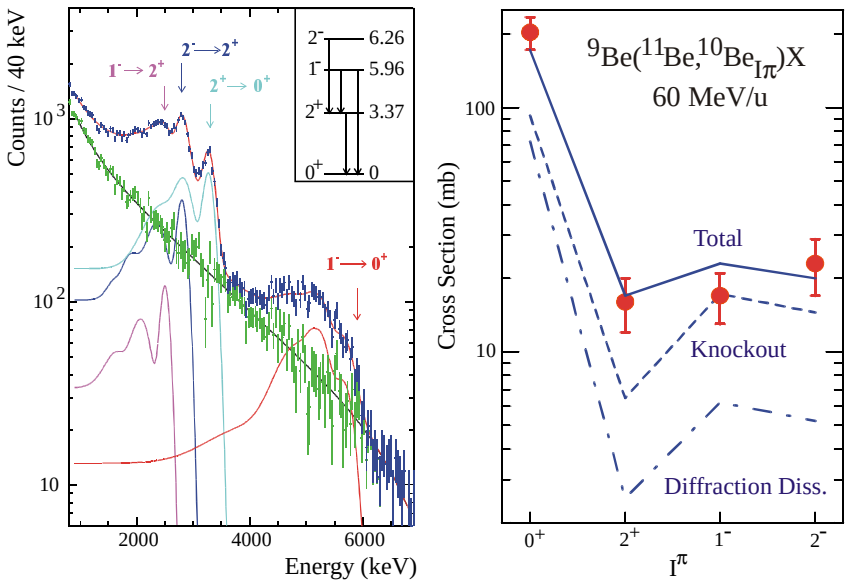


Figure 30: The γ-ray spectrum in the reaction $^{9}$Be($^{11}$Be,$^{10}$Be*)X, observed in coincidence with the projectile residue. The $^{11}$Be level scheme and γ-ray transitions are shown in the inset. The right part shows the experimental absolute cross sections compared with the total calculated values. Adapted from [aum99].

experimental work has been carried out for light nuclei [mad99], in principle the method is applicable to any mass region, and work with neutron-rich nuclei at N = 20 and 28 has already started. With RIA, even heavy fission fragments should come within reach. Early tests of the technique show that precise orbital angular momentum assignments and spectroscopic factors are obtained in known cases. It seems realistic to expect that knockout reactions in those cases where they are applicable will have spectroscopic sensitivity comparable to that of classical transfer reactions. The theoretical strength of the method has been underlined in calculations that compare two different models [bon98, tos99] that are in excellent agreement. Other important assets are, that with increasing energy the theoretical models become more reliable, with the cross sections remaining essentially constant. An important open question is how the knockout technique will be modified in the case of nuclei with large quadrupole deformations; recent theoretical work [sak99] suggests that the shape of the momentum distribution is sensitive to the single-particle motion in a deformed potential.

It is also possible to study transfer reactions with exotic beams in inverse kinematics. With transfer reactions one can study both the removal and addition of nucleons to the projectile. The cross sections for these reactions decrease dramatically with increasing beam energy as a result of the momentum mismatch. Thus the optimal beam energies are the energies available with ISOL and at the lower side of the energies available with fast fragmentation. A recent example of results which can be obtained with fragmentation beams is shown in Figure 31 for the reaction p($^{11}$Be,$^{10}$Be*)d at 35 MeV/nucleon [for99]. The results obtained from this experiment are in good agreement with those of the knockout reaction discussed above. Quite good energy resolution is obtained by observing the angle and energy of the outgoing deuteron, so that the γ-ray coincidence is not needed. However, the sensitivity, is lower because thin targets must be used.

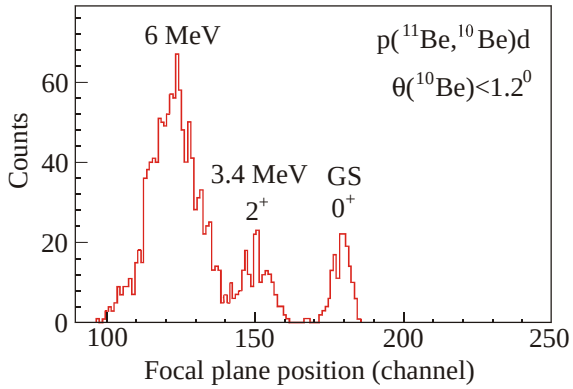


Figure 31: Excitation energy spectrum of $^{10}$Be following the pickup reaction p($^{11}$Be,$^{10}$Be)d, adapted from [for99].

## Coulomb Excitation

Coulomb excitation of even-even nuclei provides a direct measure of the collectivity of the protons in the nucleus via the energy and probability for exciting low-lying states. Coulomb excitation of odd-even nuclei provides additional information regarding single-particle structure and how single-particle degrees of freedom are connected to collective states. The in-beam γ-ray spectroscopy measurement of the energy and quadrupole (E2) transition strength to the first excited 2$^+$ state in $^{32}$Mg (Z = 12) at RIKEN [mot95] experimentally established a large degree of collectivity in this N = 20 nucleus. This is an

example of the change in shell structure away from that found in nuclei near the valley of stability, where N = 20 is a magic number.

The weakening of the N = 28 shell gap has been predicted [wer94, wer96], and the first experimental indication was deduced from half-lives measured in β-decay [sor93]. Measurements of low-lying collective states in even-even argon and sulfur isotopes [sch96a, gla97] confirmed the prediction. Figure 32 illustrates the experimental evidence for a weakening of the N = 28 shell for neutron-rich sulfur (Z = 16) isotopes. For Z = 16, N = 20 is again a magic number, as indicated by the decrease in the deformation and the sharp increase in the excitation energy of the $2^+$ state. However, N = 28 is much less magic than N = 20, as indicated by the small change in deformation and excitation energy at N = 28. The differences between the large-basis shell-model, Hartree-Fock (HF), and relativistic mean field (RMF) calculations shown in Figure 32 illustrate the theoretical uncertainties.

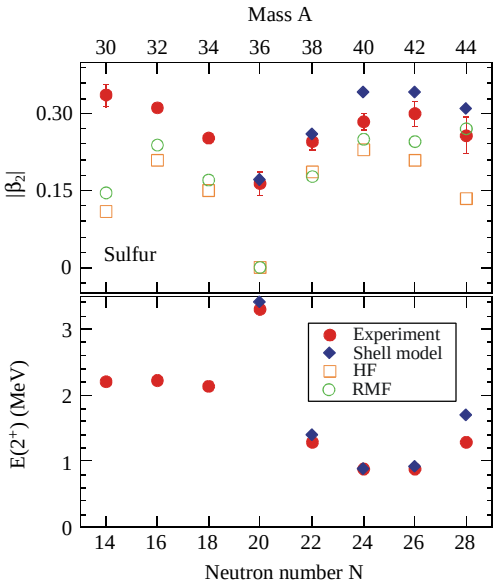


Figure 32: Quadrupole deformation parameters and excitation energies of the first excited states for even-even sulfur isotopes. Adapted from [gla97].

The experimental technique of intermediate-energy (30 MeV/nucleon < $E_{beam}$ < 150 MeV/nucleon, $\beta = v_{beam}/c \approx 0.25–0.5$) Coulomb excitation with photon detection allows for in-beam γ-ray spectroscopy of β-unstable nuclei far from stability with low beam intensities. The energy range is a perfect match for the fast exotic beams from RIA. The technique compensates for the low beam rates with targets that are up to 1,000 times thicker than in comparable low-energy Coulomb excitation experiments, and experiments with beam intensities as low as 1 particle/s are possible. The observation of photons which readily traverse thick targets identifies the inelastic scattering process. Thus one can simultaneously measure the energies of excited bound states and the Coulomb-excitation cross sections. In the last four years, intermediate-energy Coulomb excitation with photon detection has been established as an efficient tool to gain spectroscopic information on exotic beams at GANIL [ann95], RIKEN [mot95, nak97], GSI [wan97], and the NSCL [sch96a, chr97, fau97, gla97, ibb98, ibb99].

Figure 33 schematically illustrates the experimental technique. An intermediate-energy heavy-ion beam transverses a thick, heavy target (thickness ≈ 100–1000 mg/cm$^2$, Z ≈ 80) with little change in velocity. The ions are positively identified after interacting with the heavy target in the beam particle detector to distinguish Coulomb excitation from more violent reaction processes. The beam-particle detector together with the tracking detectors also ensure that the beam scattering angle θ is small. This scattering angle is a direct measure of the impact parameter between projectile and target (see, e.g., [win79, ber88]).

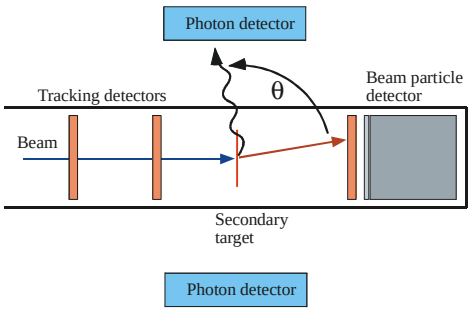


Figure 33: Schematic experimental setup for a projectile Coulomb excitation experiment. The tracking detectors and the beam particle detector ensure that the scattering angle is small, and they positively identify the beam particle after interaction with the target.

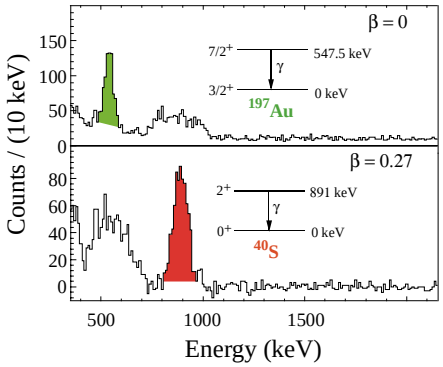


Figure 34: Photon spectra for the reaction $^{197}$Au($^{40}$S, $^{40}$S$^{*}$) at 39.5 MeV/nucleon. Top panel: Spectrum in the laboratory frame with the 547 keV transition in the gold target visible as a sharp peak. In the bottom panel, the 891 keV transition in the projectile becomes sharp after adjusting for the Doppler shift. Adapted from [sch99].

The beam particles are excited in the Coulomb field of the heavy target and de-excite in flight. A position sensitive photon detector measures the energy and interaction point of the emitted photon in the laboratory frame. If the lifetime of the excited state is such that the decay occurs in the target, one can reconstruct the photon energy in the projectile frame on an event-by-event basis. Photons emitted in flight from the projectile can be easily distinguished by their Doppler broadening from γ rays originating in the heavy target. An example of a photon spectrum measured with a position-sensitive NaI(Tl) detector array [sch99] is shown in Figure 34. The location of a peak in the photon spectrum establishes the energy of the transition between the ground state and the first excited state in the nucleus $^{40}$S, and the γ-ray yield is directly related to the Coulomb excitation cross section $\sigma(0^{+}\rightarrow 2^{+})$ [win79, ber88].

The 10% energy resolution of the photon spectrum in this particular example is limited by the intrinsic energy resolution of the NaI(Tl) detectors. With the advent of high-efficiency germanium detectors with position sensitivity (e.g. [hab97, lee97]) it is now possible to achieve energy resolutions of better than 0.5% without losing photopeak efficiency.

Coupled-channels calculations [ber99] which account for the relativistic nature of the beams show that – contrary to low-energy Coulomb excitation – the interaction time between projectile and target is not long enough at intermediate energies to allow for multiple excitations to occur. However, it is possible to excite more than one low-lying state, especially in odd-even and odd-odd nuclei, where low-lying collectivity can be spread out over several states. In this case it becomes important to account for possible feeding from higher-lying to lower-lying states [ibb99]. If the level density becomes too high (e.g., in deformed heavy nuclei with low-lying first excited states), the energy resolution achievable with scintillation detectors ($\Delta E/E \approx 8\%$) becomes insufficient. In these cases, high resolution studies ($\Delta E/E < 0.5\%$) with position-sensitive germanium

detectors are possible, but the secondary target thickness will be limited to the order of 100 mg/cm$^2$ to restrict the velocity change in the target.

Low-energy and intermediate-energy Coulomb excitation studies will complement each other. Low-energy spectroscopic studies with thin targets yield information on multiple excited states and are much less affected by absorption of low-energy photons ($E_\gamma$ < 200 keV) in the secondary target, while studies with fast beams extend the frontiers for in-beam γ-ray studies of neutron-rich nuclei several mass units further from stability.

The feasibility of Coulomb excitation of low-lying states at beam energies above 200 MeV/nucleon has been investigated at GSI with $^{50}$Ti fragments [wan97]. This experiment showed that the increase in background atomic X-rays with increasing beam energy likely limits beam energies to about 200 MeV/nucleon, within the energy range of the fast fragmentation beams from RIA. The cross section for the low-lying $2^+$ state slowly decreases with increasing energy. But the number of reactions also depends on the secondary target thickness, which can be increased with beam energy.

The experimental studies performed up to now have been limited by the available beams to an exploration of the lightest magic nuclei. The beams available from RIA will make it possible to study the N = 50, 82, and (to some extent) 126 magic numbers in the regions where the astrophysical r-process crosses the shell gaps.

## Neutron Deformations

Protons and neutrons contribute differently to transition strengths between low-lying collective states. While Coulomb excitation measurements are sensitive to protons, a strongly interacting experimental probe is needed to probe the neutron distribution in the nucleus. Measurements of both the proton and neutron matrix elements then provide a tool for understanding the relative importance of valence and core contributions to these transitions and provide an additional means for testing the predictive power of theoretical models far from stability.

Close to the valley of β stability, the proton and neutron distributions in the nucleus generally have similar degrees of deformation. However, microscopic calculations suggest that for example in the most neutron-rich sulfur isotopes (N > 28) the proton distributions are more deformed than the neutron distributions by up to a factor of two [wer94]. By comparing deformations of neutron distributions with proton distributions for the most neutron-rich nuclei, it will be possible to experimentally address the question of whether very neutron-rich nuclei have deformed neutron distributions.

Experimental methods for the determination of proton and neutron matrix elements involve the comparison of measurements of a transition using two experimental probes with different sensitivities to proton and neutron contributions. Such studies have been performed on stable targets with a variety of combinations of experimental probes [ber83]. For β-unstable isotopes it is possible to deduce information on the ratio of proton-to-neutron transition matrix elements by comparing electromagnetic excitation strengths to hadronic excitation strengths. The latter can be measured by proton scattering in inverse

kinematics (since proton targets are available and neutron targets cannot be made). This experimental method was pioneered at GSI [kra94] for $^{56}$Ni and has since been used at MSU [kel97, jew99, ril99, mar99] and at GANIL for neutron-rich argon, sulfur and oxygen isotopes. Exotic beams with energies between 30 MeV/nucleon and 100 MeV/nucleon are scattered off proton targets (either plastic targets or cryogenic targets which are 1–3 mg/cm$^2$ thick can be used), and protons with energies between 1 MeV and 20 MeV are detected in segmented silicon detectors at laboratory angles close to 90°. Forward elastic scattering in the center-of-mass corresponds to proton laboratory angles of about 60°–85°, and the same angular domain is relevant for inelastic scattering to low-lying excited states. For such measurements, a silicon strip detector array configured to cover an angular range of approximately $60° \leq \theta \leq 85°$ in the laboratory, would be ideally suited to measure elastic scattering and inelastic scattering to low lying excited states.

These measurements have been performed at the NSCL using beam rates as low as 2000 particles/s with a silicon-strip detector array that covered about 20% of the applicable solid angle. Figure 35 shows the measured proton energy plotted versus their laboratory angle for the reaction $^{38}$S(p,p′). Figure 36 shows measured elastic and inelastic proton angular distributions. The data are compared to microscopic coupled-channels calculations using collective model densities with a density dependent nucleon-nucleon interaction [jeu77, jeu77a, bau98] for the ground state (solid line) and the $2^+$ state (dashed line) [mar99]. These data are possible evidence for different deformations for neutrons and protons in $^{38}$S [kel97].

With the intensities predicted for RIA these studies can be performed in substantially more neutron rich nuclei. For example the sulfur isotopes could be studied up to $^{44}$S which is predicted to have significantly different deformations for neutrons and protons [wer94].

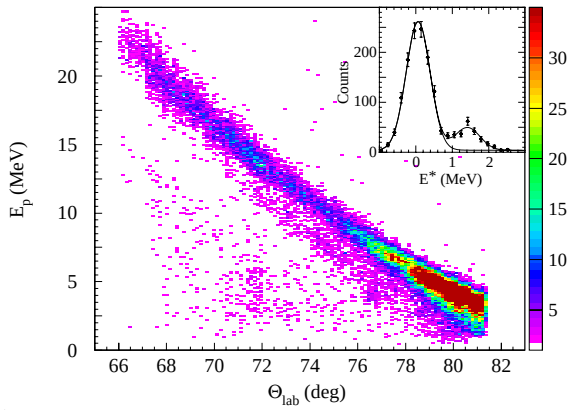


Figure 35: Proton energy versus laboratory angle scatter plot for the center of mass angular range of 27°–30°. The inset shows the excitation energy spectrum. Adapted from [kel97].

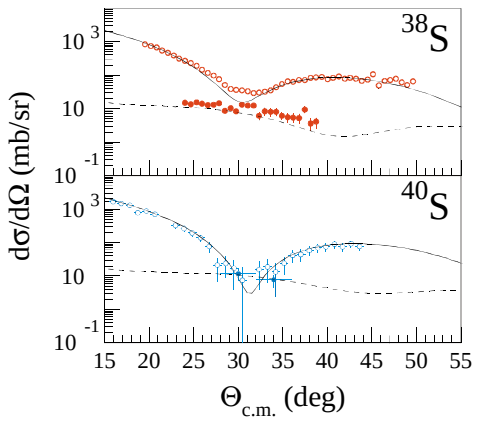


Figure 36: Angular distributions for the ground state (open circles) and the $2^+$ state at 1.29 MeV (solid circles) in the $^{38}$S(p,p′) reaction [kel97] and the $^{40}$S(p,p′) reaction [mar99].

## Gamow-Teller Transitions

Beta decay and electron capture are important both for testing nuclear models and for input into astrophysical models. Some astrophysical phenomena such as the r-process can make relatively direct use of measured β-decay half-lives, whereas the processes of electron capture and neutrino interactions depend upon rates for transitions which are energetically allowed only in hot stellar environments. In the latter case, the rates must be obtained from theoretical models that are tested against known β-decay strength. Gamow-Teller strengths can be inferred from (p,n) and (n,p) type reactions at energies greater than 120 MeV/nucleon [goo80]. It also appears that high-energy inelastic proton and $^{6}$Li scattering can be used to extract spin-dipole strengths in nuclei [aus99]. These strengths determine neutral current neutrino interactions in nuclei.

Such measurements are important for modeling supernovae and supernova nucleosynthesis (see page 66). Weak interaction rates such as electron capture and β-decay in the hot dense presupernova core are important in both Type I and Type II supernova explosions. Electron capture rates affect the number of electrons present (hence the degeneracy pressure) and the neutron-to-proton ratio in the supernova core [ful85]. In the case of core collapse supernovae, rough estimates indicate that successive electron capture and β-decay, together with the associated neutrino emission, might lower the temperature of the iron-like core by as much as 10% [auf94].

Although it is well accepted that half of the heavier element abundance is produced in the r-process, the site is uncertain. One scenario involves neutron star mergers. The nucleosynthesis in such a site is sensitive to the electron fraction and hence to neutrino and weak-interaction rates [fre99]. Neutrino-nucleus interactions are thought to play a key role in the supernova explosion mechanism, in the production of some light p-process nuclei [hof96] (see page 68), and potentially in modifications of the r-process nucleosynthesis distributions [hax97] (see page 54). The cross sections for the relevant neutrino-induced reactions can be inferred from studies of inelastic hadron scattering and charge exchange.

With fast beams from RIA, charge exchange reactions and high energy inelastic proton scattering can be studied in inverse kinematics. For example, (p,n) measurements can be studied using a radioactive beam striking a proton target. For center of mass angles of more than a few degrees, the neutrons are emitted at around 90º in the lab, with energies in the range of 0.5 to 20 MeV. Hence neutron detection is relatively simple, except that an angular resolution of about 1º is required. Similar kinematics occur for inelastic proton scattering. The (n,p) direction can be measured by use of the (t,$^{3}$He) reaction [dia98] and a tritiated polymer foil target. A possible alternative to the measurement of light target recoils is to measure the decay spectrum of the heavy partner via γ-ray de-excitation or particle emission.

The most important nuclei for which electron capture rates are needed are $^{55–60}$Co, $^{56–61}$Ni, $^{54–58}$Mn, and $^{54–59}$Fe [auf94, dea98, mar00]. Electron capture rates can be studied with the (t,$^{3}$He) reaction and require beam intensities in the $10^{6}$ to $10^{8}$ particles/s range, depending on the level of detail required in the measurements. All of these nuclei will be available at

## Core Collapse Supernovae

One of the most important and challenging problems in nuclear astrophysics is to understand the explosion mechanism of core collapse supernovae and the associated element synthesis. Core collapse supernovae are extraordinary events, releasing $10^{53}$ erg of energy in the form of neutrinos of all types at the staggering rate of $10^{57}$ neutrinos per second, and generating the conditions for the synthesis of many new nuclei. The explosion ejects these nuclei into the interstellar medium, where they can be incorporated into new stellar systems like our own, forming the basis for life itself. Left in the wake of the explosion is a relativistic object, a black hole or a neutron star that may contain new forms of hadronic matter. As a result, a supernova is a unique cosmic environment for studies of nucleosynthesis, neutrino properties, and nuclear matter at extremes of density, temperature, and neutron-to-proton ratio.

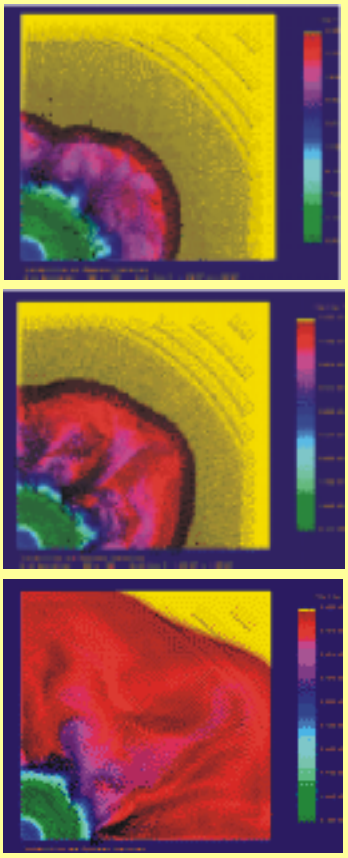

In our current picture of the supernova process, an outgoing shock wave – formed when the iron-like core of a massive fully evolved star collapses gravitationally and rebounds at high (supranuclear) densities – stalls as a result of energy losses due to nuclear dissociation and neutrino emission. A few seconds later, the shock is re-energized by the intense neutrino flux emerging from the protoneutron-star at the stellar center. The shock induces explosive nucleosynthesis in the outer layer, leading to the observed explosion. The observation of neutrinos from SN1987A gives us some confidence that this picture is at least qualitatively correct. Yet this attractive idea has not borne fruit – supernovae simulations have not consistently resulted in explosions. It is not clear where the fault lies: in inaccurate knowledge of the nuclear structure physics involved and of the nuclear equation of state, or in the manner by which energy is transported by neutrinos, or in the absence of multidimensional calculations that can fully take into account the relevant microphysics. To remedy this situation, computer simulations involving accurate multidimensional, neutrino-energy-dependent radiation transport and radiation hydrodynamics must be supported by commensurate improvements in the microphysics.

This will require the integration of state of the art supernova simulation and nuclear structure computation to model both the explosion mechanism and supernova nucleosynthesis. Only a consistent treatment of the explosion and its nucleosynthesis will allow the use of observational constraints such as isotopic abundances, $\gamma$-ray and neutrino fluxes, to obtain information on the explosion mechanism. Challenges include modeling lepton number losses during the infall stage, the stellar core equation of state, post-core-bounce neutrino heating, and the nucleosynthesis that takes place in the ejecta.

(Figure adapted from: http://www.psc.edu/science/Burrows/burrows.html
Text from: “Opportunities in Nuclear Astrophysics: Origin of the elements”)

RIA at rates of greater than $10^8$ particles/s. For the case of N = Z nuclei, (p,n) measurements can provide equivalent information. The (p,n) measurements can also be used to test large basis and Monte Carlo shell model calculations of GT-distributions. The beam intensities will be sufficient to allow these measurements to be performed for all the nuclei of interest in the *fp*-shell.

## Beta-Decay Studies

Beta-decay properties of unstable nuclides far from stability can provide valuable insight into the evolution of shell structure and nuclear deformation toward the drip lines. Precise theoretical predictions of β-decay lifetimes are difficult since the Gamow-Teller resonance, responsible for most of the β-decay strength in nuclei, lies at excitation energies around 20 MeV, well above the Q-value window (typically less than 10 MeV). The main features of β-decay are therefore governed by the tail of the Gamow-Teller resonance, and are not constrained by the limits placed on the overall Gamow-Teller strength by single-particle selection rules. For nuclei very far from stability, binding energy uncertainties and the interplay between normal and continuum states in weakly bound nuclei present additional challenges to the calculation of β-decay rates. Fully self-consistent theoretical calculations employing well-established nuclear interactions are now being performed on neutron-rich nuclei with magic neutron numbers [eng99]. These calculations reproduce the limited half-life data for neutron-rich nuclei along the N = 50 and N = 82 isotones fairly well. Extending the known β-decay rates to more exotic nuclei will require further improvements in the nuclear interactions employed in these microscopic calculations, which may eventually expand the applicability of these theoretical methods to open-shell nuclei with non-spherical ground states.

Nuclei at the drip lines offer additional opportunities to study new and unusual features of β decay. For example, "super" Gamow-Teller β transitions may exist in the heavy, neutron-deficient nuclei near the N = Z line, for which most of the Gamow-Teller resonance is predicted to lie within the β-decay Q-value window. The β decay of $^{100}$Sn is predicted to proceed with nearly 100% of the total Gamow-Teller sum-rule strength to a low-energy $1^+$ level in $^{100}$In [bro94]. Since all observed Gamow-Teller transition strengths, except for A = 3, are consistently smaller than the theoretical sum-rule estimates, this unique β decay in $^{100}$Sn could appropriately be labeled a "super" Gamow-Teller transition.

Precise β-decay half-lives, as well as β endpoint energies to determine masses, are crucial nuclear physics input parameters for network calculations of the astrophysical r-process. Studies of nuclei near the waiting points at the magic neutron shell closures N = 50, N = 82, and N = 126 are particularly important (Figure 37). The disparity between theoretical estimates and the β-decay lifetimes measured for a few N = 50 and N = 82 r-process isotopes in the last decade have clearly demonstrated the need for experimental data on very neutron-rich nuclei near neutron shell closures to improve our understanding of both nuclear structure far from stability and of r-process nucleosynthesis [kra93].

The β-decay lifetimes of neutron-deficient nuclei adjacent to the N = Z line govern the behavior of X-ray bursters and the synthesis of heavy elements in X-ray pulsars. If fast α-

## The p-process nuclei

The r- or s-processes cannot make certain rare nuclides that lie on the proton rich side of the valley of stability. Understanding the synthesis of these p-process nuclei has been a long-standing challenge, partly because at least three different processes can produce them: the gamma-process, the rp-process, and the neutrino-process. The gamma-process is the result of a high temperature stellar environment, such as that found in supernovae, and involves photo-erosion of preexisting abundant heavy nuclides by (γ,n), (γ,p), and (γ,α) reactions induced by the ambient blackbody photons. The nuclear statistical model should be applicable for the calculation of the rates of these reactions. Comparison with (n,γ) and (p,γ) data show that these rates (and their inverses) can often be predicted to within a factor of two. In contrast, (α,γ) measurements indicate that the calculated rates can be wrong by a factor of ten or more, apparently because of poorly known α-particle optical potentials at such low energies. These uncertainties might be reduced substantially by low-energy (n,α) measurements that can constrain the α-particle potentials. Studies of Coulomb-breakup of radioactive nuclei at a fragmentation facility or using a free electron laser facility should also provide information on these reactions.

The rp-process that occurs in the hydrogen-rich layer accreted on a neutron star may be responsible for production of some of the lighter p-process nuclides: isotopes of Mo and Ru, whose anomalously high abundances have been difficult to produce in the gamma-process models. An additional issue is whether the radiation pressure is sufficient to overcome the enormous gravitational attraction of the neutron star and blow a small fraction of the produced material into the interstellar medium. This depends on the rate of energy production. To determine the feasibility of the rp-process will require measurements of masses and β-decay lifetimes for the progenitors of Mo and Ru (light Pd, Ag, and Cd isotopes), and around lower-mass bottlenecks such as $^{72}$Kr.

The neutrino-process occurs in the high neutrino flux produced by the protoneutron-star in a core-collapse supernova. More abundant nuclei are excited to unbound states (which later undergo particle decay) by neutrino induced inelastic scattering or charge exchange reactions. This mechanism can affect the abundances of r-process nuclei, especially those on the lower-mass side of the r-process peaks, and produce a significant abundance of isotopes like $^{7}$Li, $^{11}$B, $^{19}$F, $^{138}$La, and $^{180}$Ta. It may also produce light p-process nuclei such as $^{92}$Mo.

("Opportunities in Nuclear Astrophysics: Origin of the elements")

decays or β-delayed α-particle decays of nuclei near the limits of stability dominate, as is expected for the decay of very neutron-deficient tellurium, iodine, and xenon isotopes, a natural halting point for the rp-process is reached. The experimental determination of β-decay rates for neutron-deficient nuclei above tin (Z = 50) will improve the predictions of astrophysical network calculations for the elemental abundances of the heaviest species produced by rp-process nucleosynthesis.

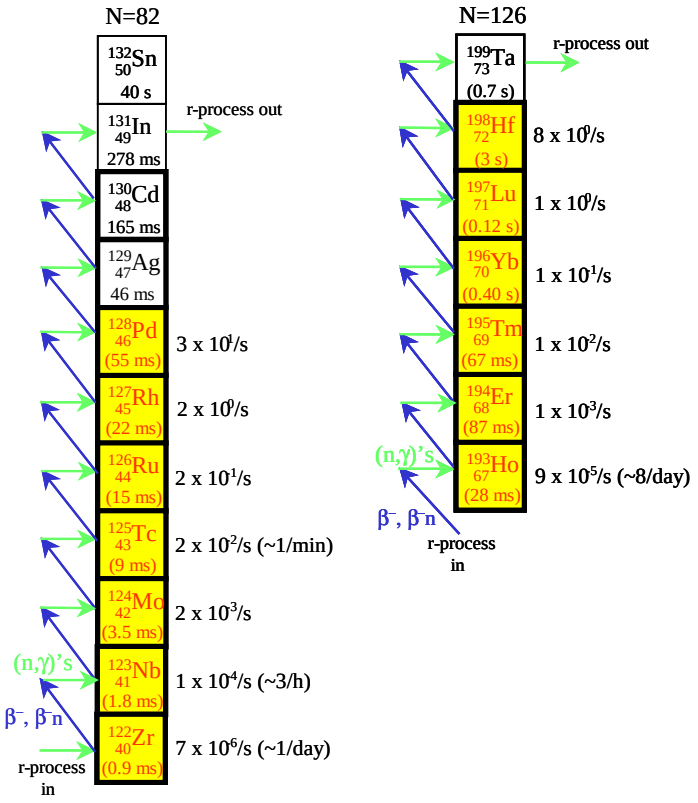


Figure 37: Possible r-process pathways through the very neutron-rich nuclei at N = 82 and N = 126. The important r-process waiting points are indicated as thick squares. Nuclei with unknown β-decay properties that are accessible at RIA are marked in yellow (predicted half-lives are listed in parentheses). The production rates predicted for fast beams from RIA are indicated to the right of each nuclide. The β-decay half-lives for N = 82 isotopes are from [kra00], for N = 126 isotopes from [moe97].

Significant progress has been made in the measurement of β-decay half-lives of exotic nuclei. This can be directly attributed to particle-detection techniques employed with fast fragmentation beams. It is necessary to have unique identification of the β-emitting source to assign the properties of the β decay correctly because the energy spectrum is continuous. For fast beams, energy loss, time-of-flight, and magnetic rigidity can be used to determine the atomic number and mass of each fragment on an event-by-event basis. Such clean particle identification, readily available with fast fragmentation beams, would be difficult to accomplish with recoil separators or on-line isotope separators at low energies.

Silicon strip detectors have proven successful in the correlation of recoil implants and rare proton decays [sel92] and are now used extensively in low count-rate β-decay measurements with fast fragmentation beams [lon98]. The high granularity of the strip detector allows the use of continuous beam implantation for rates of less than 100 particles/s. Since implants and decays are detected event-by-event, a mixed-isotope (cocktail) fragmentation beam can be utilized, and several decay measurements can be performed simultaneously. The use of silicon strip detectors to correlate fast beam implants with subsequent β-decays will be highly effective in extending half-life measurements to very exotic nuclei produced at rates of a few per day.* The detectors also provide a highly efficient means for measuring β-delayed protons and α particles. A strip detector

* For much higher intensities (>10 particles/s), more conventional techniques can be used and complete decay schemes can be obtained without particle-by-particle tagging.

arrangement can be readily complemented with a modest array of germanium detectors to directly correlate fragment implants and isomeric γ-ray transitions, or to study low-energy structure via correlated β-delayed γ-ray measurements [ree99].

The correlation of fast beam implants and subsequent β particle emissions to measure decay half-lives has been applied to a variety of very neutron-deficient and neutron-rich exotic nuclei. The study of the β decay of $^{100}$Sn at GSI [sum97] demonstrates the effectiveness of fragment-decay correlations measurements employing low implantation statistics. A half-life determination (having a 50% error) was made for a total of only seven $^{100}$Sn nuclei implanted over an 11-day period.

RIA will produce fast beams of the short-lived nuclei around $^{100}$Sn with sufficient rates to perform detailed studies of the low-energy structure of nuclear species important to rp-process nucleosynthesis. On the neutron-rich side, RIA will allow studies of the majority of r-process nuclei along the N = 82 waiting point, and make it possible to reach 5–6 of the N = 126 waiting point nuclei (Figure 37). These isotopes are 10–20 mass units beyond the current border of experimentally known nuclei. All of the short-lived r-process waiting-point nuclei marked in Figure 37 will be accessible with fast fragmentation beams at RIA.

## Static Nuclear Moments

The nuclear magnetic dipole moment has considerable sensitivity to the relative amplitudes of different components of the nuclear state wave function [gri92, gei99], while the electric quadrupole moment provides a measure of the deviation of the nuclear charge distribution from spherical symmetry. The direct measure of ground-state magnetic dipole and electric quadrupole moments of short-lived nuclei will play an important role in identifying shell structure anomalies predicted for neutron-rich nuclides [dob96a]. For self-conjugate and other mirror nuclei, the isovector and isoscalar combinations of known ground state magnetic dipole moments of mirror nuclei provide an important and sensitive framework to test isospin symmetry in nuclei [sug69].

Until recently, the main source of information on nuclear moments and charge radii has been the extensive results from laser spectroscopy and atomic-beam methods, especially those developed at ISOLDE [ott89]. For example, new and important data which probe the ground state structure of light drip-line nuclei $^{11}$Li, $^{11}$Be, and $^{17}$Ne [neu00] have helped to provide a more complete picture of the extended nature of the ground state wavefunctions of these nuclei. The recent application of nuclear magnetic resonance (NMR) and level mixing resonance (LMR) methods to spin-polarized and spin-aligned fast fragmentation beams has proven effective in deducing magnetic dipole and electric quadrupole moments of exotic nuclei. These resonance techniques, coupled with fast beams, are especially suited for short-lived, lighter nuclei, where the traditional methods of laser spectroscopy and on-line nuclear orientation are less efficient.

The substantial spin polarization observed for fast beams produced away from zero degrees by intermediate energy projectile fragmentation [asa90] is significantly larger than that measured using tilted-foil techniques on low-energy beams [rog87, lin95]. Coupled with the technique of nuclear magnetic resonance on β-emitting nuclei (β-NMR), nuclear

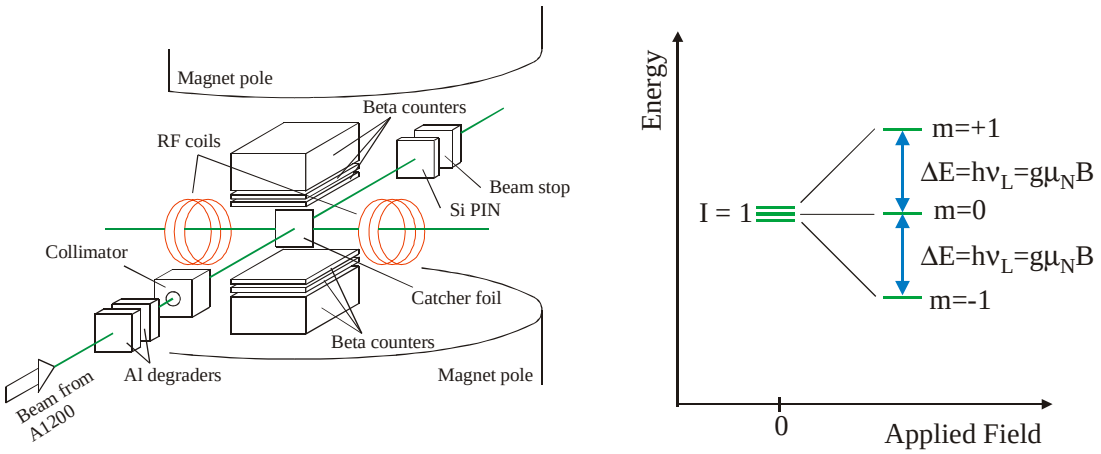


Figure 38: Left: Beta-NMR setup at the NSCL. A set of coils perpendicular to the applied magnetic field provide the rf field for the resonance measurements [man97]. Right: NMR splitting diagram for an I = 1 nucleus. At B = 0, the magnetic substates are degenerate. At B ≠ 0, the splitting between substates is directly related to the applied field strength and the magnitude of the nuclear *g* factor.

moment measurements have been performed by groups at RIKEN, GSI, and MSU on spin-polarized fast beams produced at rates of a few hundred radioactive nuclei per second (see Figure 38). In a traditional β-NMR measurement, the angular distribution of β particles emitted from implanted polarized isotopes is measured. When the polarized sample is exposed to radiofrequency (rf) radiation at the Larmor frequency, a redistribution of the magnetic substates will occur, and the β angular distribution will be altered. For a purely magnetic interaction, the nuclear *g* factor is determined directly from the Larmor frequency and the magnitude of the directional magnetic holding field. Measurement of the electric quadrupole moment involves implantation of the fast fragmentation beam having nuclear spin $I \geq 1$ into a non-cubic host. The quadrupole and dipole interactions between the short-lived impurity and host will result in multiple resonances, which can be excited simultaneously if one has knowledge of the magnitude of the magnetic interaction [izu96]. The β-NMR method is well suited for the study of short-lived nuclides, since the nuclear β decay must precede relaxation of the nuclear spin polarization, which typically occurs in a few seconds.

New methods are currently developed that optimize the magnitude of induced fragment spin-polarization before NMR is observed. Adiabatic rotation of a magnetic holding field has been used at RIKEN to determine the nuclear spin polarization of $^{18}$N fragments produced by fragmentation of a $^{22}$Ne beam [oga99]. At MSU, a pulsed magnetic field method was employed to determine the magnitude of spin polarization of $^{12}$B nuclei without the use of NMR [ant00]. Both methods can be applied at fast beam implantation rates of a few hundred ions per second.

The combined nuclear magnetic dipole and electric quadrupole moments for short-lived nuclei can be deduced using the level-mixing resonance (LMR) technique [ney97], which

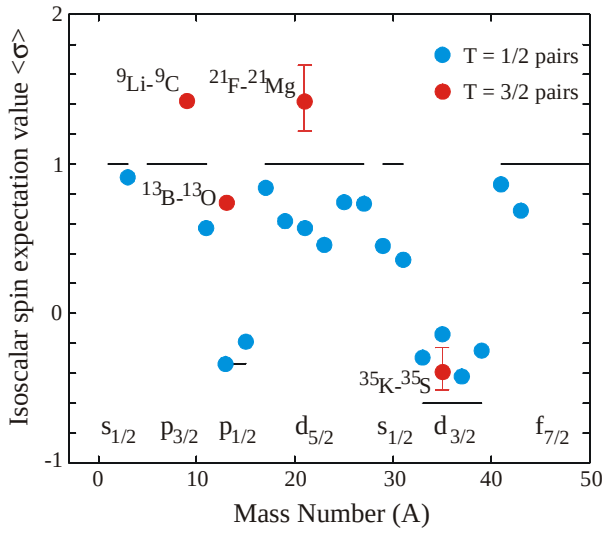


Figure 39: Isoscalar spin expectation values for T = 1/2 (blue) and T = 3/2 (red) mirror pairs. The solid lines represent the limits on <σ> calculated using the extreme single-particle model. (Adapted from [mat96] with additional data from [man98, sch98]).

relies on an initial spin alignment of a fast beam of short-lived nuclei. Spin alignment can typically be achieved in fast fragmentation reactions by selecting nuclei produced at zero degrees, where there is a maximum in the fragment angular distribution. A ratio of the nuclear electric quadrupole moment to the magnetic dipole moment, $\nu_Q/\mu$, can be determined by observing a resonant onset of β asymmetry as a function of applied magnetic field. For the implantation of nuclei with $I \geq 1$ into a non-cubic host, the induced nuclear polarization is achieved through a mixing of two hyperfine levels. To extract $\nu_Q/\mu$, the electric field gradient for the implanted exotic beam in the non-cubic host material must be known. The magnetic moment can be derived independently by adding a small radiofrequency (rf) field perpendicular to the applied magnetic field [ney99]. Allowed $\Delta m = \pm 1$ transitions induced by the applied rf on either side of the level mixing resonance can be detected by monitoring the β counting rates. The positions of the resonances due to the rf field can be used to independently derive μ.

An extreme example of the unexpected deviation of mirror moments from theoretical predictions is the small ground state magnetic moment of the $T_z = -3/2$ nucleus $^9$C [mat96, huh98]. When combined with the ground state magnetic moment of the $T_z = +3/2$ mirror partner $^9$Li, an anomalously large value of 1.44 is attained for the isoscalar spin expectation value <σ> (Figure 39). The extreme single particle model predicts a maximum of 1.00 for this <σ> value, where <σ> is twice the Pauli spin factor S. The results of shell model calculations including isospin non-conserving terms in the nuclear Hamiltonian could not fully reproduce the large <σ> value for the T = 3/2, A = 9 mirror system. Other theoretical approaches [kan95, var95] have failed to describe the observed $^9$C-$^9$Li mirror moments. The significance of the weak binding ($S_p$ = 1.3 MeV) of $^9$C, which has an extreme proton-to-neutron ratio (Z/N = 2), has not been fully investigated.

Very neutron-deficient nuclei having A > 40 will be produced in sufficient quantities and with sufficient polarization or alignment using fast fragmentation beams at RIA to allow the measurement of their ground state magnetic dipole moments. Since these heavier mirror nuclei lie along the proton drip line, they will serve as excellent laboratories to further explore details of isospin symmetry in nuclides with low proton binding energies.

## Microsecond Isomers

The previous subsections focused on the study of ground states and lowest-energy excited states of exotic nuclei, typically at low angular momentum. Probing structural details of very neutron-rich nuclei at higher energy and angular momentum is an experimental challenge that can be addressed at RIA using isomeric beams produced in fast fragmentation reactions. Experimental studies of isomeric states and their subsequent γ-ray decays help determine the evolution of single-particle states as well as the residual interactions between valence nucleons. Isomeric states in neutron-rich nuclei may also serve as models for the weakly-bound ground states of nuclei near the neutron drip line. If the excitation energy of the isomer is close to the neutron separation energy, the isomeric state simulates the ground states of even more exotic nuclei [ryk98].

Fast fragmentation beams can efficiently populate metastable states in nuclei [grz95, pfu98], including configurations of relatively high spin [pod00]. The γ-ray decay of these isomeric states can be studied after the traversing the fragment separator, which is of the order of 100 ns. Isomeric states with half-lives of microseconds or less are therefore accessible after stopping of the fast fragmentation beam.

New isomeric states in exotic nuclei, including, for example, neutron-deficient $^{66m}$As [grz98a], $^{102m}$Sn [grz97], and neutron-rich $^{78m}$Zn [dau00], have been discovered using fragmentation facilities. The decay properties of these isomeric states have provided new and unique information on nuclear properties near the N = Z line, in the close vicinity of doubly-magic $^{100}$Sn, and for neutron-rich nuclei between neutron shell closures at N = 40 and N = 50. The identification of a 210 ns, $I^{\pi} = 8^{+}$ isomer in $^{70}$Ni produced by fragmentation of a $^{86}$Kr beam at 63 MeV/nucleon [grz98] provided the first data for the energy of the first $2^{+}$ state of $^{70}$Ni (Figure 40), and confirmed the magic character of the N = 40 subshell closure at Z = 28. RIA will be ideally suited to extend the detailed studies of isomers to the most exotic nuclei, the regions beyond $^{100}$Sn and $^{78}$Ni and near $^{60}$Ca. Detailed spectroscopy of predicted isomeric states in nuclei as exotic as the N = 48 isotones of the magic systems $^{98m}$Sn and $^{76m}$Ni will be achievable with RIA.

RIA will have sufficient intensities to permit measurements of nuclear level lifetimes, angular correlations, *g*-factors, or even secondary reactions for previously discovered isomers. For example, one may envision making unique spin and parity assignments, as well as deducing the excited state *g*-factors for $^{78m}$Zn and $^{98m}$Cd, which lie at the two extremes of the N = 50 shell closure. The determination of excited-state *g*-factors using spin-aligned beams has been demonstrated for $^{45m}$Sc ions ($I = 19/2^{-}$, $T_{1/2}$ = 472 ns) [sch94] and several isomers in the region of $^{68}$Ni produced via projectile fragmentation [ney00]. In both measurements, sufficient alignment and intensity were obtained to observe the time-dependent perturbed angular distributions for several γ rays depopulating the short-lived isomers.

Isomeric studies with fast fragmentation beams are possible at implantation rates of only $10^{-3}$ particles/s. The isomers are identified by the time correlation of the implanted ion and the delayed γ-ray decay which is in the μs-range. This gating technique significantly reduces the γ-ray background (see Figure 40) and permits the identification of a μs-isomer

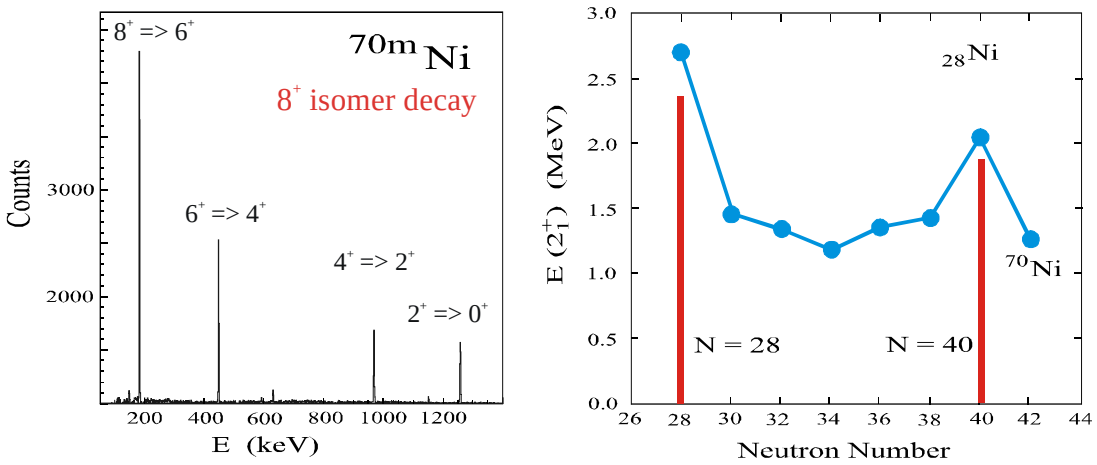


Figure 40: Left panel: Gamma-ray spectrum of $^{70m}$Ni ($T_{1/2}$ = 210 ns, $I^{\pi} = 8^{+}$) measured in the fragmentation reaction of a E/A = 63 MeV $^{86}$Kr beam and selected by the ion-γ μs-time correlations [grz98]. Right panel: E($2^{+}_{1}$) systematics for even-even Ni isotopes.

of a particular isotope with a few thousand implanted ions. This observation window can be extended down to the nanosecond time scale, in specific cases, when the ionic half-life is significantly longer than for a neutral atom. Since many fragmentation products at RIA will be transmitted as fully-stripped ions, the conversion electron channel of the isomer decay is blocked during flight. Isomeric ions are then transmitted with minimal in-flight decay losses. An example is the observation of the $T_{1/2} = 35 \pm 10$ ns, $I^{\pi} = 0^{+}$ shape isomer in $^{74}$Kr [cha97].

# Appendix A: Rate Estimates for Experiments With Fast Beams

There is a compelling scientific case for the incorporation of an advanced fast fragmentation beam capability into the base plan of RIA. Experiments with fast beams can be performed with low beam intensities. Whenever fast beams can be used, they have a solid lead in sensitivity over re-accelerated beams by as much as several orders of magnitude. This increase in sensitivity arises from the increase of luminosity due to the use of thicker secondary targets, background free tracking and tagging of individual particles, improved detection efficiency due to strongly forward focused kinematics, and fast, chemistry-free production. Many experiments with fast beams can be run simultaneously with experiments at the stopped target station or with the more intense re-accelerated beams of isotopes closer to the line of stability needed for studies that require low-energy precision beams (discussed in the 1997 Report *Scientific Opportunities with an Advanced ISOL Facility*). RIA can provide capabilities for the two complementary techniques already recognized in the 1996 LRP: the ISOL re-acceleration technique and the projectile fragmentation technique. Together, the two techniques will provide unprecedented access to the unknown territory of rare isotopes far from the line of stability.

Experiments with fast fragmentation beams will not replace those with re-accelerated ISOL beams but they will allow the study of important additional physics, primarily in the region very far off stability where production rates are low, or when high energies are required as for giant resonance excitations and charge-exchange reactions.

Table 1 summarizes the main methods and minimum beam intensities needed for important classes of experiments with fast fragmentation beams. The minimum rates listed in Table 1 were derived from actual experiments whenever possible. Individual rate estimates are explained in the following numbered paragraphs, and references are given to existing experimental work that serves as proof-of-principle or substantiates the estimates given.

1. DETECTION AND IDENTIFICATION: The limit of $10^{-5}$ particles/s corresponds to the observation of ~1 particle per day. In special cases, longer beam times with even lower count rates are justified. Two events of the proton-rich doubly-magic nucleus $^{48}$Ni were observed over several days of beam time [bla00]. Similarly, the neutron-rich doubly-magic nucleus $^{78}$Ni was observed in an experiment with 3 events over 5 ½ days [ber97].

2. STRIPPING REACTIONS: Nuclear properties beyond the drip lines have been studied using stripping or pick-up reactions from exotic nuclei produced in fragmentation reactions with beam intensities as low as ~2000 particles/s [kry95]. Typical beam energies are ~50 MeV/nucleon.

3. MASS MEASUREMENTS: Mass measurements with fast fragmentation beams have been performed, for example, at GANIL using the direct time-of-flight technique with a high-resolution magnetic spectrometer. With this technique, a mass resolution of $3 \cdot 10^{-4}$ was achieved. This resulted in an accuracy of $4 \cdot 10^{-6}$ for the mass of $^{29}$Na with the detection of

Table 1: Estimated minimum beam intensities for various experiments that are well suited for fast fragmentation beams.

| | Method | Part./s | Physics |
|---|---|---|---|
| 1. | Detection and identification | $10^{-5}$ | Limits of nuclei, Existence |
| 2. | Stripping reactions | $10^{4}$ | Nuclear properties beyond the drip lines |
| 3. | Mass measurements | $10^{-2}$ | Masses, explosive nucleosynthesis |
| 4. | Interaction cross section | $10^{-2}$ | Radii, nuclear size |
| 5. | Knockout reactions | $10^{-1}$ | Halos, cluster models, spectroscopic factors |
| 6. | Heavy-ion collisions | $10^{5}$ | Nuclear compressibility, EOS, supernovae |
| 7. | Giant dipole resonance | $10^{6}$ | Nuclear size and shape, r-process |
| 8. | Giant monopole resonance | $10^{7}$ | Nuclear compressibility, EOS, neutron stars, supernovae |
| 9. | Coulomb excitation ($2^{+}$) | 1 | Evolution of shell structure, r-process |
| 10. | Elastic scattering | $10^{3}$ | Radii, density distributions |
| 11. | Inelastic scattering | $10^{3}$ | Nuclear structure, rp-process |
| 12. | Coulomb breakup | $10^{4}$ | Proton drip line, rp-process |
| 13. | Charge exchange | $10^{6}$ | Gamow-Teller strength, supernova core evolution, |
| 14. | Lifetimes/β-decay studies | $10^{-3}$ | Nuclear deformation, shell evolution, explosive nucleosynthesis, r-process, |
| 15. | β–NMR | 10 | Ground-state moments |
| 16. | Micro-second isomers | $10^{-3}$ | Shell structure, single particle states |

only 5000 nuclei [orr91]. Assuming no further improvements in the method, the required intensity for a 7 day experiment is 0.01 particles/s.

4. INTERACTION CROSS SECTIONS: Interaction cross section measurements were among the first experiments with fast beams of exotic nuclei [tan85]. The interaction cross section of $^{8}$He on Be, C, and Al targets was measured to ±1% with a beam intensity of 500 particles/s [tan85a]. Interaction cross sections and two-neutron removal cross sections of $^{8}$Li, $^{9}$Li, and $^{11}$Li were measured with intensities as low as 0.1 particles/s [bla93]. A total of ~1000 incident particles are sufficient so that with a rate of 0.01 particles/s the experiment can be performed within one day.

5. KNOCKOUT REACTIONS: The estimate is based on a recent study of the neutron knockout reaction $^{9}$Be($^{19}$C,$^{18}$C$_{gs}$)X [mad99]. The experiment was carried out with an incident beam of 0.5–1 $^{19}$C per second, and several targets were measured over a period of 3 days. This experiment shows that it is possible to obtain precise and detailed spectroscopic information in knockout reactions with very weak beams. The estimate of the needed intensity given in the table is probably conservative; it assumes an order-of-magnitude

improvement arising from a better γ-ray detection system combining germanium and sodium iodide, from reduction of the reaction-induced background, and from the use of higher beam energies. The energy loss in the target makes the proton knockout reaction less favorable by roughly an order-of-magnitude; therefore the analogous $^{9}$Be($^{27}$P,$^{26}$Si$_{gs}$)X experiment used a target of only 14 mg/cm$^2$.

6. HEAVY-ION COLLISIONS: The flow measurements for charged particles performed at Lawrence Berkeley Laboratory with the EOS TPC [par95] were measured with stable beams having intensities of about $5 \cdot 10^3$ particles/s and target thickness in the range of several hundred mg/cm$^2$ [rai90,kea00]. For cases of special interest, flow measurements can be performed with slightly lower radioactive beam intensities of $10^3$ particles/s. To measure neutron flow requires higher beam intensities; the measurements of [zha95] were performed with beam intensities of $10^5$ particles/s [kea00]. The projectile fragmentation measurements with the ALADIN spectrometer (see right panel of Figure 19) were performed with stable beam intensities less than $10^4$ particles/s and targets with thicknesses in the range of several hundred mg/cm$^2$ [sch96]. For cases of special interest projectile fragmentation measurements should be possible with radioactive beam intensities of $10^3$ particles/s. Measurements of multifragmentation in central collisions and neck fragmentation in peripheral collisions require incident energies of the order of E/A = 35–100 MeV and targets with thicknesses of 5–10 mg/cm$^2$. Similar multifragmentation measurements were performed with stable Au beams with average intensities less than $10^5$ particles/s [tsa93]. This would also mark the lower intensity range for such measurements with radioactive beams.

7. GIANT DIPOLE RESONANCE: The GDR in exotic nuclei can be studied with virtual photon scattering (measuring the γ-ray decay back to the ground-state) [var99] or with virtual photon absorption (the GDR is reconstructed from the energies and angles of the decay products) [aum99a]. The first virtual photon scattering experiments were limited by presently available beam intensities ($< 5 \cdot 10^5$ particles/s), but beam intensities of $> 10^6$ particles/s should be sufficient to extract the GDR. Virtual photon absorption has a larger cross section and experiments should be possible with even lower intensities.

8. GIANT MONOPOLE RESONANCE: The study of the GMR in exotic nuclei will be extremely difficult. So far no experiments have been performed, partly because of the large intensity needed. The low energies of the scattered target nuclei requires the use of gas targets. Beam intensities $>10^7$ particles/s will be necessary.

9. COULOMB EXCITATION: At intermediate energies, Coulomb excitation experiments have been performed at RIKEN, Michigan State, and GANIL [ann95, mot95, nak97, wan97, sch96, chr97, fau97, gla97, ibb98, ibb99]. The lowest beam rates used were 15 particles/s in the study of $^{44}$S [sch96] and 3 particles/s in the study of $^{31}$Na [pri00]. Each experiment lasted three days. In the latter case, the first excited state of $^{31}$Na was studied at a secondary beam energy of 59 MeV/nucleon with a 702 mg/cm$^2$ thick gold target. The efficiency of the photon detector used can be increased by a factor of about 5 (for low γ-ray energies) to 20 (for high γ-ray energies) and the target thickness by 30–50%. In a three-day experiment, rates of 0.5 particles/s will result in publishable data.

10.-11. ELASTIC AND INELASTIC SCATTERING: At intermediate energies, proton elastic scattering angular distributions which allow the extraction of an optical model (i.e., they include at least one minimum in the angular distribution) have been measured with beam rates as low $2 \cdot 10^3$ particles/s [mar99]. The $(CH_2)_n$ target used was about 2 mg/cm$^2$ thick. The inverse kinematics mechanism focuses the projectiles into a small scattering cone which allows for efficient particle detection. At the angle of the minimum in the angular distribution the elastic scattering cross sections are comparable to inelastic cross sections.
At low energies, the scattering cross sections are comparable to those at higher energies and targets of similar thickness can be used. With a detector of large solid angle, scattering experiments which can yield optical model parameters should be possible at rates similar to the ones used in fast-beam experiments. In cases where the cross sections are more favorable, meaningful experiments can be performed with even lower rates. Quasi-elastic scattering of $^{11}$Li from $^{12}$C was studied at 60 MeV/nucleon with beam rates of 50–200 particles/s on a 592 mg/cm$^2$ thick target [kol92].

12. COULOMB BREAKUP: Coulomb break-up reactions for astrophysically interesting nuclei have been performed at RIKEN with $10^4$ particles/s of $^8$B and $^{14}$O at 91.2 MeV/nucleon [mot91, mot94]. $^8$B breakup was measured at GSI with $10^3$ particles/s at 350 MeV/nucleon [iwa99].

13. CHARGE EXCHANGE: The charge exchange reaction p($^6$He,$^6$Li)n has been studied with an intensity of $4 \cdot 10^5$ particles/s [bro96a]; and based on this experience, intensities between $10^6$ to $10^8$ particles/s for the (t,$^3$He) reaction should be sufficient.

14. LIFETIMES/BETA-DECAY STUDIES: With fast fragmentation beams, β-decay half-lives have been determined with intensities as low as $10^{-5}$ particles/s in the case of $^{100}$Sn at GSI [sum97], but uncertainties were large (~50%). In the same experiment, the half-life of $^{105}$Sb was determined with an accuracy of 10% on the basis of a factor-of-10 more events [sch95]. This level of accuracy requires therefore a beam intensity of $10^{-4}$ particles/s. Similarly in a recent experiment at GANIL, the half-life of $^{86}$Tc was determined with an accuracy of 25% and a beam intensity of the order of $10^{-4}$ particles/s [lon98].

15. BETA-NMR: Ground-state magnetic-moment measurements have been made at implantation rates below 10 particles per second for $^9$C ($T_{1/2}$ = 127 ms) at the NSCL [huh98] and $^{17}$B ($T_{1/2}$ = 5.1 ms) at RIKEN [uen96]. Both measurements took advantage of the large polarizations observed for fragments collected off the normal beam axis following intermediate-energy heavy-ion reactions [asa90]. The induced fragment polarization is significantly larger than that obtained using the tilted foil technique on slow-moving beams [rog86].

16. MICRO-SECOND ISOMERS: A large number of μs-isomers were observed in a fragmentation reaction with individual intensities as low as ~$2 \cdot 10^{-3}$ particles/s [grz95]. The lifetime of the new isomer $^{66m}$As was later measured with $1.7 \cdot 10^5$ implants in 96 hours (0.5 particles/s) [grz98]. The technique relies on coincidences between the implanted ion and a γ ray within the μs range, which significantly reduces the γ-ray background. About a thousand implanted ions are sufficient to detect new μs-isomers, which makes possible experiments with intensities of $10^{-3}$ particles/s.

# Appendix B: On the Possibility of Operating RIA With Parallel Main Users

An important argument for the implementation of both, fast beam capabilities and ISOL capabilities at RIA is that it will allow twice the experimental time (and possibly more) to be allocated to users with little reduction in the intensity that each user receives. The essential technical point is that in the production mode envisaged, high-energy fragmentation reactions, the yield curves cover a broad mass range. Hence, the reactions will always produce other interesting products at momentum settings in the vicinity of any given value. It should be possible to design the first stage of the fragment separator to separate beams of somewhat different magnetic rigidities and to deliver these into separate beam lines. One line could serve the ISOL stopper and post-accelerator, while another line delivers the direct fragmentation beam for fast-beam experiments. Should simultaneous operation of a standard ISOL target be possible with the same primary beam, the beam from the linac could be RF switched between the fragmentation line and a standard ISOL target. This possibility would allow a minimum of three simultaneous experiments.

As an example, one can imagine ISOL operation with a re-accelerated beam of doubly magic $^{132}$Sn simultaneously with an in-flight experiment using Sn beams with masses around 140. Since each user presumably will have the same conditions as if he or she were alone on the machine, this will mean a real gain in service to the user community and in scientific output from the facility.

The design of such an integrated pre-separator and switchyard element will clearly require a dedicated study. The task will be simplified if, as expected, the main demand for fast-beam studies is for the most neutron-rich species, which will have higher rigidity than the higher intensity isotopes needed to feed the gas stopping station.

# Appendix C: Experimental Equipment Required for Fast Beam Studies

This section provides examples and rough cost estimates of experimental equipment needed to implement a fast beam arena at RIA. The present list is based upon experience gathered worldwide in recent years and is neither intended to be complete, nor to guess at the priority ranking the community may give to these capabilities. Most certainly, techniques, needs, and opportunities will evolve with the coming generation of fast beam experiments at the upgraded NSCL facility and elsewhere in the world. In addition, the initial instrumentation at RIA must be optimized with regard to other facility features and thus requires a broader discussion in the US physics community than can be provided in the current context. Nevertheless, the community and the funding agencies may find this list useful as a baseline for future discussions and deliberations.

The considerations presented here indicate that an investment of the order of $50 M will provide the basic equipment needed for the experiments discussed in this document. Additional investments will add to this basic capability and will provide a highly versatile

Table 2: Examples of experimental equipment for a fast beam arena, rough estimated cost, anticipated use.

| Equipment item | Use | Cost (M$) |
|---|---|---|
| High Bay for 6 experimental vaults, beam lines, vacuum system, utilities | Building plus infrastructure | 23 |
| High resolution fragment separator | In-flight separation of fast fragments | 17 |
| Velocity (Wien) Filter | Additional removal of contaminants, especially at lower velocities | 10 |
| High resolution spectrograph | Precision particle detection for direct reactions in inverse kinematics, e.g., knockout and charge-exchange studies. | 18 |
| Sweeper magnet | Neutron measurements at zero degrees (needed to deflect intense charged particle flux from line-of-sight of neutron wall) | 5 |
| Large Area Neutron Detector | Structure of neutron-rich nuclei, EOS | 2 |
| Position sensitive Ge-array | Coulomb excitation, tagging of knockout reactions, decay studies | 10 |
| Large area Si-array | Inverse kinematics studies | 3 |
| Implantation Station | Half lives, decay modes | 1 |
| Time Projection Chamber | EOS, quantum transport phenomena | 4 |

fast beam arena for experiments at the cutting edge of technology. The various equipment items and rough cost estimates are listed in Table 2. Most estimates are based on approximate scaling of existing equipment at in-flight experimental facilities around the world.

The base needs follow from the desire to deliver fragment beams to the RIA gas stopping station for ISOL experiments and fast beams for the experimental program described in this document simultaneously. It would be most efficient to feed the high-energy area by its own high-resolution fragment separator. Less rigid secondary beams (typically of higher intensity) could be sent to the gas stopper while, simultaneously, more rigid (less intense) beams could be used for fast beam experiments. The separator for the high-energy area should be tailored for in-flight experiments, i.e., low contamination (since no isobar separator will be available) and a somewhat reduced momentum acceptance. The large 20% momentum acceptance, envisioned to feed the gas stopper, may be difficult to accommodate in fast beam experiments and would have significant contamination of other isotopes. A high-resolution separator with a large solid angle, 6% momentum acceptance, and an 8 Tm bending power would be adequate for fast beam separation. The reduction in secondary beam intensity compared to the large acceptance separator would be roughly a

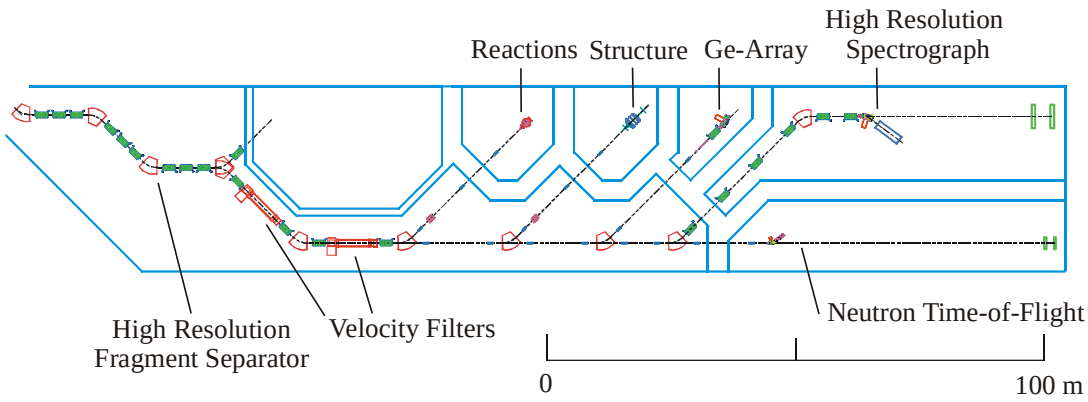


Figure 41: Schematic layout of the beam transport and the experimental areas of the fast fragmentation beams of RIA.

factor of 2. This device could be a scaled up version of the 6 Tm device (A1900) at the NSCL.

The performance of the high-energy separator could be enhanced by the addition of a series of Wien filters for velocity selection. Such additional velocity filters could remove remaining contaminants and provide relatively pure beams. This is particularly useful for experiments with very weak beams, such as those used for decay studies of nuclei produced at the 1 particle/day level. This technique has been successfully used with LISE3 at GANIL and with the RPMS at the NSCL. Approximately 20 m of Wien filter are required to provide sufficient separation at energies of 100 to 200 MeV/nucleon.

The cost estimate for the high bay, beam transport system, vault shielding, utilities, etc. was scaled up from the present NSCL facility costs. A schematic layout which accommodates all listed equipment is shown in Figure 41. Some cost saving could be realized by starting with a smaller number of equipped vaults.

One of the important equipment items is the high-resolution magnetic spectrograph needed in direct reactions, such as knockout, charge-exchange, transfer, and other reactions in which a good particle ID tag is required. The rigidity of the device can be somewhat less than the full 8 Tm, since less rigid breakup products will usually be measured. A similar spectrograph at the NSCL, the S800, has a 20 msr solid angle and an energy resolving power of 10,000. These parameters are ideal for knockout studies and are desirable for the new device. The maximum rigidity of the S800 is 4 Tm, and hence the new device will have to be scaled up by 50% in size assuming the same field strengths. The actual design of the new spectrograph would probably look different than the S800, but the key element, as in the S800, would be large-bend and large-volume dipoles to provide the needed resolving power.

Many experiments involve neutron-rich, weakly bound nuclei, and often the final states will be neutron-unbound. To measure these states it is necessary to detect the decay products, i.e., a charged particle in coincidence with a fast neutron, both typically emitted close to the beam axis. This requires the use of a sweeper magnet that deflects the main

charged particle flux to a shielded location at larger angles, where the charged particles are stopped or detected without producing background neutrons in the neutron detector (located near zero degrees). A sweeper magnet must also be used in forward-angle neutron coincidence experiments when the charged particles are detected with the high-resolution spectrograph. At the largest expected energy (400 MeV), a long flight path is required for adequate neutron energy resolution. For high-resolution studies, a minimum flight path of 50 m should be available. Thus, a large class of neutron coincidence studies requires a sweeper magnet, a large area neutron detector, and a long flight path for neutrons. The new sweeper magnet at the NSCL will have a bending power of 4 Tm and is being constructed for a cost of $1M. A scaled up 8 Tm version would cost approximately five times this amount. The fully equipped facility could use three such sweeper magnets for optimum flexibility and convenience: a full rigidity version for stand-alone operation, a 6 Tm version for use with the spectrograph, and a 4 Tm sweeper (similar to the NSCL sweeper magnet) for high-resolution neutron experiments with long flight paths. The present large-area neutron detector at the NSCL could be used, but an additional larger detector optimized for higher energy neutrons would also be needed. In a restricted funding scenario, at least one such device should be built and shared with different coincidence equipment. Similarly, the neutron detector should be movable to allow coincidence experiments with the TPC (discussed below).

Many experiments described in this report require γ-ray detection. Since the γ-ray emitting nuclei are typically moving with 20–60% of the speed of light, the γ-ray detector will need position resolution of the order of a few millimeter. Concepts for such a detector are being developed at the NSCL, LBNL, and ANL, as well as at laboratories in Europe. The requirements for the fast beam device will be somewhat easier to meet than those discussed for GRETA at LBNL for example.

A large-area silicon detector is needed for inverse kinematics studies. Elastic and inelastic studies require coverage around 90°, and (p,d) and (d,p) reactions require coverage near 0° and 180° in the lab, respectively. A prototype array is being developed by a collaboration of Washington University, Indiana University, and the NSCL. A similar device, the MUST array, has been constructed at GANIL.

Experiments to identify fragments and to measure their half-lives and decay modes will require a highly segmented implantation station with 4π neutron detection. Such a station should allow half-life measurements to be performed with single atoms per day, similar to what is now done at GSI.

A significant part of the program will involve high-energy reactions to investigate isospin dependencies of the EOS, liquid gas transitions, and quantum-transport phenomena. This program will require a 4π detector for charged particles. Such a detector should have a broad dynamics range in particle type and energy and a low particle detection threshold. It further needs high granularity to allow detection of all fragments in multi-fragmentation events. A good solution is a time projection chamber, TPC. It may be possible to reuse an existing TPC. For example, if available, the EOS TPC is probably a good match to RIA requirements.

As a final comment, it should be pointed out that the experimental studies described in this document do not require a storage ring. However, given the success of the ESR at GSI, it may be desirable to design the facility layout in such a way that there is sufficient space to accommodate an accumulator and storage ring which could then be implemented at a later time.

# REFERENCES

The references given here serve to point the reader to pertinent work discussed in Section 4 and Appendix A, but no attempts have been made to be complete.


[abo95] Y. Aboussir, J. M. Pearson, A. K. Dutta, and F. Tondeur, At. Data Nucl. Data Tables **61**, 127 (1995).

[alk96] J. S. Al-Khalili, J. A. Tostevin, and I. J. Thompson, Phys. Rev. C **54**, 1843 (1996).

[ann94] R. Anne, R. Bimbot, S. Dogny, *et al.*, Nucl. Phys. **A575**, 125 (1994).

[ann95] R. Anne, D. Bazin, R. Bimbot, *et al.*, Z. Phys. **A352**, 397 (1995).

[ant00] D. Anthony, P. F. Mantica, D. J. Morrissey, and G. Georgiev, Hyperfine Int., accepted for publication (2000).

[asa90] K. Asahi, M. Ishihara, N. Inabe, *et al.*, Phys. Lett. **B251**, 488 (1990).

[auf94] M. B. Aufderheide, I. Fushiki, G. M. Fuller and T. A. Weaver, Ap. J. **424**, 257 (1994).

[aum99] T. Aumann, A. Navin, D. P. Balamuth, *et al.*, Phys. Rev. Lett. **84**, 35 (2000).

[aum99a] T. Aumann, A. Leistenschneider, K. Boretzky *et al.*, Nucl. Phys. **A649**, 297c (1999).

[aum99b] T. Aumann, D. Aleksandrov, L. Axelsson, *et al.*, Phys. Rev. C **59**, 1252 (1999).

[aus95] S. M. Austin and G. F. Bertsch, Scientific American **272**, 62 (1995).

[aus99] S. M. Austin, private communication.

[axe96] L. Axelsson, M. J. G. Borge, S. Fayans, *et al.*, Phys. Rev. C **54**, R1511 (1996).

[azh98] A. Azhari, T. Baumann, J. A. Brown, *et al.*, Phys. Rev. C **57**, 628 (1998).

[bau98] E. Bauge, J. P. Delaroche, and M. Girod, Phys. Rev. C **58**, 1118 (1998).

[ber83] A. M. Bernstein, V. R. Brown, V. A. Madsen, Comm. Nucl. Part. Phys. **11**, 203 (1983).

[ber88] C. A. Bertulani and G. Baur, Phys. Rep. **163**, 299 (1988).

[ber89] G. F. Bertsch, B. A. Brown, and H. Sagawa, Phys. Rev. C **39**, 1154 (1989).

[ber97] M. Bernas, P. Armbruster, S. Czajkowski, *et al.*, Nucl. Phys. **A616**, 352c (1997).

[ber99] C. A. Bertulani, Comp. Phys. Comm. **116**, 345 (1999).

[bil00] L. Bildsten, in "Cosmic Explosions", edited by S. S. Holt and W. W. Zhang, New York, AIP, to be published (2000).

[bla80] J. P. Blaizot, Phys. Rep. **64**, 171 (1980).

[bla93] B. Blank, J.-J. Gaimard, H. Geissel, *et al.*, Nucl. Phys. **A555**, 408 (1993).

[bla00] B. Blank, M. Chartier, S. Czajkowski, *et al.*, Phys. Rev. Lett. **84**, 1116, (2000).

[boh70] G. Bohm and F. Wysotzki, Nucl. Phys. **B15**, 628 (1970); G. Bohm, J. Klabuhn, U. Krecker, *et al.*, Nucl. Phys. **B4**, 511 (1968).

[boh88] H. G. Bohlen, B. Gebauer, D. Kolbert, *et al.*, Z. Phys. **A330**, 227 (1988).

[boh93] H. G. Bohlen, B. Gebauer, M. von Lucke-Petsch, *et al.*, Z. Phys. **A344**, 381 (1993).

[bol99] G. Bollen, private communication.

[bon95] J. P. Bondorf , A. S. Botvina, A. S. Iljinov, *et al.*, Phys. Rep. **257**, 133 (1995).

[bon98] A. Bonaccorso and D. M. Brink, Phys. Rev. C **58**, 2864 (1998).

[bor93] M. J. G. Borge, L. Johannsen, B. Jonson, *et al.*, Nucl. Phys. **A560**, 664 (1993).

[bra99] "Proceedings of the Topical Conference on Giant Resonances", edited by A. Bracco and P. F. Bortignon, Nucl. Phys. A **649** (1999).
[bro88] B. A. Brown and B. H. Wildenthal, Ann. Rev. Nucl. Part. Sci. **38**, 29 (1988).
[bro94] B. A. Brown and K. Rykaczewski, Phys. Rev. C **50**, 2270 (1994).
[bro96] B. A. Brown and P. G. Hansen, Phys. Lett. **B381**, 391 (1996).
[bro96a] J. A. Brown, D. Bazin, W. Benenson, *et al*., Phys. Rev. C **54**, R2105 (1996).
[bro98] B. A. Brown, International School of Heavy Ion Physics, 4th course: Exotic Nuclei; R. A. Broglia and P. G. Hansen (eds.) (World Scientific, Singapore, 1998), p 1.
[bro98a] B. A. Brown, Phys. Rev. C **58**, 220 (1998).
[bue84] M. Buenerd, J. Phys. (Paris), Colloq. **C-4**, 115 (1984).
[cag99] J. A. Caggiano, D. Bazin, W. Benenson, *et al.*, Phys. Rev. C **60**, 064322 (1999).
[cha97] Ch. Chandler, P. H. Regan, C. J. Pearson, *et al*., Phys. Rev. C **56**, R2924 (1997).
[cha97a] E. Chabanat, P. Bonche, P. Haensel, J. Meyer and F. Schaeffer, Nucl. Phys. **A627**, 710 (1997).
[che00] L. Chen *et al.*, to be published (2000).
[cho99] Ph. Chomaz and F. Gulminelli, Phys. Lett. **B447**, 221 (1999).
[chr97] M. J. Chromik, B. A. Brown, M. Fauerbach, *et al.*, Phys. Rev. C **55**, 1676 (1997).
[chr99] M. J. Chromik, B. A. Brown, M. Fauerbach, *et al.*, Proceedings of the International Conference on Nuclear Structure 98, edited by C. Baktash, AIP Conference Proceedings **481**, p. 187 (1999).
[col98] M. Colonna, M. DiToro, G. Fabbri, and S. Maccarone, Phys. Rev. C **57**, 1410 (1998).
[dag96] M. D'Agostino, A. S. Botvina, P. M. Milazzo, *et al.*, Phys. Lett. **B371**, 175 (1996).
[dan85] P. Danielewicz and G. Odyniec, Phys. Lett. **B157**, 146 (1985).
[dan98] B. V. Danilin, I. J. Thompson, J. S. Vaagen, M. V. Zhukov, Nucl. Phys. **A632**, 383 (1998).
[dan98a] P. Danielewicz, nucl-th 9907098.
[dau98] J. M. Daugas, M. Lewitowicz, R. Anne, *et al.*, Proceedings of the International Conference on Exotic Nuclei and Atomic Masses, ENAM98, edited by B. M. Sherrill, D. J. Morrissey, and C. N. Davids, AIP Conference Proceedings **455**, p. 494 (1998).
[dau00] J. M. Daugas *et al*., submitted to Phys. Lett. **B**, (2000).
[dav96] C. N. Davids, P. J. Woods, H. T. Penttilä, *et al.*, Phys. Rev. Lett. **76**, 592 (1996).
[dav98] C. N. Davids, P. J. Woods, D. Seweryniak, *et al.*, Phys. Rev. Lett. **80**, 1849 (1998).
[dea98] D. J. Dean, K. Langanke, L. Chatterjee, P. B. Radha, and M. R. Strayer, Phys. Rev. C **58**, 536 (1998).
[dec80] J. Decharge and D. Gogny, Phys. Rev. C **21**, 1568 (1980).
[des94] C. Desfrancois, H. Abdoul-Carime, C. Adjouri, N. Khelifa, and J. P. Schermann, Europhys. Lett. **26**, 25 (1994).
[det91] C. Détraz, Z. Phys. **A340**, 227 (1991).

[dia98] I. Daito, H. Akimune, S. M. Austin, *et al.*, Phys. Lett. **B418**, 27 (1998).
[dob84] J. Dobaczewski, H. Flocard and J. Treiner, Nucl. Phys. **A422**, 103 (1984).
[dob94] J. Dobaczewski, I. Hamamoto, W. Nazarewicz and J. A. Sheikh, Phys. Rev. Lett. **72**, 981 (1994).
[dob96] J. Dobaczewski, W. Nazarewicz, T. R. Werner, *et al.*, Phys. Rev. C **53**, 2809 (1996).
[dob96a] J. Dobaczewski, W. Nazarewicz, and T. Werner, Phys. Scripta **T56**, 15 (1995).
[efi70] V. M. Efimov, Sov. J. Nucl. Phys. **12**, 589 (1970); Comments Nucl. Part. Phys. **19**, 271 (1990).
[end90] P. M. Endt, Nucl. Phys. **A521**, 1 (1990).
[eng99] J. Engel, M. Bender, J. Dobaczewski, W. Nazarewicz, and R. Surman, Phys. Rev. C **60**, 014302 (1999).
[far97] Michel Farine, J. M. Pearson and F. Tondeur, Nucl. Phys. **A615**, 135 (1997), T. v. Chossy and W. Stocker, Phys. Rev. C **56**, 2518 (1997), I. Hamamoto, H. Sagawa, and X. Z. Zhang, Phys. Rev. C **56**, 3121 (1997), D. Vretenar, G.A. Lalazissis, R. Behnsch, W. Pöschl, and P. Ring, Nucl. Phys. **A621**, 853 (1997), Z. Ma , N. Van Giai, H. Toki, and M. L'Huillier, Phys. Rev. C **55**, 2385 (1997).
[fau97] M. Fauerbach, M. J. Chromik, T. Glasmacher, *et al.*, Phys. Rev. C **56**, R1 (1997).
[fay98] S. A. Fayans, Proceedings of the International Conference on Exotic Nuclei and Atomic Masses, ENAM98, edited by B. M. Sherrill, D. J. Morrissey, and C. N. Davids, AIP Conference Proceedings **455**, p. 310 (1998).
[for99] S. Fortier, S. Pita, J. S. Winfield, *et al.*, Phys. Lett. **B461**, 22 (1999).
[fri90] W. A. Friedman, Phys. Rev. C **42**, 667 (1990).
[fre99] C. Freiburghaus, S. Rosswog and F.-K. Thielemann, Ap. J. **525**, L121 (1999).
[fuk93] N. Fukunishi, T. Otsuka, and I. Tanihata, Phys. Rev. C **48**, 1648 (1993).
[ful85] G. M. Fuller, W. A. Fowler, and M. J. Newman, Ap. J. **293**, 1 (1985).
[gar98] E. Garrido, D. V. Fedorov, and A. S. Jensen, Phys. Rev. C **58**, R2654 (1998).
[gei99] W. Geithner, S. Kappertz, M. Keim, *et al.*, Phys. Rev. Lett. **83**, 3792 (1999).
[gla97] T. Glasmacher, B. A. Brown, M. J. Chromik, *et al.*, Phys. Lett. **B395**, 163 (1997).
[gla98] T. Glasmacher, Ann. Rev. Nucl. Part. Sci. **48**,1 (1998).
[gol60] V. I. Goldanskii, Nucl. Phys. **19**, 482 (1960).
[goo80] C. D. Goodman, C. A. Goulding, M. B. Greenfield, *et al.*, Phy. Rev. Lett. **44**, 1755 (1980).
[gor95] J. Görres, M. Wiescher, and F.-K. Thielemann, Phys. Rev. C **51**, 392 (1995).
[gor98] S. Goriely, Phys. Lett. **B436**, 10 (1998).
[gri92] A. G. Griffiths, C. J. Ashworth, J. Rikovska, *et al.*, Phys. Rev. C **46**, 2228 (1992).
[grz95] R. Grzywacz, R. Anne, G. Auger, *et al.*, Phys. Lett. **B355**, 439 (1995).
[grz97] R. Grzywacz, R. Anne, G. Auger, *et al.*, Phys. Rev. C **55**, 1126 (1997).
[grz98] R. Grzywacz, R. Béraud, C. Borcea, *et al.*, Phys. Rev. Lett. **81**, 766 (1998).
[grz98a] R. Grzywacz, S. Andriamonje, B. Blank, *et al.*, Phys. Lett. **B429**. 247 (1998).
[gro97] D. H. E. Gross, Phys. Rep. **279**, 120 (1997).

[gui90] D. Guillemaud-Mueller, J. C. Jacmart, E. Kashy, *et al.*, Phys. Rev. C **41**, 937 (1990).
[hab97] D. Habs, D. Rudolph, P. Thirolf, *et al.*, Prog. Part. Nucl. Phys. **38**, 111 (1997).
[han95] P. G. Hansen, A. S. Jensen, and B. Jonson, Ann. Rev. Nucl. Part. Sci. **45**, 591 (1995).
[han99] P. G. Hansen, private communication.
[hax97] W. C. Haxton, K. Langanke, Y.-Z. Qian, and P. Vogel, Phys. Rev. Lett. **78**, 2694 (1997); Y.-Z. Qian, P. Vogel, and G. J. Wasserburg, Ap. J. **513**, 956 (1999).
[hen96] K. Hencken, G. Bertsch, and H. Esbensen, Phys. Rev. C **54**, 3043 (1996)
[hof96] R. D. Hoffman, S. E. Woosley, G. M. Fuller, and B. S. Meyer, Ap. J. **460**, 478 (1996).
[hua96] M. J. Huang, R. C. Lemmon, F. Daffin, *et al.*, Phys. Rev. Lett. **77**, 3739 (1996).
[huh98] M. Huhta, P. F. Mantica, D. W. Anthony, *et al.*, Phys. Rev. C **57**, R2790 (1998).
[ibb98] R. W. Ibbotson, T. Glasmacher, B. A. Brown, *et al.*, Phys. Rev. Lett. **80**, 2081 (1998).
[ibb99] R. W. Ibbotson, T. Glasmacher, P. F. Mantica, and H. Scheit, Phys. Rev. C **59**, 642 (1999).
[iwa99] N. Iwasa, F. Boué, G. Surówka, *et al.*, Phys. Rev. Lett. **83**, 2910 (1999).
[izu96] H. Izumi, K. Asahi, H. Ueno, *et al.*, Phys. Lett. **B366**, 51 (1996).
[jan99] Z. Janas, C. Chandler, B. Blank, *et al.*, Phys. Rev. Lett. **82**, 295 (1999), and references therein.
[jeu77] J. -P. Jeukenne, A. Lejeune, and C. Mahaux, Phys. Rev. C **15**, 10 (1977).
[jeu77a] J. -P. Jeukenne, A. Lejeune, and C. Mahaux, Phys. Rev. C **16**, 80 (1977).
[jew99] J. K. Jewell, L.A. Riley, P.D. Cottle, *et al.*, Phys. Lett. **B454**, 181 (1999).
[joh73] R. C. Johnson, F. D. Santos, R. C. Brown, *et al.*, Nucl. Phys. **A208**, 221 (1973).
[joh99] R. C. Johnson and J. A. Tostevin, private communication.
[kan95] Y. Kanada-En'yo and H. Horiuchi, Phys. Rev. C **54**, R468 (1995).
[kea00] D. Keane, private communication.
[kel97] J. H. Kelley, T. Suomijärvi, S. E. Hirzebruch, *et al.*, Phys. Rev. C **56** , R1206 (1997).
[kob89] T. Kobayashi, S. Shimoura, I. Tanihata, *et al.*, Phys. Lett. **B232**, 51 (1989).
[koi99] O. Koike, M. Hashimoto, K. Arai, and S. Wanajo, Astron. Astrophys. **342**, 464 (1999).
[kol92] J. J. Kolata, M. Zahar, R. Smith, *et al.*, Phys. Rev. Lett. **69**, 2631 (1992).
[kor94] A. A. Korsheninnikov, K. Yoshida, D. V. Aleksandrov, *et al.*, Phys. Lett. **B326**, 31 (1994).
[kor99] A. A. Korsheninnikov, M. S. Golovkov, A. Ozawa, *et al.*, Phys. Rev. Lett. **82**, 3581 (1999).
[kra93] K.-L. Kratz, J.-P. Bitouzet, F.-K. Thielemann, P. Möller, and B. Pfeiffer, Ap. J. **403**, 216 (1993).
[kra94] G. Kraus, P. Egelhof, C. Fischer, *et al.*, Phys. Rev. Lett. **73**, 1773 (1994).
[kra94a] A. Krasznahorkay, A. Balanda, J.A. Bordewijk, *et al.*, Nucl. Phys. **A567**, 521 (1994).

[kra99] A. Krasznahorkay, M. Fujiwara, P. von Aarle, *et al.*, Phys. Rev. Lett. **82**, 3216 (1999).
[kra00] K.-L. Kratz, private communication.
[kry93] R. A. Kryger, A. Azhari, A. Galonsky, *et al.*, Phys. Rev. C **47**, R2439 (1993).
[kry95] R. A. Kryger, A. Azhari, M. Hellström, *et al.*, Phys. Rev. Lett. **74**, 860 (1995).
[lal97] G. A. Lalazissis, J. Konig and P. Ring, Phys. Rev. C **55**, 540 (1997).
[lal99] G. A. Lalazissis, S. Raman, and P. Ring, At. Data Nucl. Data Tables **71**, 1 (1999).
[lee97] I. Y. Lee, Prog. Part. Nucl. Phys. **38**, 65 (1997).
[lep98] A. Lépine-Szily, J. M. Oliveira, Jr., A. N. Ostrowski, *et al.*, Phys. Rev. Lett. **80**, 1601 (1998).
[lin95] M. Lindroos, C. Broude, G. Goldring, *et al.*, Nucl. Instrum. Methods Phys. Res. **A361**, 53 (1995).
[llo99] W. Llope, private communication
[lon98] C. Longour, J. Garcés Narro, B. Blank, *et al.*, Phys. Rev. Lett. **81**, 3337 (1998).
[mad99] V. Maddalena *et al.*, to be published.
[man97] P. F. Mantica, R. W. Ibbotson, D. W. Anthony, *et al.*, Phys. Rev. C **55,** 2501 (1997).
[man98] P. F. Mantica, D. W. Anthony, B. A. Brown, *et al.*, Proceedings of the International Conference on Exotic Nuclei and Atomic Masses, ENAM98, edited by B. M. Sherrill, D. J. Morrissey, and C. N. Davids, AIP Conference Proceedings **455**, p. 66 (1998).
[man99] P. F. Mantica, private communication.
[mar99] F. Maréchal, T. Suomijärvi, Y. Blumenfeld, *et al.*, Phys. Rev. C **60**, 034615 (1999).
[mar00] G. Martinez-Pinedo, K. Langanke, and D. J. Dean, Ap. J., in press (2000)
[mat96] K. Matsuta, T. Minamisono, M. Tanigaki, *et al.*, Hyperfine Int. **97/98**, 519 (1996).
[mil83] D. J. Millener, J. W. Olness, E. K. Warburton, and S. S. Hanna, Phys. Rev. C **28**, 497 (1983).
[moe95] P. Möller, J. R. Nix, W. D. Meyers, and W. J. Swiatecki, At. Data Nucl. Data Tables **59**, 185 (1995).
[moe97] P. Möller, J. R. Nix, and K.-L. Kratz, At. Data Nucl. Data Tables **66**, 131 (1997).
[moh91] M. F. Mohar, D. Bazin, W. Benenson, *et al.*, Phys. Rev. Lett. **66**, 1571 (1991).
[mot91] T. Motobayashi, T. Takei, S. Kox, *et al.*, Phys. Lett. **B264**, 259 (1991).
[mot94] T. Motobayashi, N. Iwasa, Y. Ando, *et al.*, Phys. Rev. Lett. **73**, 2680 (1994).
[mot95] T. Motobayashi, Y. Ikeda, Y. Ando, *et al.*, Phys. Lett. **B346**, 259 (1991).
[muk98] I. Mukha, L. Axelsson, J. Äystö, *et al.*, Nucl. Phys. **A630**, 394c (1998).
[nak97] T. Nakamura, T. Motobayashi, Y. Ando, *et al.*, Phys. Lett. **B394**, 11 (1997).
[nak99] T. Nakamura, N. Fukuda, T. Motobayashi, *et al.*, Phys. Rev. Lett. **83**, 1112 (1999).
[nav98] A. Navin, D. Bazin, B. A. Brown, *et al.*, Phys. Rev. Lett. **81**, 5089 (1998).
[naz99] W. Nazarewicz, Nucl. Phys. **A654,** 195c (1999).
[neg96] F. Negoita, C. Borcea, and F. Carstoiu, Phys. Rev. C **54**, 1787 (1996).

[neu00] R. Neugart, Hyperfine Int., accepted for publication (2000); W. Geithner, S. Kappertz, M. Keim, *et al.*, Phys. Rev. Lett. **83**, 3792 (1999).
[ney97] G. Neyens, N. Coulier, S. Ternier, *et al.*, Phys. Lett. **B393**, 36 (1997).
[ney99] G. Neyens, N. Coulier, S. Teughels, *et al.*, Phy. Rev. Lett. **82**, 497 (1999).
[ney00] G. Neyens, private communication.
[nin99] V. Ninov, K. E. Gregorich, W. Loveland, *et al.*, Phys. Rev. Lett. **83**, 1104 (1999).
[oga99] H. Ogawa, K. Asahi, K. Sakai, *et al.*, Phys. Lett. **B451**, 11 (1999).
[orr91] N. A. Orr, W. Mittig, L. K. Fifield, *et al.*, Phys. Lett. **B258**, 29 (1991).
[ott89] E. W. Otten, in "Treatise on Heavy-Ion Science", edited by D. A. Bromley, Vol. **8**, p. 517 (Plenum Press, 1989).
[pan93] Q. Pan and P. Danielewicz, Phys. Rev. Lett. **70**, 2062 (1993).
[pak97] R. Pak, W. Benenson, O. Bjarki, *et al.*, Phys. Rev. Lett. **78**, 1022 (1997).
[par95] M. D. Partlan, S. Albergo, F. Bieser, *et al.*, Phys. Rev. Lett. **75**, 2100 (1995).
[pea92] J. M. Pearson, M. Farine, F. Tondeur, Proceedings of Nuclei Far from Stability/Atomic Masses and Fundamental Constants 1992, IPC Series No. **132**, p. 857 (1992).
[pea94] G. F. Peaslee, M. B. Tsang, C. Schwarz, *et al.*, Phys. Rev. C **49**, R2271 (1994).
[pea96] J. M. Pearson, R. C. Nayak, and S. Goriely, Phys. Lett. **B387**, 455 (1996).
[pfe97] B. Pfeiffer, K.–L. Kratz, and F.–K. Thielemann, *et al.*, Z. Phys. **A357**, 235 (1997).
[pfu98] M. Pfützner, P. Armbruster, T. Baumann, *et al.*, Phys. Lett. **B444**, 32 (1998).
[pod00] Z. Podolyak *et al.*, submitted to Phys. Rev. Lett. (2000)
[pri00] B. Prityckenko *et al.*, submitted to Phys. Rev. Lett. (2000).
[pud96] B. S. Pudliner, A. Smerzi, J. Carlson, *et al.*, Phys. Rev. Lett. **76**, 2416 (1996).
[rad97] T. Radon, Th. Kerscher, B. Schlitt, *et al.*, Phys. Rev. Lett. **78**, 4701 (1997).
[rai90] G. Rai, A. Arthur, F. Bieser, *et al.*, IEEE Trans. Nucl. Sci. **37**, 56 (1990).
[ree99] A. T. Reed, O. Tarasov, R. D. Page, *et al.*, Phys. Rev. C **60**, 024311 (1999).
[rei99] P.-G. Reinhard, D. J. Dean, W. Nazarewicz, *et al.*, Phys. Rev. C **60**, 014316 (1999)
[ril99] L. A. Riley, J. K. Jewell, P. D. Cottle, *et al.*, Phys. Rev. Lett. **82**, 4196 (1999).
[rog86] W. F. Rogers, D. L. Clark, S. B. Dutta, and A. G. Martin, Phys. Lett. **B177**, 293 (1986); M. Lindroos, C. Broude, G. Goldring, *et al.*, Nucl. Instrum. Methods Phys. Res. **A361**, 53 (1995).
[rog87] W. F. Rogers, D. L. Clark, S. B. Dutta, and A. G. Martin, Nucl. Instrum. Methods Phys. Res. **A253**, 256 (1987).
[ryk98] K. Rykaczewski, R. Grzywacz, M. Lewitowicz, and M. Pfützner, Nucl. Phys. **A630**, 307c (1998).
[sag93] H. Sagawa, B. A. Brown, and H. Esbensen, Phys. Lett. **B309**, 1 (1993).
[sag98] H. Sagawa, I. Hamamoto, and X. Z. Zhang, J. Phys. G **24**, 1445 (1998).
[sak99] A. Sakharuk and V. Zelevinsky, Phys. Rev. C **61,** 014609 (2000).
[sca99] L. Scalone, M. Colonna, and M. Di Toro, Phys. Lett. **B461**, 9 (1999).
[sch94] W.-D. Schmidt-Ott, K. Asahi, Y. Fujita, *et al.*, Z. Phys. **A350**, 215 (1994).
[sch94a] W. Schöllkopf and J. P. Toennies, Science **266**, 1345 (1994).

[sch95] R. Schneider, T. Faestermann, J. Friese, *et al.*, Nucl. Phys. **A588**, 191c (1995).
[sch96] A. Schüttauf, W.D. Kunze, A. Wörner, *et al.*, Nucl. Phys. **A607**, 457 (1996).
[sch96a] H. Scheit, T. Glasmacher, B. A. Brown, *et al.*, Phys. Rev. Lett. **77**, 3967 (1996).
[sch98] M. Schäffer, W.–D. Schmidt-Ott, T. Dörfler, *et al.*, Phys. Rev. C **57**, 2205 (1998).
[sch98a] H. Schatz, A. Aprahamian, J. Görres, *et al.*, Phys. Rep. **294**, 168 (1998).
[sch99] H. Scheit, T. Glasmacher, R. W. Ibbotson, and P. G. Thirolf, Nucl. Instr. Meth. **A422**, 124 (1999).
[sch99a] K. Schmidt, P. J. Woods, *et al.*,"Proton decay studies of heavy nuclei produced by projectile fragmentation reactions", GSI proposal (1999).
[sel92] P. J. Sellin, P. J. Woods, D. Branford, *et al.*, Nucl. Instrum. Methods Phys. Res. **A311**, 217 (1992).
[set87] K. K. Seth, M. Artuso, D. Barlow, *et al.*, Phys. Rev. Lett. **58**, 1930 (1987).
[sim99] H. Simon, D. Aleksandrov, T. Aumann, *et al.*, Phys. Rev. Lett. **83**, 496 (1999).
[sor93] O. Sorlin, D. Guillemaud-Mueller, A. C. Mueller, *et al.*, Phys. Rev. C **47**, 2941 (1993).
[sug69] K. Sugimoto, Phys. Rev. **182**, 1051 (1969).
[sum97] K. Sümmerer, R. Schneider, T. Faestermann, *et al*., Nucl. Phys. **A616**, 341c (1997).
[sum99] K. Sümmerer, B. Blank, private communication.
[suz95] T. Suzuki, H. Geissel, O. Bochkarev, *et al*., Phys. Rev. Lett. **75**, 3241 (1995).
[tal60] I. Talmi and I. Unna, Phys. Rev. Lett. **4**, 469 (1960).
[tan85] I. Tanihata, H. Hamagaki, O. Hashimoto, *et al.*, Phys. Rev. Lett. **55**, 2676 (1985).
[tan85a] I. Tanihata, H. Hamagaki, O. Hashimoto, *et al*., Phys. Lett. **160B**, 380 (1985).
[tan92] I. Tanihata, D. Hirata, T. Kobayashi, *et al*., Phys. Lett. **B289**, 261 (1992)
[tho99] M. Thoennessen, S. Yokoyama, A. Azhari, *et al.*, Phys. Rev. C **59**, 111 (1999);
[tho00] M. Thoennessen *et al.,* to be published.
[tos99] J. A. Tostevin, J. Phys. G **25**, 735 (1999).
[tsa93] M. B. Tsang, W. C. Hsi, W. G. Lynch, *et al.*, Phys. Rev. Lett. **71**, 1502 (1993).
[uen96] H. Ueno, K. Asahi, H. Izumi, *et al.*, Phys. Rev. C **53**, 2142 (1996).
[var95] K. Varga, Y. Suzuki, and I. Tanihata, Phys. Rev. C **52**, 3013 (1995).
[var99] R. L. Varner *et al.*, Proceedings of the International Workshop on Collective Excitations in Fermi and Bose Systems, edited by C. Bertulani, World Scientific (1999), p.264.
[wan97] S. Wan, P. Reiter, J. Cub, *et al.*, Z. Phys. **A358**, 213 (1997).
[war96] R. E. Warner, R. A. Patty, P. M. Voyles, *et al*., Phys. Rev. C **54**, 1700 (1996)
[war97] R. E. Warner, Phys. Rev. C **55**, 298 (1997)
[war00] R. E. Warner *et al*., submitted to Phys. Rev. C (2000)
[wef99] E. Wefers *et al*., Proceedings of ENPE99 in Sevilla, Spain, edited by B. Rubio, M. Lozano, and W. Gelletly, AIP Conference Proceedings **495**, 375 (1999).
[wer94] T. R. Werner, J. A. Sheikh, W. Nazarewicz, *et al.*, Phys. Lett. **B335**, 259 (1994).
[wer96] T. R. Werner, J.A. Sheikh, M. Misu, *et al.*, Nucl. Phys. **A597**, 327 (1996).
[win79] A. Winther and K. Alder, Nucl. Phys. **A319**, 518 (1979).

[win93] J. A. Winger, D. P. Bazin, W. Benenson, *et al.*, Phys. Lett. **B299**, 214 (1993).
[woo97] P. J. Woods and C. N. Davids, Ann. Rev. Nucl. Part. Sci. **47**, 541 (1997).
[xia98] C. Xiangzhou, F. Jun, S. Wenqin, *et al*., Phys. Rev. C **58**, 572 (1998).
[xu99] H. Xu, private communication.
[you93] B. M. Young, D. Bazin, W. Benenson, *et al.*, Phys. Lett. **B311**, 22 (1993).
[you96] D. H. Youngblood, H. L.Clark, and Y.-W.Lui, Phys. Rev. Lett. **76**, 1429 (1996).
[you97] D. H. Youngblood, Y.-W. Lui, and H. L. Clark, Phys. Rev. C **55**, 2811 (1997).
[you99] D. H. Youngblood, H. L. Clark, and Y.-W.Lui, Phys. Rev. Lett. **82**, 691 (1999).
[zha95] W. M. Zhang, R. Madey, J. Schambach, *et al.*, Phys. Rev. C **52**, 2643 (1995).

# ACKNOWLEDGEMENTS

The document was prepared by the National Superconducting Cyclotron Laboratory with the significant input of many scientists around the world. A rough first draft of the science sections served as a basis for further discussion, consultation, and input. Subsequently more than 250 physicists and colleagues from other institutions were contacted electronically and asked whether they were willing to read, critique, and augment the science laid out in various sections. Over 140 scientists from other institutions provided advice, comments, and suggestions for changes, often in considerable depth and detail. The overwhelmingly positive response indicates the great scientific interest in a fast fragmentation beam capability at RIA. This process resulted in a much-improved document which can now serve as a basis for discussions and further deliberations by the nuclear physics community. We would like to thank the following scientists for their contribution and apologize to everyone we failed to contact or who commented and are inadvertently not listed below:

Navin Alahari, Bhabha Atomic Research Center, India
Nicolas Alamanos, CEA, Scalay, France
Jim Al-Khalili, University of Surrey, England
Ani Aprahamian, University of Notre Dame
Koichiro Asahi, Tokyo Institute of Technology, Japan
Juha Aysto, ISOLDE, CERN
David Balamuth, University of Pennsylvania
Bruce Barrett, University of Arizona
Noemie Benczer-Koller, Rutgers University
Georg Berg, Indiana University
George Bertsch, University of Washington
Bertram Blank, University of Bordeaux, France
Yorick Blumenfeld, Université de Paris Sud, Orsay, France
Georg Bollen, Technische Universität München, Germany
Angela Bonaccorso, University of Pisa, Italy
Jakob Bondorf, Niels Bohr Institute, Copenhagen, Denmark
Maria Borge, CSIC, Madrid, Spain
Richard Boyd, Ohio State University
Angela Bracco, University of Milan, Italy
Daeg Brenner, Clark University
David Brink, Oxford University, England
Jim Brown, Millikin University
Rick Casten, Yale University
Ed Cecil, Colorado School of Mines
Art Champagne, University of North Carolina
Marielle Chartier, University of Bordeaux, France
Phillippe Chomaz, GANIL, Caen, France
Maria Colonna, INFN and University of Catania, Italy

John D'Auria, TRIUMF, Canada
Cary Davids, Argonne National Laboratory
David Dean, Oak Ridge National Laboratory
Piotr Decowski, Smith College
Marie-Agnes Deleplanque-Stephens, Lawrence Berkeley National Laboratory
Peter Dendooven, University of Jyväskylä, Finland
Romualdo de Souza, Indiana University
Massimo DiToro, INFN and University of Catania, Italy
Jacek Dobaczewski, University of Warsaw, Poland
Dominique Durand, University of Caen, France
Hans Emling, GSI, Darmstadt, Germany
Paul Fallon, Lawrence Berkeley National Laboratory
Hubert Flocard, IPN, Orsay, France
John Fox, Oak Ridge National Laboratory
Stefan Frauendorf, University of Notre Dame
William Friedman, University of Wisconsin
Mamoru Fujiwara, Osaka University, Japan
Charles Gale, McGill University, Canada
Sidney Gales, Université de Paris Sud, Orsay, France
Alejandro Garcia, University of Notre Dame
Joachim Görres, University of Notre Dmae
Uwe Greife, Colorado School of Mines
Henry Griffin, University of Michigan
Carl Gross, Oak Ridge National Laboratory
Robert Grzywacz, Oak Ridge National Laboratory
Dominique Guillemaud-Mueller, GANIL, Caen, France
Greg Hackman, University of Kansas
Mel Halbert, Oak Ridge National Laboratory
Joe Hamilton, Vanderbilt University
John Hardy, Texas A&M University
Dieter Hartmann, Clemson University
Peter Haustein, Brookhaven National Laboratory
Kris Heyde, University of Ghent, Belgium
Andrew Hirsch, Purdue University
Ruth Howes, Ball State University
Aksel Jensen, University of Aarhus, Denmark
Ron Johnson, University of Surrey, England
Björn Jonson, Chalmers University, Gothenburg, Sweden
Declan Keane, Kent State University
Kirby Kemper, Florida State University
Che-Ming Ko, Texas A&M University
Hans-Joachim Körner, Technische Universität München, Germany
James Kolata, University of Notre Dame
Steve Koonin, California Institute of Technology

Ray Kozub, Tennessee Technical University
Karl-Ludwig Kratz, Universität Mainz, Germany
Toshiyuki Kubo, RIKEN, Japan
Dimitri Kusnezov, Yale University
Roy Lacey, SUNY Stony Brook
Karlheinz Langanke, Aarhus University, Denmark
I-Yang Lee, Lawrence Berkeley National Laboratory
Bao-An Li, Arkansas State University
Uli Lynen, GSI, Darmstadt, Germany
Adam Maj, University of Krakow, Poland
Grant Mathews, University of Notre Dame
Alberto Mengoni, ENEA, Bologna, Italy
Volker Metag, Universität Giessen, Germany
John Millener, Brookhaven National Laboratory
Igor Mishustin, NBI, Kopenhagen, Denmark
Wolfgang Mittig, GANIL, Caen, France
Luciano Moretto, University of Berkeley
Arialdo Moroni, INFN and University of Milan, Italy
Ulrich Mosel, Universität Giessen, Germany
Alex Mueller, Université de Paris Sud, France
Tetsuya Murakami, University of Kyoto, Japan
Joe Natowitz, Texas A&M University
Witek Nazarewicz, University of Tennessee
Giancarlo Nebbia, INFN, Padua, Italy
Takaharu Otsuka, University of Tokyo, Japan
Peter Parker, Yale University
Peter Paul, Brookhaven National Laboratory
Larry Phair, Lawrence Berkeley National Laboratory
Stuart Pittel, University of Delaware
Eric Plagnol, GANIL, Caen, France
Norbert Porile, Purdue University
Alfredo Poves, University of Madrid, Spain
Jorgen Randrup, Lawrance Berkeley National Laboratory
Paddy Regan, University of Surrey, England
Willi Reisdorf, GSI, Darmstadt, Germany
Achim Richter, Technische Universität Darmstadt, Germany
Karsten Riisager, Aarhus University, Denmark
Ernst Roeckl, GSI, Darmstadt, Germany
Krzysztof Rykaczewski, Oak Ridge National Laboratory
Steve Sanders, University of Kansas
John Schiffer, Argonne National Laboratory
Wolf Schmidt-Ott, Universität Göttingen, Germany
Gerhard Schrieder, GSI, Darmstadt, Germany
Udo Schröder, University of Rochester

Paul Semmes, Tennessee Technological University
Rolf Siemssen, KVI, Groningen, The Netherlands
Geirr Sletten, NBI, Kopenhagen, Denmark
Lee Sobotka, Washington University
Irina Stone, Oxford University, England
Andrew Stuchberry, Australian National University, Canberra, Australia
Klaus Sümmerer, GSI, Darmstadt, Germany
Sam Tabor, Florida State University
Peter Thirolf, Ludwig Maximilian Universität, München, Germany
Ian Thompson, University of Surrey, England
Jeff Tostevin, University of Surrey, England
Wolfgang Trautmann, GSI, Darmstadt, Germany
Bob Tribble, Texas A&M University
Jan Vaagen, Oslo University, Norway
Ad van den Berg, KVI, Groningen, The Netherlands
Robert Varner, Oak Ridge National Laboratory
Jean Vervier, Louvain-la-Neuve, Belgium
Giuseppe Viesti, INFN, Padova, Italy
Domenico Vinciguerra, INFN and University of Catania, Italy
Vic Viola, Indiana University
Bill Walters, University of Maryland
Bob Warner, Oberlin College
Michael Wiescher, University of Notre Dame
Jeff Winger, Mississippi State University
Frank Wolfs, University of Rochester
Hermann Wolter, Ludwig Maximilian Universität, München, Germany
Phil Woods, University of Edinburgh, Scottland
Gordon Wozniak, Lawrence Berkeley National Laboratory
Allan Wuosmaa, Argonne National Laboratory
Steve Yates, University of Kentucky
Sherry Yennello, Texas A&M University